

# **Development and Application of Microreactors for Biocatalytic Reactions**

Zur Erlangung des akademischen Grades eines  
**Dr.-Ing.**  
von der Fakultät Bio- und Chemieingenieurwesen  
der Technischen Universität Dortmund  
genehmigte Dissertation

vorgelegt von

**Rohan Karande, M.Sc.**

aus

Karad, Indien

Tag der mündlichen Prüfung: 15.11.2012

1. Gutachter: Prof. Dr. Andreas Schmid
2. Gutachter: Prof. Dr. David Agar

**Dortmund 2012**



## Acknowledgements

I would like to express my deepest gratitude to the two most important people, Prof. Andreas Schmid and Dr. Katja Bühler. Andreas, thank you for giving me the opportunity to perform doctoral thesis on the very interesting topic. I enjoyed the freedom you gave me during the entire thesis work. Your vast knowledge, broad vision and ideas drove me to overcome challenges and added to my research experience. In simple words, I learned from you to look challenge as an opportunity and not as an obstacle. Katja, very special thanks for your encouragement, patience and dedication that you invested to complete my thesis work. You introduced me to the BT laboratory during my master studies and then onwards guided me through my master and doctoral thesis. I am truly thankful for providing me with direction and shaping my scientific career. I don't know whether I will ever be able to convey my appreciation fully, but I owe you both my eternal gratitude.

I thank the members of the examination committee, Prof. David Agar, Prof. Norbert Kockmann and Prof. Rolf Wichmann for the time and efforts taken to review my thesis.

I am deeply indebted to Dr. Reto Ruinatscha, Dr. Babu Halan, Dr. Daniel Kuhn and Bart for fruitful discussions and sharing your research experience with me. For the good atmosphere in the lab, many thanks goes to my current and former colleagues from the BT chair: Anders, Birgitta, Bruno, Christian D., Christian W., Darius, Dusny, Eleni, Francesco, Freddy, Frank, Jana, Jan H., Jan V., Jianan, Jochen, Jon, Karo, Karsten, Kerstin, Kirsten, Kamila, Lars, Linde, Marcel, Mani (always ready to help), Martin, Marvin, Mattijs, Michael, Nadine (a good office colleague), Oliver, Özde, Patty, Rainer, Sabine, Sjef, Suresh, Verena and Volker.

My sincere thanks to Christine Wasielewski and Anja Kulmsee for their excellent administrative support. I would also like to thank Jochen, Patty and Sabine for their help in many ways during the laboratory work. Furthermore, I thank Sammy Majdi and his team for managing the IT structures.

I thank all my friends Gaurang, Prasad, Madhav, Yogesh, Kiran, Sachin, Bharat, Vijay W., Babu S., and Srikant for making my stay in Germany very comfortable.

I am grateful to my parents, my brother and his family for their love and moral support during my stay in Germany. A special thanks to my wife Shubhangi for caring, understanding and supporting me over our stay in Germany. I highly appreciate your skills to manage our loving son (Yug) and my schedules very efficiently. Shubhangi, thank you very much!

# Table of Contents

Summary	VI
Zusammenfassung	VIII
List of Abbreviations	X
Chapter 1: General Introduction	1
General criteria to choose a microreactor design	2
The different types of biocatalysts	3
Multiphase biocatalysis	8
Multiphase biocatalytic microreactors	17
Concluding remarks	21
Scope of the thesis	22
Chapter 2: Evaluating Enzyme Stability in an Aqueous/Organic Segmented Flow System	23
Summary	24
Introduction	25
Materials and methods	27
Results and discussion	30
Conclusions	38
Chapter 3: Stabilizing Enzyme Activity in an Aqueous/Organic Segmented Flow	39
Summary	40
Introduction	41
Materials and methods	43
Results and discussion	46
Conclusions	53
Chapter 4: Miniaturizing biocatalysis: Enzyme Catalyzed Reactions in an Aqueous/Organic Segmented Flow Capillary Microreactor	54
Summary	55
Introduction	56
Materials and methods	58
Results and discussion	60
Conclusions	72
Chapter 5: The Segmented Flow Biofilm Microreactor-A Novel Reactor Concept	73
Summary	74
Introduction	75
Materials and methods	77
Results and discussion	80
Conclusions	88

Chapter 6: (Aqueous-air-organic) Three-phase Segmented Flow Biofilm Microreactor	89
Summary	90
Introduction	91
Materials and methods	93
Results and discussion	95
Perspective	98
Chapter 7: General Discussion	99
Outlook	112
References	113
Curriculum Vitae	121

## Summary

In the recent years, microreactors have been recognized as a potent technology for enhancing reaction rates at low energy input and simplified scale up issues. The aim of this thesis was to develop and apply microreactors for biocatalytic reactions. In this context, the potential advantages of microreactors were explored for both forms of biocatalysts, isolated enzymes and whole cells.

Fast inactivation of the respective enzyme was a key problem when applying it in aqueous-organic segmented flow microreactors. The large aqueous-organic interfacial area and the strong fluidic forces within the segments mostly accounted for enzyme inactivation. Enzyme immobilization and addition of surfactant to the aqueous phase were explored as possible solutions to overcome fast enzyme inactivation. At an optimal concentration of surfactant (Tween 20), the direct contact of enzymes with the interface was prevented, resulting in almost 100 % recovered enzyme activity as compared to 45% without any medium modification. After stabilizing enzyme activity, the enzymatic performance was evaluated in the segmented flow reactor for 1-heptanol synthesis by using thermostable alcohol dehydrogenase (TADH) and formate dehydrogenase (FDH). An average volumetric productivity of  $10.4 \text{ g}_{\text{product}} \text{ L}_{\text{org}}^{-1} \text{ hr}^{-1}$  ( $90 \text{ mM h}^{-1}$ ) was obtained in the 0.5 mm (i.d.) capillary microreactor. The study performed revealed that the capillary diameter, flow velocity, and enzyme as well as substrate concentrations were important parameters regarding reactor performance. These parameters govern the interplay between reaction rates and mass transfer rates and for the systematic optimization of the enzymatic microreactor an operational window approach was proposed.

The concept of segmented flow was expanded to whole-cell catalysis by utilizing biofilms as biocatalysts in the microreactor system. The development and maintenance of a stable biofilm without clogging the capillary was achieved by following a three step procedure: i) Development of a first-stage biofilm during single phase flow. ii) Introduction of air segments which leads to a significant detachment of the biofilm. iii) Development of an adapted second-stage biofilm under segmented flow conditions. Based on this concept, two reactor set-ups (aqueous-air) segmented flow biofilm membrane reactor (SFBMR) and (aqueous-air-organic) segmented flow biofilm reactor (SFBR) were developed, and their applicability were investigated for several reactions. For styrene epoxidation to (*S*)-styrene oxide oxygen availability was identified as key limiting parameter in the SFBMR, and by enhancing the air flow rates the volumetric productivity was improved by 4-fold ( $11 \text{ to } 46 \text{ g}_{\text{sty. oxid.}} \text{ L}_{\text{tube}}^{-1} \text{ day}^{-1}$ ).

In summary, this thesis shows the development of the segmented flow microreactor technology for enzyme and biofilm catalysed reactions, and emphasizes the potential of this technology for biocatalytic reactions.

## Zusammenfassung

In den vergangenen Jahren rückten Mikroreaktoren vermehrt in den Fokus des allgemeinen Interesses. Diese Systeme zeichnen sich durch eine erhöhte Reaktionsleistung unter niedrigem Energieeintrag und relativ einfache Maßstabs Vergrößerung aus. Ziel dieser Arbeit war die Entwicklung und Anwendung von Mikroreaktoren auf biokatalytische Synthesereaktionen. In diesem Zusammenhang wurde das Potenzial von diesen Reaktorsystemen sowohl für isolierte Enzyme als auch für ganze Zellen untersucht.

Aufgrund der großen Phasengrenzfläche zwischen wässriger und organischer Phase und der starken Konvektivkräfte werden isolierte Enzyme in einem (wässrig-organisch) segmentierten Durchfluss Reaktor sehr schnell inaktiviert. Durch Zugabe von Tween20 wurde der direkte Kontakt der Enzymmoleküle mit der Phasengrenzfläche verhindert. So konnten fast 100% Enzymaktivität zurückgewonnen werden, verglichen mit 45% Restaktivität ohne Stabilisator. Anhand der Synthese von 1-Heptanol mittels thermostabiler *Thermus* Alkohol Dehydrogenase (TADH) und Format Dehydrogenase (FDH) zur Kofaktorregeneration wurde die Anwendbarkeit dieser Technologie untersucht. Im segmentierten Fluss in einer 0.5 mm (i.d.) Kapillare wurde eine mittlere Produktivität von  $10.4 \text{ g}_{\text{Produkt}} \text{ L}_{\text{org}}^{-1} \text{ hr}^{-1}$  ( $90 \text{ mM h}^{-1}$ ) erreicht. Der Durchmesser der verwendeten Kapillare, die Fließgeschwindigkeit und die Enzym / Substrat Konzentrationen erwiesen sich als entscheidend für die Leistung des Systems. Diese Parameter, welche das Zusammenspiel von Massentransfer und Reaktionsrate bestimmen, wurden in einem Prozessfenster zusammengefasst, welches nun als Hilfsmittel für eine systematische Optimierung dieser Systeme zur Verfügung steht.

Das Konzept der segmentierten Durchfluss-Mikroreaktoren wurde auf die Ganzzellbiokatalyse ausgedehnt, mit einem Biofilm als Modellsystem. In einem 3-stufigen Prozess konnte ein stabiler Biofilm in den Kapillaren etabliert werden. i) Anzucht eines Primärbiofilms im wässrigen Fluss. ii) Zuschalten der Gasphase in segmentierten Fluss. Dadurch kommt es zur starken Abscherung des größten Teils der Biomasse. iii) Wachstum des adaptierten Sekundärbiofilms im segmentierten Fluss. Mit dem „Segmentierter-Fluss (wässrig / Luft) Biofilm-Membran-Reaktor“ (SFBMR) und dem „Segmentierter-Fluss (wässrig / Luft / organisch) Biofilm-Reaktor (SFBR)“ wurden zwei unterschiedliche Durchfluss-Reaktoren entwickelt. Es zeigte sich, dass die Biofilm katalysierten Biotransformationen hauptsächlich durch Sauerstoff limitiert wurden. Mit der Erhöhung des Sauerstofftransfers im SFBMR konnte eine vierfache Erhöhung der volumetrischen Produktivität (11 bis  $46 \text{ g}_{\text{Sty.oxid.}} \text{ L}^{-1} \text{ Tag}^{-1}$ ) erreicht werden. Im SFBR war es aufgrund der limitierten Verweilzeit im Reaktor nicht möglich, den Sauerstofftransfer wesentlich



zu erhöhen. Dies führte zu sehr niedrigen Umsatzraten und zeigt einen klaren Nachteil des SFBR's im Vergleich zum SFBMRs.

Zusammenfassend zeigt diese Arbeit die Entwicklung und Anwendung von segmentierten Durchfluss-Mikroreaktoren für Enzym und Biofilm katalysierte Reaktionen, und verdeutlicht das Potenzial dieser Technologie für die Biotechnologie.

## Abbreviations

$a$	Interfacial area per volume ( $\text{m}^2 \text{m}^{-3}$ )
$A_{\text{aq}}$	Aqueous phase surface area ( $\text{m}^2$ )
BEHP	Bis(2-ethylhexyl) phthalate
$C_{\text{As}}$	Substrate concentration on the surface (mM)
$C_{\text{ab}}$	Substrate concentration in the bulk liquid (mM)
$C_{\text{Ai}}$	Equilibrium substrate concentration in the aqueous phase (mM)
$C_{\text{AL}}$	Substrate concentration in the bulk aqueous phase (mM)
CDW	Cell dry weight
$d$	Diameter (mm)
$D_{\text{A}}$	Substrate diffusion coefficient ( $\text{m}^2 \text{s}^{-1}$ )
$D_{\text{Ae}}$	Effective diffusion coefficient ( $\text{m}^2 \text{s}^{-1}$ )
DCPK	Dicyclopropyl ketone
$Da_{\text{I}}$	First Damköhler number
$Da_{\text{II}}$	Second Damköhler number
$Da_{\text{app}}$	Apparent Damköhler number
$e_0$	Enzyme concentration (mM)
e.e.	Enantiomeric excess
$E_{\text{a}}$	Active form of the enzyme
$E_{\text{i}}$	Inactive form of the enzyme
$E_{\text{inact}}$	Enzyme inactivated ( $\mu\text{g mL}^{-1}$ )
$F$	Laminar friction constant
FDH	Formate dehydrogenase
For.	Formate
Fr.	Flow ratio
GC	Gas chromatography
i.d.	Inner diameter
IPTG	Isopropyl $\beta$ -D-1-thiogalactopyranoside
$k_{\text{a}}$	Rate constant for adsorption [ $\text{mL } \mu\text{g}^{-1} \text{s}^{-1}$ ]
$k_{\text{L}}$	Mass transfer coefficient ( $\text{m s}^{-1}$ )
$k_{\text{d}}$	Enzyme inactivation coefficient ( $\text{s}^{-1}$ )
$K_{\text{m}}$	Michaelis constant (mM)
$K_{\text{org/aq}}$	Substrate partition coefficient in the organic and aqueous phases
$k_{\text{cat}}$	Turnover number ( $\text{s}^{-1}$ )

$\text{Log}P_{\text{O/W}}$	Logarithm of octanol-water partition coefficient
$L_{\text{UC}}$	Segment length (mm)
$\text{NAD}^+/\text{H}$	Oxidized/reduced nicotinamide adenine dinucleotide
OD	Optical density
OTR	Oxygen transfer rate
P	Power (W)
Pe	Peclet number
PTFE	Polytetrafluoroethylene
$r_A$	Rate of reaction in the aqueous phase
$r_{A,\text{obs}}$	Observed reaction rate ( $\text{mM s}^{-1}$ )
$r_d$	Rate of enzyme inactivation ( $\text{mM s}^{-1}$ )
rxs.	Reactions
SFBMR	Segmented flow biofilm membrane reactor
SFBR	Segmented flow biofilm reactor
SFER	Segmented flow enzymatic microreactor
Sty. oxid.	Styrene oxide
STY	Space time yield ( $\text{mM h}^{-1}$ )
$S_X$	External surface area ( $\text{mm}^2$ )
$t_r$	Reaction time (min)
TADH	Thermus alcohol dehydrogenase
U	Activity unit equal to 1 $\mu\text{mol}$ product formed per minute
V	Volume (L)
$V_{\text{act.lost}}$	Loss in volumetric enzyme activity (%)
$V_{\text{aq.}}$	Particle volume ( $\text{mm}^3$ )
$V_p$	Aqueous phase volume ( $\text{m}^3$ )
$V_{\text{max}}$	Maximum reaction rate ( $\text{mM s}^{-1}$ )
$Y_{\text{so2}}$	Yield of biomass on oxygen ( $\text{mg mg}^{-1}$ )
$\tau$	Residence time (min)
$\varphi$	Phase ratio
$\mu$	Viscosity (Pa s)
$\epsilon_L$	Liquid holdup
$\epsilon_G$	Gas holdup
$\delta$	Diffusion layer thickness (mm)
$\Omega$	Observable modulus

$\Phi$	Weisz modulus
$\theta$	Fractional surface area covered by enzymes
$\Gamma$	Surface excess energy

# Chapter 1

## General Introduction

Rohan Karande, Andreas Schmid and Katja Buehler

Katja Buehler and Andreas Schmid coordinated and supervised the project and corrected the manuscript

## Introduction

Current academic and industry research is gaining pace on developing and applying novel miniaturized systems (Hessel et al. 2009). Microreactors are characterized by sub-millimetre dimensions, which enhance the surface area to volume ratios and decreases diffusion time. Such devices are gaining importance in process development as they profit from an excellent heat and mass transfer, efficient mixing, low energy input, compact size and improved safety (Ehrfeld et al. 2000; Kockmann 2006).

### 1.1 General criteria to choose a microreactor design

Reactions that necessitate high mass and/or heat transfer rates to improve the apparent reaction rates are generally considered to be well suited for microreactors (Ehrfeld et al. 2000; Renken and Kiwi-Minsker 2010). The reactants mass transfer time and the reaction time are important measures regarding the influence of chemical parameters (catalyst, solvent, temperature, etc.) or physical parameters (reactor type, stirring speed, solvent viscosity etc.) on the product yield of such reactions. Figure 1.1 compares the time scale of chemical and physical processes such as mass and heat transfer, and mixing (Renken and Kiwi-Minsker 2010). The reaction time is the *time necessary* to completely convert the reactant or substrate supplied. It is the ratio of the reactant concentration ( $s$ ) and the reaction rate ( $r$ ). As a thumb rule, the time scale for the physical processes should be one order of magnitude smaller than the reaction time to overcome mass transfer limitations. The characteristic time range for physical processes is in between  $10^{-2}$  s in conventional reactors and from  $10^{-2}$  s to  $10^{-5}$  s in microreactors. Therefore, very fast or instantaneous reactions having a time scale in the range of  $10^{-3}$  to  $10^{-5}$  s are influenced by physical parameters in microreactors.

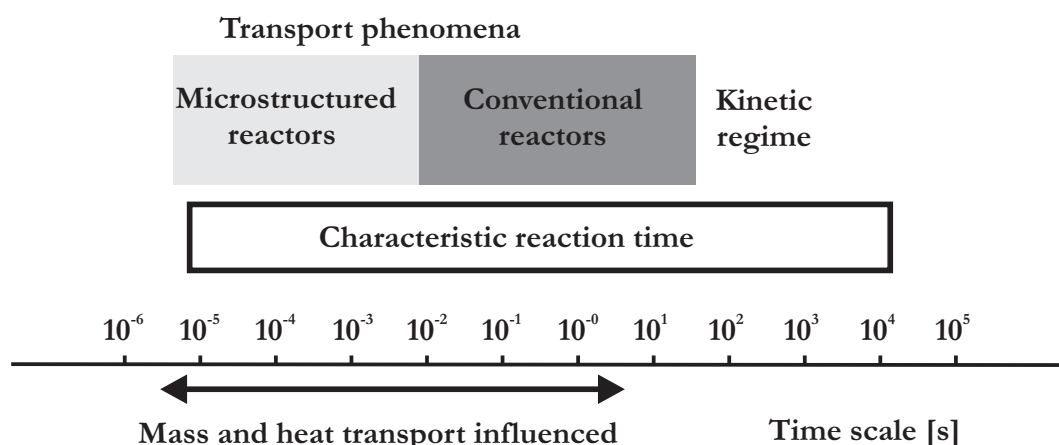


Figure 1.1: Overview of the time scale of chemical and physical processes adapted from (Renken and Kiwi-Minsker 2010).

For slow reactions, the reaction performance is dependent on the intrinsic reaction kinetics of the catalyst. Such reactions would profit least if employed in microreactors. Thus, application of biocatalytic reactions in microreactors calls for understanding the characteristic reaction and mass transfer times, which depend on the nature of the biocatalyst applied.

## 1.2 The different types of biocatalysts

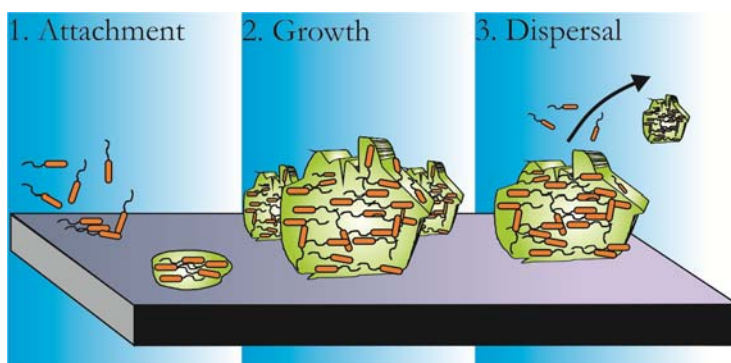
Biocatalysts perform chemical transformation of various compounds mostly in an aqueous medium, at ambient conditions (temperatures, pH) and atmospheric pressure. Enzymes form the major class of biocatalysts and are employed either in an isolated form or contained in whole cells (Table 1.1). The advantages of isolated enzymes are the higher specificity and less mass transfer resistance, but they usually require high preparation costs and recycling of expensive cofactors in case of cofactor dependent enzymes. In contrast, whole cells recycle the necessary cofactors intrinsically and enzyme stability is higher inside the cells. On the downside whole cell biocatalysis might be limited by (cell membrane) mass transfer over the cell membrane, protein production, cellular metabolism and side reactions. Whole cells can be applied as growing culture or resting cells. A brief overview of different types of biocatalysts and its advantages and disadvantages is given in Table 1.1.

**Table 1.1: Biocatalyst forms and its advantages and disadvantages (adapted and modified from (Faber 2004; Gross 2010)).**

Biocatalyst	Form	Advantages	Disadvantages
Isolated enzymes	Free enzymes	Simple work-up and no side reactions	Cofactor recycling, lower stability and expensive purification
	Immobilized enzymes	Higher stability, easy recovery, and reuse	Activity loss during immobilization, extra preparation costs and additional mass transfer resistance
Whole cells	Free cells-growing culture	Higher activities and no cofactor recycling necessary	Large amount of biomass and unwanted by-products
	Free cells-resting state	Easy work-up and fewer by-products	Lower activities and stability
	Artificially immobilized whole cells	Re-use possible and higher stability	Lower activities, substrate mass transfer limitation
	Natural immobilized whole cells- (biofilm)	Higher activities and high tolerance to toxic chemicals	Slow growth and mass transfer limitation of nutrients

Enzymes or whole cells may be immobilized to gain structural stability, high catalyst density, and to achieve multiple uses. Several methods for immobilization are known, such as crosslinking, binding to carrier particles, microencapsulation etc., and detailed description of these methods can be found in several texts and review papers (Buchholz et al. 2005; Cao. L 2005; Sheldon 2007).

A natural way of immobilization is biofilm formation. Biofilms formed by microbes have the ability to self-attach (and thus immobilize) to solid surfaces (substratum) and encase themselves in an excreted extra-polymeric matrix called EPS. Key compounds of EPS are polysaccharides, proteins, free nucleic acids, and water. It acts as a glue to hold the biofilm to its substratum and shields the organisms against various toxic substances. The development of biofilms comprises three major steps (Figure 1.2), (1) reversible attachment of the cells to the substratum, (2) formation of micro-colonies, EPS secretion and biofilm maturation, (3) steady state, an equilibrium between biofilm detached and regrowth. A schematic view of biofilm development is shown in figure 1.2 and a detailed description on each step can be found in Halan and co-workers (Halan et al. 2012).



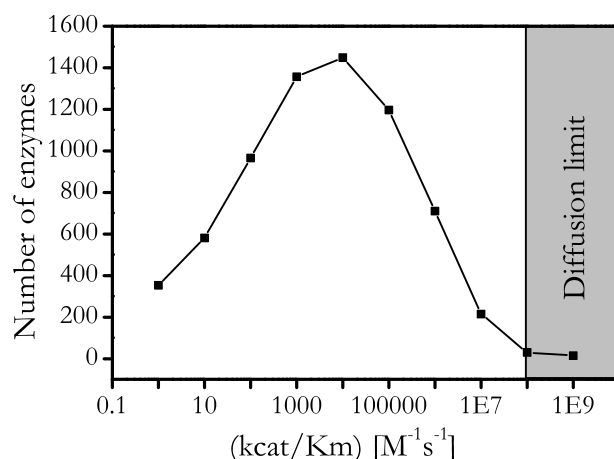
**Figure 1.2: Schematic model showing the three major biofilm development steps (1) biofilm attachment, (2) development of micro- and macrocolonies, and (3) steady-state dispersal and reproduction.**

### 1.2.1 Characteristic reaction times for free enzymes or suspended whole cells

The key to understand biological reaction rates is to examine the kinetic parameters of biocatalysts. The kinetic parameters of 6870 enzymes taken from the Brenda database ([www.brenda-enzymes.info](http://www.brenda-enzymes.info)) are plotted in Figure 1.3 as a function of  $k_{cat}/K_m$  over the number of enzymes. The turnover number  $k_{cat}/K_m$ , is the second order rate constant, and an enzyme is very efficient if its turnover number is high. In fact, 45 (0.65%) of the enzymes reported in the Brenda database perform catalysis at a turnover number of  $10^8$  to  $10^9 \text{ M}^{-1} \text{ s}^{-1}$ , which is considered to be the uppermost limit of bimolecular reactions. At these rate constants, the frequency of the collision between substrate and enzyme, and the product formation are the same. In such



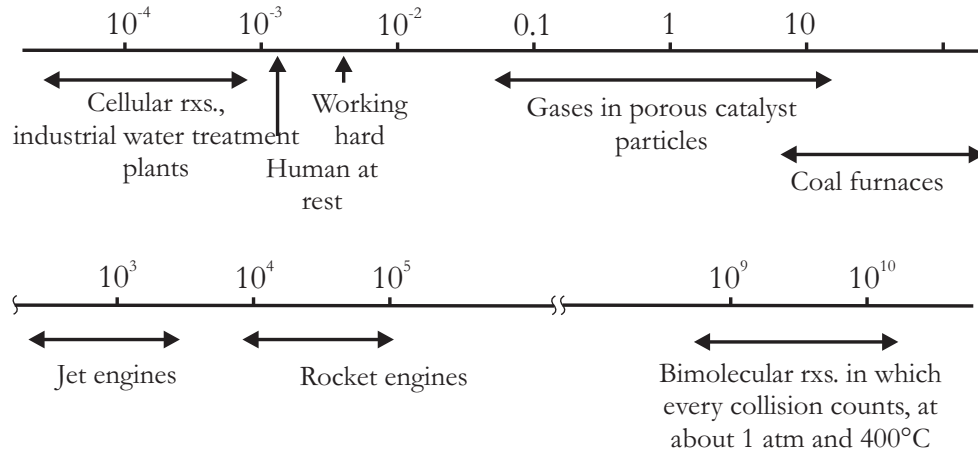
condition, every collision of substrate molecules with the catalyst leads to a product molecule. Such bimolecular reactions are diffusion controlled.



**Figure 1.3: Distribution of the second order rate constants ( $k_{\text{cat}}/K_M$ ) for enzymes.** Data taken from Brenda database ([www.brenda-enzymes.info](http://www.brenda-enzymes.info)).

The average rate constant for most of the enzymes have  $k_{\text{cat}}/K_M$  values in the range of  $10^4$  to  $10^5$   $\text{M}^{-1} \text{s}^{-1}$ . Thus, some enzymatic reactions occur very fast, while others are slow. To estimate the velocity of enzymatic reactions relative to other chemical transformations, the rate of reactions (Figure 1.4) adapted from (Levenspiel 1999) can be applied. The relative reaction rates vary from days in waste water treatment plants to few seconds in rocket engines. Interestingly, the uppermost limit is set to bimolecular reactions occurring at 1 atm and  $400^\circ\text{C}$ , where every collision of the respective reactants with the catalyst results in a product molecule. Similar is also true for the upper limit of enzymatic reactions at a turnover number of  $10^8$  to  $10^9$   $\text{M}^{-1} \text{s}^{-1}$  (see above). Furthermore, based on the moderate catalytic speed ( $k_{\text{cat}}/K_M$  in the range of  $10^4$  to  $10^5$ ) of enzymes and assuming that the substrate and enzyme concentration in the solution is 1 M, we estimated the reaction rates. Essentially, the moderate enzymatic reaction rates are in the range of  $10^4$ - $10^5$   $\text{mole m}^{-3} \text{s}^{-1}$ , which is similar to the speed of rocket engines as stated in figure 1.4. However, these reaction rates are only possible at a substrate and enzyme concentration of 1 M. In practice, the available substrate and enzyme concentrations in the aqueous phase are 100 to 1000 fold lower than this theoretical value, which severely diminishes the reaction performance. Especially, the interesting organic substrates exhibit a very low solubility (below 20 mM) in the aqueous phase. If we assume 1 mM of enzyme with the rate constant in the range of  $10^4$ - $10^5$   $\text{M}^{-1} \text{s}^{-1}$  (moderate speed) then it would take 5 to 0.5 s to completely convert 20 mM of substrate in the aqueous phase. Obviously, the addition of a second organic phase is necessary to replenish water insoluble substrate molecules. The second organic phase serves as a substrate reservoir to overcome the substrate availability limitation. In two-phase biocatalysis, the transformation of the respective molecules (rate of reaction) might severely depend on the transport of the substrate

over the phase boundary to the biocatalyst. For such a situation, volumetric mass transfer governs the reaction performance.



**Figure 1.4: Rates of reactions (moles  $\text{m}^{-3} \text{s}^{-1}$ ) adapted from (Levenspiel 1999).**

A similar situation arises, if aerobic microorganism's (suspended whole cells) are employed as biocatalysts where oxygen is a key nutrient for growth and metabolism. However, the solubility of oxygen in the aqueous phase is (approx.) 0.2 mM. Typically, the oxygen uptake rate for a microorganism such as *Azotobacter vinelandii* is  $12.5 \text{ mmol g}^{-1} \text{ h}^{-1}$  (Doran 2004). If we assume a cell concentration  $10 \text{ g L}^{-1}$  then it would take 6 s to completely consume the oxygen present in the aqueous phase. Thus, the continuous supply of air becomes obligatory in bioreactors, and the oxygen transfer rate might play a key role in the reactor performance. The oxygen mass transfer rate is a function of the volumetric mass transfer coefficient and the concentration gradient (Garcia-Ochoa and Gomez 2009). Thus, the maximum oxygen transfer rate per unit aqueous volume is given as:

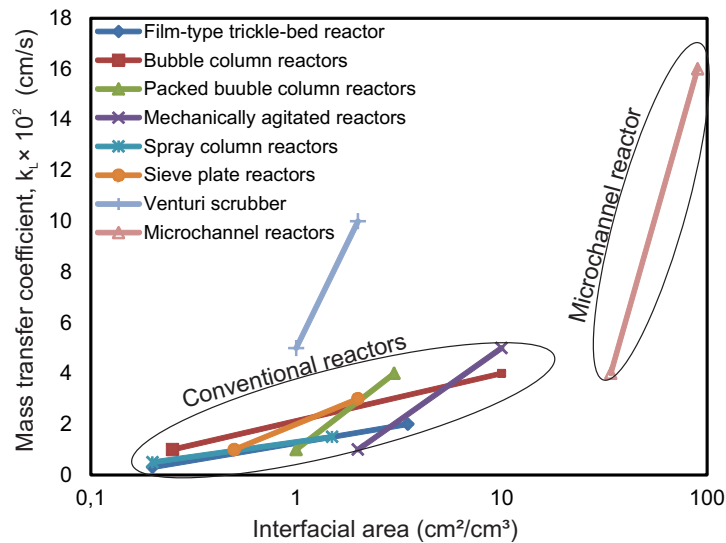
$$\text{OTR}_{\text{max}} = k_L a C_{A_i} \quad (1.1)$$

By assuming the oxygen concentration to be constant (due to the solubility limit), the maximum oxygen transfer from the gas phase to the liquid phase is characterized by the volumetric mass transfer coefficient ( $k_L a$ ). The oxygen mass transfer time is quantified by the mass transfer coefficients in the aqueous phase.

$$t_m = (k_L a)^{-1} = (k_L A_{\text{aq}} / V_{\text{aq}})^{-1} \quad (1.2)$$

where,  $A_{\text{aq}}$  is the aqueous phase surface area and  $V_{\text{aq}}$  is the aqueous phase volume. For gas-liquid reactors, the surface area to volume ratio in micro-channel reactors is reported to be in the range of 3000 to 9000  $\text{m}^2 \text{ m}^{-3}$  (Kashid et al. 2011a; Yue et al. 2007), while in conventional reactors a maximum surface area to volume ratio of 2000  $\text{m}^2 \text{ m}^{-3}$  is reached (Doraiswamy and Sharma 1984). Overall, the mass transfer coefficients ( $k_L a$ ) in microchannel reactors are several folds

higher than in conventional reactors (Figure 1.5). Thus, biological reactions that are limited by mass transfer could benefit from relatively high  $k_L a$  values in microreactors.



**Figure 1.5: Mass transfer coefficient versus interfacial area generated in various reactor types.** The data for conventional reactors are adapted from (Doraiswamy and Sharma 1984), while data for microchannel reactors are adapted from (Yue et al. 2007).

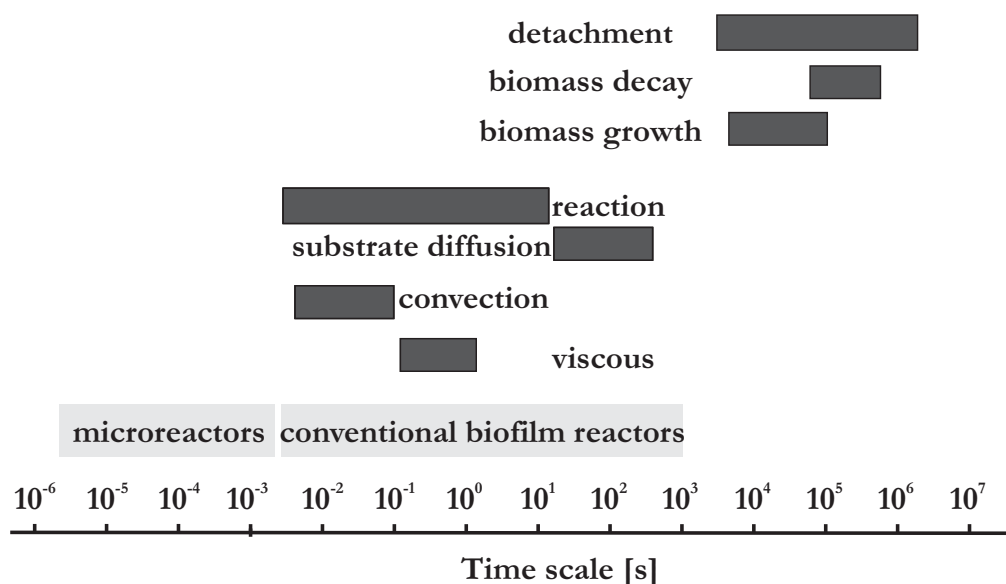
### 1.2.2 Characteristic reaction and mass transfer times for immobilized biocatalysts

Almost 40% of the reported biocatalytic processes applied on industrial scale involve immobilized biocatalysts (Liese et al. 2006). As discussed above, the biocatalyst could be immobilized either artificially (enzymes or whole cells) within solid particles or gels, or naturally (only whole cells) in a self-made polymeric material (biofilms). Based on the characteristic times scale of reaction and physical processes we would like to evaluate whether immobilized biocatalysts have the potential to be applied in microreactors.

To address this issue, we have selected biofilms as an immobilized form of biocatalyst. Biofilms are highly dynamic structures and various processes, such as biomass growth, biomass decay, detachment, reaction and multicomponent diffusion, take place during biofilm development (Picioreanu et al. 2000). These processes have completely different time scales (Figure 1.6), which makes biofilms the most complex form of immobilized biocatalysts for such an evaluation.

Biomass growth, biomass decay and detachment are slow processes that occur at a time scale of hours to days (Figure 1.6). These processes take longer time to reach a steady state but they define the biofilm volume or biocatalyst concentration. However, biofilm reactors are usually operated for longer time periods (weeks to months), and once the steady state is reached (1 to 3 days for biofilm growth and detachment to be in equilibrium) a constant biomass could be assumed in the reactor.

Multicomponent diffusion of molecules takes place from the bulk phase into the biofilm, which contains nutrients for biofilm growth and substrates for reactions. In conventional biofilm reactors, the characteristic reaction time is smaller than the substrate diffusion time into the biofilm. This means that the reaction is diffusion limited and the catalytically active biomass is performing below the possible maximum. As the characteristic reaction time for physical processes in microreactors ( $10^{-3}$  to  $10^{-5}$  s) are lower than in conventional biofilm reactors, the reactor performance could be considerably improved for biofilm reactions. However, the key bottleneck to realize such a microreactor is the development and maintenance of a stable biofilm without clogging the microchannel. This key challenge is addressed in the later part of this thesis (chapter 5 and 6). Overall, based on the concept of the characteristic time scale of biocatalytic reactions and mass transfer, the potential of microreactors could be explored for biocatalytic reactions limited by mass transfer rates.



**Figure 1.6: Characteristic times for processes occurring in biofilms.** Data adapted and modified from (Piciooreanu et al. 2000).

### 1.3 Multiphase biocatalysis: defining an operational regime by non-dimensional numbers

Several biocatalytic reactions involve multiple phases such as gas-liquid, liquid-liquid and liquid-solid phases. However, to explore these reactions in microreactors it is utmost important to understand whether the reactor performance is mass transfer limited. As described in the above section, characteristic times for mass transfer of compounds and characteristic reaction times allow an approximation possible mass transfer limitations. In chemical engineering literature, such characteristic times are typically described by non-dimensional numbers.

In the following section, non-dimensional numbers are applied to understand the operational regime (mass transfer limited or kinetically limited) for solid-liquid and liquid-liquid phase biocatalytic reactions described in the literature.

### 1.3.1 Liquid-solid biocatalysis

In heterogeneous biocatalysis, the reaction is performed in the solid particles leading to a two-step mass transfer resistance (Kasche and Kuhlmann 1980). First, the substrate needs to diffuse from the adjoining liquid bulk phase to the solid surface, which is often referred to as external mass transfer. In the second mass transfer resistance step, the substrate has to diffuse through the solid in order to reach the biocatalyst, referred to as internal mass transfer resistance.

**External mass transfer resistance:** This mass transfer resistance may occur by a liquid film surrounding the catalyst particle, which is assumed to be stagnant film based on the film theory. To assess the influence of external mass transfer resistance on the biocatalytic reaction rate, an observable modulus,  $\Omega$ , (Doran 2004) is applied:

$$\Omega = \frac{V_P}{S_X} \left( \frac{r_{A,obs}}{k_L C_{Ab}} \right) = \frac{\text{reaction rate}}{\text{external mass transfer rate}} \quad (1.3)$$

$$\Omega = \frac{\text{external diffusion time } (\tau_{\text{ext. diffusion}})}{\text{reaction time } (\tau_{\text{reaction}})} \quad (1.4)$$

Where  $V_p$  is the particle volume,  $S_x$  the external surface area,  $r_{A,obs}$  the observed reaction rate per unit volume of catalyst,  $k_L$  the liquid phase mass transfer coefficient and  $C_{Ab}$  is the substrate concentration in the bulk liquid. Equation 1.3 is further simplified by assuming that the liquid mass transfer coefficient ( $k_L$ ) is proportional to the substrate diffusivity ( $D_A$ ) and inversely proportional to the liquid film thickness ( $\delta$ ),

$$\Omega = \frac{V_P}{S_X} \left( \frac{r_{A,obs} \delta}{D_A C_{Ab}} \right) \quad (1.5)$$

The observable modulus,  $\Omega$ , is used to quantitatively illustrate the impact of external mass transfer on the biocatalytic reaction (Table 1.2). If  $\Omega$  is much smaller than 1, the substrate surface concentration is equal to the substrate bulk concentration ( $C_{As} \sim C_{Ab}$ ) and the external mass transfer is insignificant. In case of high external mass transfer resistance ( $\Omega > 1$ ), the substrate surface concentration is much lower than the substrate bulk concentration ( $C_{As} \ll C_{Ab}$ ), and the reaction rate is assumed to be restricted by the external mass transfer rate. In such cases, several strategies can be employed to lower the observable modulus such as increasing the surface area to volume ratio, decreasing the film thickness by flow velocity, decreasing the reaction rate, or by increasing substrate concentration. In the following section, several experimental examples are evaluated from the literature to determine the operation regime.

**Examples:** Horvath and coworkers covalently immobilized trypsin and urease on the inner surface of capillaries and studied the impact of substrate concentration and flow velocity on the reactor performance (Horvath and Solomon 1972). To interpret the impact of external mass transfer on the reaction performance we have estimated the observable modulus ( $\Omega$ ) for two reactor formats (Table 1.2). The estimation of  $\Omega$ , was based on the assumption of a diffusion layer thickness ( $\delta$ ) of 0.1 times capillary radius (Kerby et al. 2006) and a substrate diffusion coefficient of  $6.9 \times 10^{-6} \text{ cm}^2 \text{ s}^{-1}$ . The impact of substrate concentrations ( $C_{Ab}$ ), 1 and 10 mM, on the observable modulus ( $\Omega$ ) is stated in table 1.2. The low  $\Omega$  values in the first reactor setup suggest that the reaction is not mass transfer limited and the substrate concentration at the surface of immobilized enzyme ( $C_{As}$ ) is equal to the bulk substrate concentration ( $C_{Ab}$ ) (Table 1.2). This means that the increase in substrate concentration will not affect the reaction performance dramatically. The experimental results confirmed our predictions as slight improvement in the reaction rates from 8 to 12 mmol  $\text{s}^{-1}$  were seen with a 10-fold increase in substrate concentration (1 to 10 mM). Additionally, the reaction rate was found to be independent on the flow rate affirming no impact of external mass transfer resistance.

For the second reactor setup (Table 1.2), the high  $\Omega$  value at lower substrate concentration indicates that the system is mass transfer limited and the reaction is controlled by the substrate diffusion from the bulk phase to the surface of biocatalyst. The experimental results are in good agreement to the conclusions drawn from the observable modulus as the reaction rates were improved from 12 to 55 mmol  $\text{s}^{-1}$  by the 10-fold increase in substrate concentration (1 to 10 mM). Moreover, the reaction rates were observed to be strongly dependent on the flow rates which clearly emphasize the role of external mass transfer limitation.

Thus, the simple observable modulus is sufficient to define the operational regime where the reactor will be operated (mass transfer or kinetically limited). Once the operability is known, further steps to optimize the reactor performance can be undertaken. For example, the first reactor setup is operated in a kinetically limited regime. To maximize the reaction rate in such setups, either the enzyme loading should be increased or enzymes having higher  $k_{cat}$  values should be employed for immobilization.

In an another study, soybean peroxidase (SBP) was immobilized on a glass surface coated with poly(maleic anhydride-alt- $\alpha$ -olefin) (PMA) by Lee and co-workers (Lee et al. 2003). In this example, the amount of immobilized enzyme in the reaction was varied to study the impact of reaction rate on the reactor performance. At a  $V_{max}$  of 1.4 mM  $\text{min}^{-1}$  it would take 5.4 s to completely convert 0.13 mM of substrate. Despite the fast reaction rate, the residence time of the substrate in the microchannel was higher than 30 s, which clearly suggests that the system will

run into a substrate limitation within seconds. By loading a lower amount of enzyme on the chip the reaction rate was lowered, which enabled 80% substrate conversion. It has to be emphasized here that it is more often the applied substrate concentration rather than substrate transfer being the controlling step in such microreactor formats.

**Internal mass transfer resistance:** The second mass transfer resistance step comes into play, if the substrate has to diffuse through the solid in order to reach the biocatalyst and is also referred to as internal mass transfer resistance. Although a high biocatalyst concentration per unit volume can be attained with immobilized enzymes maximizing the volumetric productivity, diffusion obstruction may impede the overall reaction performance. Therefore, it is important to predict the inner particle mass transfer in order to identify limiting parameters. The impact of the internal mass transfer resistance on biocatalytic reactions can be estimated by the Thiele modulus. However, this necessitates a detailed kinetic study, as it is based on the true kinetic parameters like  $K_m$  and  $V_{max}$  of the catalyst. Therefore, the observable Thiele modulus also called Weisz modulus  $\Phi$ , is much more feasible and allows a quicker estimation of the internal mass transfer (Doran 2004).

$$\Phi = \left(\frac{V_p}{S_x}\right)^2 \left(\frac{r_{A,obs}}{D_{Ac}C_{As}}\right) \quad (1.6)$$

$$\Phi = \left(\frac{\text{reaction rate}}{\text{internal mass transfer}}\right) = \left(\frac{\text{internal diffusion time } (\tau_{int. diffusion})}{\text{reaction time } (\tau_{reaction})}\right) \quad (1.7)$$

where,  $r_{A,obs}$  is the observed reaction rate per unit volume of catalyst and  $D_{Ac}$  is the effective diffusion coefficient of a substrate. The internal mass transfer limitations are significant if  $\Phi$  is higher than 3 and negligible if  $\Phi$  is equal to or less than 1.

**Examples:** Heydorn and coworker studied biofilm forming *P. aureofaciens* in flow cells (Heydorn et al. 2000). The biofilm of *P. aureofaciens* was grown with various citrate concentrations as sole carbon and energy source, and the biofilm thickness was measured accordingly. We estimated the Weisz modulus for different citrate concentrations with the objective to understand the impact of internal mass transfer resistance. Therefore, the biofilm thickness was assumed to 1 mm which is the maximum depth of the cultivation device and thus upper limit to which the biofilm could be grown. Interestingly, the Weisz modulus for the different substrate concentrations was greater than 3, indicating that the internal mass transfer was significant and thus the system will be strongly citrate mass transfer limited (Table 1.3). Furthermore, the substrate penetration depth to which the internal mass transfer allows biotransformation during its conversion was extrapolated. This was done by assuming the Weisz modulus equals 1, and estimating the ratio  $(V_p/S_x)$  in the equation 1.6. This ratio  $(V_p/S_x)$  has the dimension of length (m) and is considered to be the distance necessary for a substrate to penetrate into the solid phase. In biofilms, the depth to

which the internal mass transfer allows substrate delivery (for consumption), is considered to be the “active thickness”. Our predictions show good agreement with the experimental biofilm thickness values observed after 10 days (Table 1.3). In a similar manner, the Weisz modulus and biofilm thickness have been estimated regarding oxygen transfer in gel beads with incorporated cells (Table 1.3).

In another example, Halan and coworkers studied biofilm growth in the presence of solvent (styrene) stress in a flow-cell system (Halan et al. 2011). Here, it is important to determine the penetration depth of the solvent molecules into the biofilm. Based on  $\Phi=1$  a penetration depth of 277  $\mu\text{m}$  was estimated while the experimental biofilm thickness in the flow cell was reported to be 120  $\mu\text{m}$ . As the penetration depth of styrene is higher than the biofilm thickness it can be assumed that styrene is present throughout the biofilm. Furthermore, the penetration depth of second substrate (oxygen) was estimated and it was found out to be significantly lower (144  $\mu\text{m}$ ) than that of styrene (277  $\mu\text{m}$ ), indicating oxygen to be the limiting substrate. As oxygen is key component for biofilm growth and activity, its depletion limits biofilm growth and consequently active biofilm thickness. This illustrates the important role of the simple Weisz modulus for determining the limiting substrate that governs reaction performance. Once the limiting substrate is known further strategies for its optimization such as increase in flow velocity or oxygen rich air can be applied.



**Table 1.2: Estimation of observable modulus for monolith enzyme microreactors**

Biocatalyst Reactor setups (diameter×length)	Reaction	Biocatalyst characteristics $V_{\max}$ (mM min <sup>-1</sup> ), De (cm <sup>2</sup> s <sup>-1</sup> )	Observable modulus ( $\Omega$ )		Limitations	Experimental observations	References																																
<b><u>Trypsin</u></b>																																							
Reactor 1: (0.1 cm×100 cm)	Hydrolysis of <i>N</i> - benzoyl-L-arginine ethyl ester to <i>N</i> - benzoyl-L-arginine	1.1, 6.9×10 <sup>-6</sup>	<b><u>1 mM</u></b> 0.34	<b><u>10 mM</u></b> 0.034	Kinetically limited Mass transfer/kin- etically limited	No influence of fluid flow Impact of substrate concentration and fluid flow	(Horvath and Solomon 1972)																																
Reactor 2: (0.05 cm×25 cm)		74, 6.9×10 <sup>-6</sup>	5.5	0.55				<b><u>Lipase</u></b>								Reactor: (0.05 cm×500 cm)	Hydrolysis of 4- nitrophenyl acetate to 4- nitrophenolate	60, 6.9×10 <sup>-6</sup>	<b><u>1 mM</u></b> 0.036	<b><u>5 mM</u></b> 0.18	Kinetically limited	$V_{\max}$ for immobilized and free enzyme similar to	(Costantini et al. 2010)	<b><u>Soybean peroxidase</u></b>								Reactor 1: (0.02 cm×3 cm)	Oxidation of p- cresol	1.4, 14×10 <sup>-6</sup>	<b><u>0.12 mM</u></b> 0.06	-----	Kinetically limited Kinetically limited	Complete substrate conversion 80% conversion in 2 min	(Lee et al. 2003)
<b><u>Lipase</u></b>																																							
Reactor: (0.05 cm×500 cm)	Hydrolysis of 4- nitrophenyl acetate to 4- nitrophenolate	60, 6.9×10 <sup>-6</sup>	<b><u>1 mM</u></b> 0.036	<b><u>5 mM</u></b> 0.18	Kinetically limited	$V_{\max}$ for immobilized and free enzyme similar to	(Costantini et al. 2010)																																
<b><u>Soybean peroxidase</u></b>																																							
Reactor 1: (0.02 cm×3 cm)	Oxidation of p- cresol	1.4, 14×10 <sup>-6</sup>	<b><u>0.12 mM</u></b> 0.06	-----	Kinetically limited Kinetically limited	Complete substrate conversion 80% conversion in 2 min	(Lee et al. 2003)																																
Reactor 2: (0.02 cm×3 cm)		0.94, 14×10 <sup>-6</sup>	0.04	-----																																			

### 1.3.2 Liquid-liquid biocatalysis

Liquid-liquid two-phase systems are applied for biocatalytic reactions with barely water soluble substrates and/or for reactions with substrates or products being toxic or inhibitory to the biocatalyst. The function of the organic phase is to partition the substrate and product, and thereby reducing the respective concentrations in the aqueous phase (Woodley and Lilly 1990). Additionally, it serves as a source to deliver substrate below the toxicity or inhibitory limits in order to operate the reactor at maximum catalyst activity. However, if the substrate mass transfer rate is lower than the reaction rate then the mass transfer is the limiting step. Therefore, evaluating the limiting step is necessary to work around the bottlenecks and optimize the reaction performance. Due to the hydrophobicity of the substrate, its partitioning into the aqueous phase is lower than into the organic phase. Therefore the mass transfer limitations are assumed to be more prominent in the aqueous phase. The impact of the reaction rate on the mass transfer rate is described by the second Damköhler number ( $Da_{II}$ ),

$$Da_{II} = \frac{k_{cat} e_o \varphi}{k_L a C_A} \quad (1.8)$$

where,  $\varphi$  is the phase volume ratio ( $V_{aq}/V_{org}$ ),  $k_L$  is the aqueous phase mass transfer coefficients,  $a$  is the interfacial area per volume,  $e_o$  is the enzyme concentration,  $C_A$  is the substrate concentration and  $k_{cat}$  is the turnover number. In equation 1.8, the true kinetic parameter  $k_{cat}$  is essential and therefore detailed kinetic studies are required, similar to the Thiele modulus discussed above. To make a rough estimation the apparent Damköhler number can be applied, which is determined as  $Da_{app}$ ,

$$Da_{app} = \frac{V_{app} \varphi \delta}{D_e a C_A} = \frac{\tau_{diffusion}}{\tau_{reaction}} \quad (1.9)$$

The apparent Damköhler number,  $Da_{app}$ , is used as a quantitative measure for the impact of mass transfer on the biocatalytic efficiency in liquid-liquid biocatalytic reactions (Table 1.4).

**Examples:** A study performed by Swarts et al., 2007, determined kinetic parameters in a water/n-decane two phase system on microscale and compared the kinetic parameters with the bench scale (Swarts et al. 2008). The kinetic parameters were found to be similar between the micro and the bench scale. We estimated the apparent Damköhler number to understand the impact of substrate mass transfer on the reaction rate. The very low Damköhler number value suggests that the system is kinetically limited as there is no influence of substrate molecules being transformed from the organic phase to the aqueous phase (Table 1.4). Obviously, as there is no influence of substrate molecule transfer on the reaction rate, the kinetic parameters that have been determined were found to be similar to the bench scale setups.

Overall, what lesson do we learn from applying such dimensionless numbers? In short, such dimensionless numbers gives a clear insight about the processes that could be neglected in microreactors or the ones that could benefit from microreactors.

**Table 1.3: Estimation of Weisz modulus for liquid-solid biocatalytic reactions from selected literature studies**

Reactor setup	Biocatalyst	Substrate	Parameters De (m <sup>2</sup> s <sup>-1</sup> ), S (mg L <sup>-1</sup> ), a (mm <sup>-1</sup> ) r (mg L <sup>-1</sup> s <sup>-1</sup> )	Weisz modulus ( $\Phi$ )	Estimated biofilm thickness ( $\Phi=1$ )	Experim. thickness	Remarks	References
Flow cell: 0.01 cm×0.4 cm×4 cm	<i>Pseudomonas aureofaciens</i>	Citrate	1.2 ×10 <sup>-10</sup> , 6.4, 1, 18	23148	<b>6.5 μm</b>	<b>5.81 μm</b>	The penetration depth increases with the substrate concentration	(Heydorn et al. 2000)
			1.2 ×10 <sup>-10</sup> , 21.4, 1, 18	6944	<b>12 μm</b>	<b>5.8 μm</b>		
			1.2 ×10 <sup>-10</sup> , 107, 1, 18	1388	<b>26 μm</b>	<b>24.6 μm</b>		
Immobilized cells in gels: 2 mm diameter sphere	<i>Nitrobacter agilis</i>	Oxygen	2 ×10 <sup>-9</sup> , 0.384, 3, 0.15	22	<b>210 μm</b>	<b>400 μm</b>	The penetration depth decreases with the reaction rate	(Picioreanu et al. 2000)
			2 ×10 <sup>-9</sup> , 0.384, 3, 1.5	225	<b>67 μm</b>	<b>100 μm</b>		
			2 ×10 <sup>-9</sup> , 0.384, 3, 15	2250	<b>21 μm</b>	<b>20 μm</b>		
Flow cell: 10 mm× 1 mm	<i>Pseudomonas sp.VLB120ΔC</i>	Oxygen	1.5 ×10 <sup>-9</sup> , 6, 2, 0.44	12	<b>144 μm</b>	<b>120 μm</b>	Oxygen is the limiting substrates	(Halan et al. 2011)
		Styrene	2.4 ×10 <sup>-10</sup> , 312, 2, 0.97	3	<b>277 μm</b>			

**Table 1.4: Estimation of the Damköhler number apparent for liquid-liquid biocatalytic**

Flow pattern	Reaction	Biocatalyst	Reactor setup	Biocatalyst character. V (mM h <sup>-1</sup> ), C <sub>A</sub> (mM), a (m <sup>2</sup> m <sup>-3</sup> )	Da <sub>app</sub>	Remarks	References
Parallel flow	Oxidation of cholesterol to 4-cholesten-3-one	Lipase	Wide 220 μm, depth 50 μm, length 332 μm	3, 0.1, 9090	<b>0.005</b>	Kinetically limited	(Marques et al. 2010)
Parallel flow	Esterification of 1- butanol and propionic acid to butyl propionate	Lipase	Wide 90 μm, depth 40 cm	3240, 850, 11111	<b>0.001</b>	Kinetically limited	(Swarts et al. 2008)

## 1.4 Multiphase biocatalytic microreactors

Different microreactor configurations to perform multiphase biocatalytic reactions and to ensure the advantages over conventional bioreactors are currently being investigated at academic and industrial research level. A brief overview of multiphase microreactors is given in the following sections with a summary in Table 1.5.

### 1.4.1 Packed bed microreactors

Such reactor formats are extensively applied for liquid-solid biocatalysis. In packed bed microreactors, the biocatalyst is immobilized on polymer resins, glass, magnetic beads, and other surfaces, and packed within the microspace (Schilke et al. 2010; Sotowa et al. 2005). Catalyst pellets in conventional packed bed reactors have a diameter in the range of 4-8 mm, while in packed bed microreactors these are 50  $\mu\text{m}$ , which results in a 100-fold increase of the surface area to volume ratio (Dencic et al. 2011). Several new materials have been designed at nano-scale to maximize the surface area for biocatalyst loading. For example, nanosprings made from silicon dioxide exhibit a surface area of 300  $\text{m}^2 \text{g}^{-1}$ , which is 3 fold higher than that of a standard polymeric material (Schilke et al. 2010).

The most important features of packed bed microreactors are a high enzyme loading, a high liquid-solid surface area, and good mixing, which altogether results in high reactor productivities. However, major drawbacks of this technology are high pressure drop, incorporation of beads in the microspace, and clogging of the system due to biocatalyst leaching. Further, the enzyme immobilization method should be flexible to replace enzyme without disassembling the micro-device (Bolivar et al. 2011).

### 1.4.2 Falling film microreactors

In falling film microreactors, a very thin layer of liquid flows according to the force of gravity and gas passes this layer in a co-flow or counter-flow manner. The biocatalysts is either deposited on the wall or suspended in the liquid phase. Compared to the liquid film thickness in conventional film reactors (0.5 to 3 mm), falling film microreactors can generate stable film thickness less than 0.1 mm (Karimi and Kawaji 1998). This reduces the diffusion distance corresponding to lower mass transfer resistance.

The most important aspect of this reactor setup is its compact design, with a very high specific interfacial area up to 20000  $\text{m}^2 \text{m}^{-3}$ , which is (a few) orders of magnitude higher than the interfacial area reached in conventional reactor formats (Hessel et al. 2005). In addition, the pressure drop in this system is low compared to the packed bed microreactors. Moreover, a maximum liquid throughput of 25  $\text{cm}^3 \text{min}^{-1}$  can be achieved in this device. Such falling film

microreactor devices are commercially available, easy to scale up and have the potential to become a key technology for biocatalytic reactions involving liquid-gas, solid-liquid, and solid-liquid-gas phases. However, due to high mass transfer rates and very low residence time of only a few seconds, this technology is restricted to extremely fast biocatalytic reactions. The residence time may be prolonged by an increase in channel length or descent angle.

#### 1.4.3 Monolith microreactors

In monolith microreactors, biocatalysts are immobilized on the inner surface of materials such as silicon, poly(dimethylsiloxane), fused silica and several other surfaces of tubing or channels. Several immobilization techniques including physical adsorption, covalent immobilization and cross linking have been reported to attach the biocatalyst to the microreactor surface (Chen et al. 2011; Horvath et al. 1973). Monolith reactors are extensively applied for liquid-solid biocatalytic reactions and current research is expanding their application for liquid-gas-solid biocatalytic reactions.

In this reactor configuration, the capillary or channel diameter is of utmost importance regarding the surface area to volume ratio. Decreasing the capillary diameter from 2 mm to 0.5 mm (4 fold), the surface area to volume ratio is enhanced by a factor of 8. In comparison to the packed bed formats, the pressure drop in the monolith microreactors is lower, as the passage of fluidic flow encounters less restriction (Kreutzer et al. 2005). Additionally, scale-up of monolith reactors is achieved by simply increasing the number of tubings or channels (Kreutzer et al. 2006).

#### 1.4.4 Segmented flow microreactors

Segmented flow is also known as slug flow, plug flow bubble train or Taylor flow, refer to a flow pattern in which alternate immiscible segments are flowing through a capillary channel (Kashid and Agar 2007; Tice et al. 2003). The phase with high affinity to the capillary wall establishes a continuous phase while the second immiscible phase cuts the continuous phase and develops an alternate segmented type of flow (Harries et al. 2003). Due to large surface area of the segments, interfacial forces are very dominant in this type of flow pattern. The shearing motion due to the flow and wall generates recirculation or vortex motions which enhance mixing within the segments. The mass transfer between the segments occurs by diffusion. A high mass transfer rate is achieved within such flow patterns compared to the parallel flow because of the large surface area to volume ratio and the good mixing rate within the segments (Harries et al. 2003). These reactor formats are suited for liquid-liquid, gas-liquid, or gas-liquid-solid biocatalytic reactions. However, inactivation of soluble enzyme due to high shear stress and interfacial area between aqueous and *e.g.*, organic phase might result into lower reaction performance (Marques and Fernandes 2011).

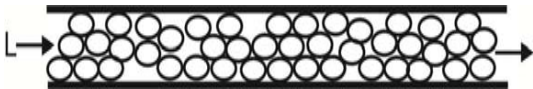
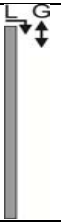

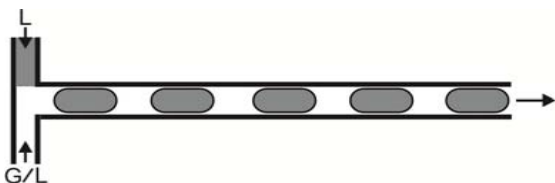
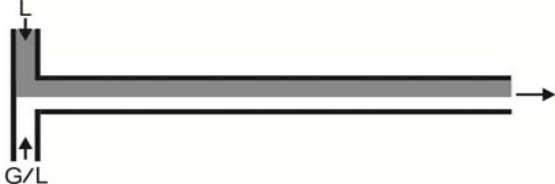
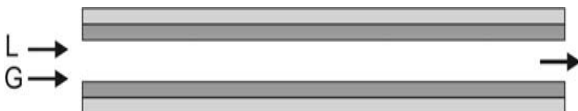
#### 1.4.5 Co-flow microreactors

In co-flow patterns, the two immiscible phases run in parallel streams alongside one another. This type of flow is generated when the ratio of the flow rates for the wetting phase to the non-wetting phase is very small (Marques and Fernandes 2011). These reactor formats are applied for liquid-liquid and liquid-gas biocatalytic reactions. In this flow pattern, mass transfer occurs through diffusion at the interface which is along the axial direction of the channel. One of the important advantages of the co-flow pattern is the easy downstream separation of the phases based on the affinity of the phases towards the material (Marques and Fernandes 2011). Additionally, due to low shear stress the enzyme inactivation in such fluidic reactors was observed to be lower as compared to the segmented flow type (Marques and Fernandes 2011).

#### 1.4.6 Membrane microreactors

In membrane microreactors, the substrates and products are separated from the enzyme by a membrane barrier (Table 1.5), thereby enhancing the rates of product-inhibited or thermodynamically limited reactions (Machsun et al. 2010). Biocatalysts, including both isolated enzymes and whole cells can be stabilized by immobilization on the membrane by physical adsorption, ionic binding, covalent binding, gelification, or by entrapment (Li et al. 2008; Machsun et al. 2010). In addition, suspended biocatalyst can also be used in this type of microreactors. Size of the membrane matrix play an important role on the reactor performance as it affects the diffusion length. Membrane microreactors are applied for liquid-solid, liquid-liquid, or liquid-gas-solid phases.

**Table 1.5: Microreactor types applied for multiphasic biocatalytic reactions**

Reactors	Reactor type	Phases	Advantages	Limitations	References
Packed bed microreactor		L-S G-L-S	High liquid-solid surface High enzyme loading Easy operation	- High pressure drop - Flow maldistribution	(Schilke et al. 2010; Sotowa et al. 2005)
Falling film microreactor		G-L L-S G-L-S	High liquid-gas surface area Low pressure drop	- Very low residence time	(Al-Rawashdeh et al. 2012; Dabir et al. 1996; Vankayala et al. 2007)
Monolith microreactor		L-S G-L-S	Low pressure drop Less transport limitation	- Specific liquid-solid surface area - Catalyst immobilization	(Chen et al. 2011; Honda et al. 2006; Horvath and Solomon 1972)
Segmented flow microreactor		L-L G-L-S L-L-G-S	High liquid-gas or liquid-liquid surface area Low pressure drop	- Specific liquid-solid surface area - Limited range of flow rates - Interfacial inactivation of enzymes	(Karande et al. 2011; Martin et al. 2003; Mohr et al. 2010; Voloshin et al. 2005)
Co-flow microreactor		L-L	Mass transfer by diffusion Low pressure drop Easy phase separation	- Limited range of flow rates	(Marques et al. 2010; Maruyama et al. 2003; Swarts et al. 2010)
Membrane reactor		S-L G-L-S	Easy phase separation	- High cost - Enzyme adsorption and interfacial inactivation	(Gross et al. 2007; Gross et al. 2010; Machsun et al. 2010)

Abbreviations: L liquid phase, S solid phase and G gas phase



## 1.5 Concluding remarks

From the characteristic time scale of mass transfer and biocatalytic reactions, it seems that there are several biocatalytic reactions that could benefit from microreactors. Interestingly, there are different concepts of integrating biocatalytic reactions into fluidic microreactors (section 1.4), and the selection of an ideal microreactor configuration depends on several factors (section 1.2). First, the biological parameters such as cell growth, enzyme kinetics, and stability under technical conditions need to be well understood. Second, the physical parameters such as phase properties and ratios, flow rate (residence time), and the mechanism of transport between the phases, and its impact on the reactor performance needs to be explored. In order to maximize the product yield in the microreactor, the biological parameters need to be combined with the physical parameters. Indeed, the accurate tuning of these parameters to maximize the reactor performance might even lead to innovative microreactor design concepts.

## 1.6 Scope of the thesis

The primary goal of this thesis was the development and application of multiphasic microreactors for biocatalytic reactions. In this context, several questions regarding biological and technical challenges are addressed.

In **chapter 2**, we investigated isolated enzyme stability in aqueous-organic segmented flow capillary systems applying thermostable alcohol dehydrogenase (TADH) as biocatalyst. Several possibilities to retain maximum enzyme activity in the liquid-liquid segmented flow have been studied and are presented in **chapter 3**. A simple, fast and cost effective method was selected to retain maximum enzyme activity in the aforementioned setup.

**Chapter 4** explores the potential of segmented flow microreactors for isolated enzyme based catalysis. The impacts of important biological, physical and technical parameters on the reactor performance are addressed. Furthermore, all key parameters governing reaction performance are summarized in an operational window for an easy assessment of the various system constraints.

The concept of multiphase segmented flow systems was expanded to whole cell catalysis by utilizing biofilms as biocatalysts in the microreactor system (**chapter 5 and 6**). A method for the development and maintenance of stable biofilm growth under high fluidic stress due to segmented flow was established. Aqueous-air segmented flow biofilm membrane reactors (SFBMR) as well as an aqueous-air-organic segmented flow biofilm reactor (SFBR) were developed. These designs integrated the characteristics of catalytic biofilms with the advantages of segmented flow and microreactors. Furthermore, several different reactions were investigated to check the adaptability of these systems.

Finally, **chapter 7** concludes the overall work performed in the thesis with a broader perspective.

## Chapter 2

### Evaluating Enzyme Stability in an Aqueous/Organic Segmented Flow System

Rohan Karande, Andreas Schmid and Katja Buehler

Katja Buehler and Andreas Schmid coordinated and supervised the project and corrected the manuscript

Published in parts in Langmuir, 2010, 26 (11), 9152-9159.

## 2.1 Summary

Multiphase flow microreactors benefit from rapid mixing and high mass transfer rates, yet their application in biocatalysis is very often limited due to the fast inactivation of isolated enzymes. In this study, an alcohol dehydrogenase from *Thermus* species was used to study enzyme stability in segmented flow microsystems. Enzyme inactivation during segmented flow is due to the large interfacial area between aqueous and organic phase. High Peclet number points to strong convective forces within the segments which lead to rapid inactivation of the enzyme. Theoretical models were used to compare protein adsorption kinetics to the interface in the segmented flow microreactor and drop tensiometry experiments. Based on the experimental observations and the investigation of the dynamic surface tension, a three step enzyme inactivation mechanism was proposed for isolated enzymes in such microreactors. Overall, strong inactivation of enzyme in segmented flow limits the applicability of this system and an approach to stabilize enzyme activity is essential.

## 2.2 Introduction

During the past decades, industrial and academic research focused on discovering new enzymatic reactions for chemical synthesis (Schmid et al. 2001). Although a number of enzymatic reactions are exploited at industrial level, the biocatalytic performance is often limited by the insufficient solubility of the substrate and/or inactivation of the enzymes. One possibility to overcome this barrier is the application of an immiscible two liquid phase system (Woodley and Lilly 1990). It involves an organic phase, which acts as substrate reservoir and product sink, whereas an aqueous phase contains the biocatalyst. The two liquid phase concept is usually applied in conventional batch or semi-batch systems (Cremonesi et al. 1975; Neuhauser et al. 1998). These are rather flexible in adapting to the necessary reaction conditions and may be used for multipurpose processes. However, mass transfer between the two phases, especially when considering scale up, is critical in such setups (Panke et al. 2002). Intense mixing of the two liquid phases is essential, but the resulting emulsion requires additional separation efforts in downstream processing (Baldascini and Janssen 2005; Colombie et al. 2001). This requires a high energy input, which is often neglected when working on a laboratory scale, but needs to be considered on a technical scale (Panke et al. 2002).

These challenges could be surmounted by utilizing continuous drop flow in a microsystem (Burns and Ramshaw 2002; Dumann et al. 2003). Drop flow is formed by contacting two immiscible phases using a T or Y shaped connector in a capillary tubing. It forms a replica of a moving train with each single phase compartment linked to the second phase. Liquid-liquid drop flow in a microreactor has several synonyms, such as plug flow (Tice et al. 2003), slug flow (Kashid and Agar 2007) and segmented flow (Nord et al. 1987). Johansson and co-workers have used the concept of liquid-liquid segmented flow to extract chemical compounds from different phases (Johansson et al. 1980). Later, Kinkel and Tomlinson developed a flow splitter to separate the segmented flow based on the wetting properties of fluids with the solid (Kinkel and Tomlinson 1980); hence no additional efforts to separate the phases are required. In a recent publication (Kashid et al. 2007), it has been shown that the mass transfer coefficients in a segmented flow microreactor are much higher as compared to conventional extraction systems. Thus, liquid-liquid segmented flow microreactor is an attractive tool to perform multiphase enzymatic syntheses and to overcome issues concerned with low substrate mass transfer, high energy input and downstream separation of phases.

Reducing the dimensions of the reaction compartment in bioprocesses from meters to millimeters enlarges the surface to volume ratio (Janasek et al. 2006). From the context of enzyme based catalysis, this typically would enhance the contact of the enzyme to the interfacial

area, resulting in a loss of its structural integrity (Ross et al. 2000; Tanaka et al. 2001). Enzyme inactivation in liquid-liquid bubble column systems was found to be proportional to the interfacial area (Ghatorae et al. 1994a). For liquid-liquid segmented flow microreactors, the interfacial area was found to be 2 to 3 times higher than in stirred tank systems (Kashid et al. 2007). Thus, it is crucial to investigate enzyme stability under the liquid-liquid segmented flow conditions to explore such reactor formats for biocatalysis. In this context, the influence of enzyme concentration, segment length, fluid flow velocity and capillary diameter on the activity of the applied enzyme was evaluated. Thermophilic alcohol dehydrogenase (TADH) from *Thermus* sp. ATN1, recombinantly synthesized in *Escherichia coli* BL21 (DE3), was used as a model enzyme in this set-up because of its broad substrate spectrum and its capability to produce chiral alcohols via asymmetric hydrogenation of ketones (Höllrigl et al. 2008).

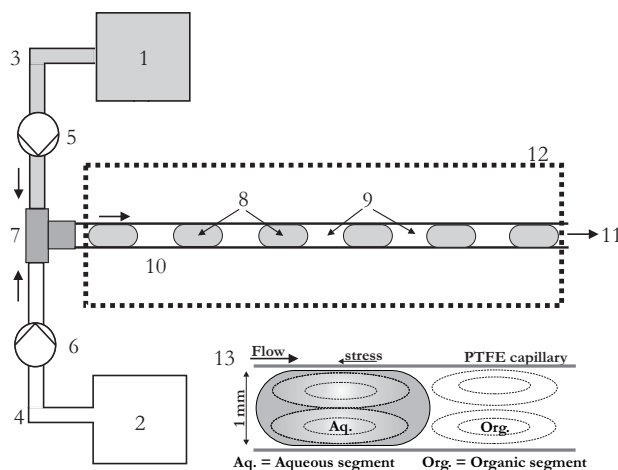
## 2.3 Materials and methods

### 2.3.1 Chemicals

All chemicals were purchased either from Sigma-Aldrich (Steinheim, Germany) or Carl Roth GmbH (Karlsruhe, Germany), unless indicated otherwise. Chemicals used in tensiometry experiments were Bis-Tris ( $C_8H_{19}NO_5$ , Assay 99% purity) from Fluka, Hexadecane ( $C_{16}H_{34}$ , minimum 99% purity) was from Sigma-Aldrich (Steinheim, Germany). All chemicals were used without further purification. Seralpur Pro 90 CN (Seral, Ransbach-Baumbach, Germany) filtered water was used to prepare all aqueous solutions. Buffer composition in all experiments was 100 mM Bis-Tris, pH 6.5 at 55°C, unless stated otherwise.

### 2.3.2 Liquid-liquid segmented flow setup

The setup of the liquid-liquid segmented flow reactor is shown in Figure 2.1. Aqueous and organic liquid was pumped separately by using a two-channel peristaltic pump (Ismatec REGLO, Glattbrugg, Switzerland) fitted with 0.7 mm inner diameter solvent resistant pump tubing (Ismatec Tygon MHL, Glattbrugg, Switzerland). Segmented flow was achieved through a 1 mm inner diameter T-piece connector (Roland Vetter RTA-TB6, Ammerbuch, Germany), and introduced into 1 mm or 2.15 mm inner diameter PTFE tubing (VICI, MACHEREY-NAGEL, Dueren, Germany). All segmented flow experiments were conducted at 55°C.



**Figure 2.1: Schematic view of the liquid-liquid segmented flow setup.** 1: aqueous phase reservoir; 2: organic phase reservoir; 3, 4: solvent resistant tubing; 5, 6: two channel peristaltic pump; 7: T shaped mixer; 8: aqueous phase segment; 9: organic phase segment; 10: 1 mm or 2.15 mm inner diameter PTFE capillary; 11: samples collected for offline analysis; 12: Thermo-bath to maintain temperature; 13: Magnified sketch of segments showing internal circulations generated within a segment (adapted from Kashid et al. 2007). The stress applied by the solid wall on the moving segments creates internal circulations, thus increasing convective forces within each segment.

The segment length was dependent on the inlet flow rates of both phases and was controlled by using the flow ratio  $Fr$  ( $Fr = v_a/v_o$ , where  $v_a$  is the aqueous phase flow rate and  $v_o$  is the organic phase flow rate). For 1 mm inner diameter PTFE capillary, at equal inlet flow rates, the flow ratio

was equal to 1 ( $Fr=1$ ) and the aqueous segment length was  $\sim 3$  mm. By varying the flow ratio from 0.3 to 3.33, the aqueous segment lengths were varied from  $\sim 1$  mm to  $\sim 7$  mm. The residence time of the segments was controlled either by varying the flow rates at a constant flow ratio or by changing the capillary length. TADH inactivation in the segmented flow was determined from the difference in TADH activity before and after passing through the reactor using a UV spectrophotometer, unless stated otherwise.

### 2.3.3 Drop tensiometry experiments

The pendant drop technique was used to measure the dynamic interfacial tension between the hexadecane-buffer system at room temperature, based on the shape of a gravity-distorted liquid drop, using a video-based contact angle meter (OCA15) manufactured by DataPhysics Instruments (Filderstadt, Germany).

A syringe was filled with the aqueous solution containing different amounts of TADH and fitted to the dosing unit. The height of the syringe was adjusted to dip the needle into a cuvette containing hexadecane, while the camera was focused on its tip. By applying pressure to the syringe an aqueous droplet of (approx.) 20  $\mu\text{L}$  was formed inside the hexadecane. Simultaneously, sequential drop images were obtained at specific time intervals. From the Young-Laplace equation, the droplet profile was fitted by the instrument to determine the interfacial tension. The surface pressure is defined as the difference between the interfacial tension of the hexadecane-buffer system without TADH and the hexadecane-buffer system in the presence of TADH. The interfacial tension between Hexadecane and Bis-Tris buffer was 42-40  $\text{mN m}^{-1}$  and was stable over time.

### 2.3.4 Preparation of TADH

*E. coli* BL21 (DE3) pLysS pASZ2 cultivated in a 3 L conical flask with baffles using 300 mL of Terrific Broth (Sambrook and Russell 2001) as medium supplemented with ampicillin (100  $\mu\text{g mL}^{-1}$ ) and chloramphenicol (20  $\mu\text{g mL}^{-1}$ ) to express TADH gene. After reaching an  $\text{OD}_{450}$  of 4 - 4.5, enzyme production was induced by adding 0.5 mM IPTG and the cells were cultivated for another 6 hours. Subsequently cells were harvested by centrifugation at 4618 $\times$ g, 4°C for 20 minutes in a Sorvall RC-5B centrifuge (Thermo Electron Corporation, Langensfeld, Germany). Enzyme purification was done according to (Höllrigl et al. 2008), reaching a final purity of 90 to 95% (no contaminating activities were found) and stored at -20°C.

### 2.3.5 Spectrophotometric determination of TADH activity

TADH activity was measured by UV-Vis absorption at 340 nm using a Cary 300 Bio UV-VIS spectrophotometer (Darmstadt, Germany). The assay mixture contained 160 mM 3-



methylcyclohexanone and 0.2 mM NADH in 100 mM Bis-Tris to a total volume of 200  $\mu$ L, pH 6.5 at 55°C. The reaction mixture was thermostated at 55°C and started by the addition of TADH. The decrease in absorbance at 340 nm was monitored for 60 seconds and enzyme activities were calculated using a specific absorption coefficient of  $\epsilon = 6220 \text{ M}^{-1} \text{ cm}^{-1}$  for NADH at 340 nm. 1 unit of enzyme activity was defined as 1  $\mu$ mole of NADH consumed per minute.

### 2.3.6 Gas chromatography analysis

From the substrate and product measurements, 0.5 mL of reaction solutions were extracted with 1 mL of ether and quantified by gas chromatography (Focus GC, Thermo Electron Corporation, Dreieich, Germany) using a chiral RT- $\beta$ Dex-sm column (30 m $\times$ 0.25 mm $\times$ 0.25  $\mu$ m Restek GmbH, Bad Homburg, Germany) column according to the method reported by Höllrigl et al., 2007.

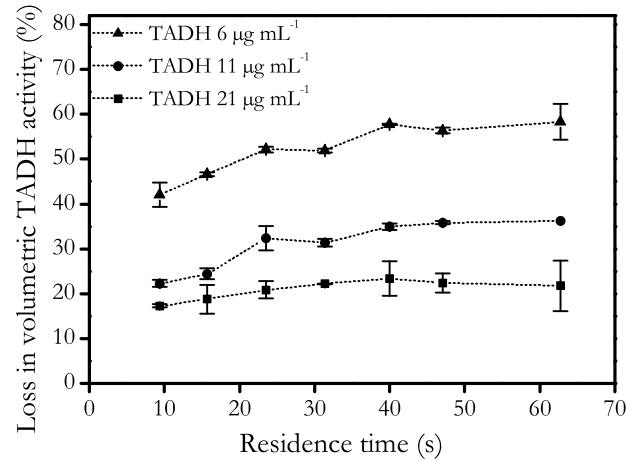
### 2.3.7 Protein quantification

Protein concentration was measured by the method given by Bradford (Bradford 1976), using the quick start Bradford dye (Bio-Rad, Munich, Germany), with a standard curve prepared using bovine serum albumin.

## 2.4 Results

### 2.4.1 Inactivation of TADH in a hexadecane-buffer segmented flow microreactor

Höllrigl and co-workers reported that organic solvents have a detrimental effect on TADH activity in a two-phase batch system (Höllrigl et al. 2008). In this context, the amount of enzyme activity lost in an aqueous-organic segmented flow microreactor was quantified as a function of TADH concentrations, segment length and capillary diameter at varying residence time.



**Figure 2.2: Influence of enzyme concentration on TADH activity in the liquid-liquid segmented flow reactor.** The flow rates were adjusted from 0.075 to 1 mL/min in a 200 mm long, 1 mm inner diameter capillary, at a constant flow ratio of 1 ( $Fr=1$ ), to achieve the respective residence time. TADH concentration in the different experiments is indicated in the graph.

The loss in TADH volumetric activity was inversely dependent on the applied initial enzyme concentration, with a rapid increase for first 20 to 40 seconds (Figure 2.2). The amount of TADH inactivated in a time period of 60 seconds was calculated by using equation 2.1,

$$E_{inact.} = E_o \times V_{act.loss} \quad (2.1)$$

Here,  $E_{inact.}$  [ $\mu\text{g mL}^{-1}$ ] is the amount TADH inactivated,  $E_o$  [ $\mu\text{g mL}^{-1}$ ] the initial TADH concentration and  $V_{act.loss}$  [%] is the loss in volumetric activity. Interestingly, the absolute amount of TADH losing its activity was always in the range of 3.4 - 3.6  $\mu\text{g mL}^{-1}$ . Since the experiment was performed at equal inlet flow rates of aqueous to organic phase ( $Fr=1$ ), the interfacial area between the adjacent segments remained constant. From these data it may be concluded that TADH inactivation might occur from the complete coverage of interfacial area by the enzyme.

Noting that a similar amount of TADH was inactivated due to the constant interfacial area, the following experiment was focused on varying the interfacial area between the segments. By changing the aqueous segment length from 1 mm to 7 mm, the interfacial surface area to volume ratio was varied from  $\sim 1.7$  to  $1.1 \text{ mm}^{-1}$ . If the loss in TADH activity is due to the constant liquid-liquid interfacial area, the maximum loss in TADH activity should be seen at a lower segmented

length, because of the resulting large interfacial area to volume ratio. However, results were in contrast to our prediction and maximal loss in TADH activity was seen in the longer segments (Table 2.1). These results clearly indicate that the surface area to volume ratio alone cannot be the only reason for TADH inactivation.

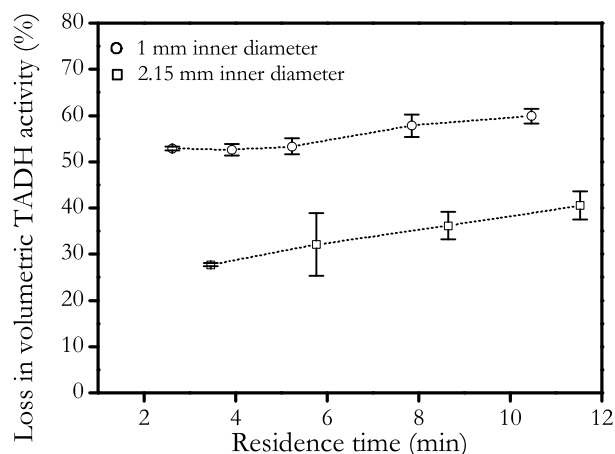
**Table 2.1: Loss in volumetric TADH activity at varying segment length and time**

Aqueous flow (mL/min)	Organic flow (mL/min)	Flow ratio (Fr)	Residence time (min)	Aqueous segment (mm)	$Pe_{aq} \times 10^3$	Loss in vol. TADH act. (%)
0.50	0.15	3.33	2.5	7	1480	81
0.32	0.32	1.00	2.5	3	270	47
0.21	0.43	0.50	2.5	1	130	46
0.17	0.05	3.33	8.0	7	510	56
0.11	0.11	1.00	8.0	3	90	51
0.07	0.15	0.50	8.0	1	40	47

Further elucidation of these results was made by calculating the Peclet number  $Pe = UL/D$ , where U, L and D represent flow velocity, segmented length and diffusion coefficient, respectively. The Peclet number is a good indicator to determine whether diffusion or convective transport is dominating in a system (Baret et al. 2009). If the Peclet number is larger than 1, transport occurs mainly by convection, while at a Peclet number smaller than 1 it will be vice-versa. To determine the Peclet number, the flow velocity and the segment size of the aqueous phase were measured while protein diffusion coefficient was assumed to be  $5 \times 10^{-7} \text{ cm}^2 \text{ s}^{-1}$  (Young et al. 1980). The maximum loss in TADH activity was seen in segments of 7 mm (length) at a residence time of 2.5 min. As indicated by the corresponding high Peclet number (Table 2.1), this may be attributed to the very high convective force within the segment. Increase in the residence time to 8 min was achieved at the expense of flow velocity, thus decreasing the Peclet number and resulting in a lower convective force and a more stable enzyme. The same explanation holds for the reduced loss in TADH activity for 3 and 1 mm segment lengths compared to 7 mm segment length. Thus it could be concluded that above a certain Peclet number the convective forces within the segmented flow is responsible for the increase in TADH inactivation, while below this value the residence time itself has a high influence on TADH inactivation.

Next, the influence of the capillary inner diameter on TADH activity was investigated in the segmented flow microreactor. According to Nord et al., and Kashid et al., a decrease in the capillary inner diameter increased mass transfer rates due to the enhanced convective transport within the segments (Kashid et al. 2007; Nord and Karlberg 1984). In our case, this would mean that the increase in capillary diameter should reduce the loss in enzyme activity. For comparison of TADH activity at a constant residence time, the length of 1 mm inner diameter capillary was doubled to that of 2.15 mm inner capillary diameter. Increasing the capillary inner diameter from

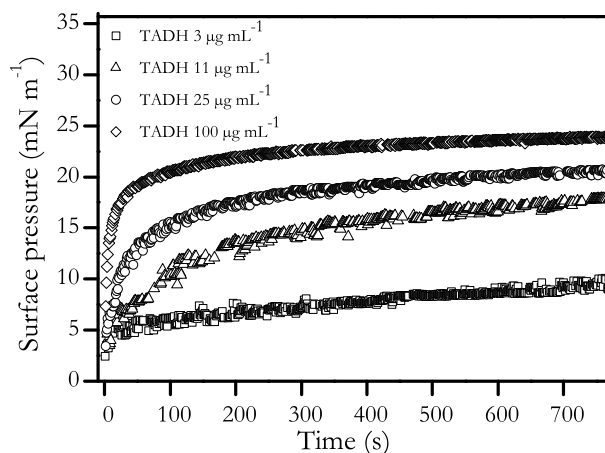
1 mm to 2.15 mm had a beneficial effect on TADH activity and the loss in volumetric TADH activity was reduced by 20 % (Figure 2.3).



**Figure 2.3: Influence of capillary inner diameters on TADH activity.** The flow rates were adjusted from 0.075 mL/min to 0.5 mL/min, at a constant flow ratio of 1 ( $Fr=1$ ) to achieve the respective residence time in the 2000 mm long, 1 mm inner diameter capillary and in the 1000 mm long, 2.1 mm inner capillary, respectively. 100 % volumetric TADH activity corresponds to 0.5 U/mL.

#### 2.4.2 Drop tensiometry to examine enzyme adsorption

To investigate TADH adsorption to the liquid-liquid interface, drop tensiometry experiments were performed. Tensiometry is a simple and useful tool to study adsorption phenomena to aqueous-organic or aqueous-air interfaces, and to determine the adsorption isotherms based on the final equilibrium values (Baret et al. 2009).



**Figure 2.4: Influence of TADH concentration on the dynamic surface tension at the hexadecane-buffer interface** (100 mM Bis-Tris pH 6.5 at 55°C).

In this work, the rates of enzyme adsorption on the aqueous-organic interface were determined by using dynamic surface pressure. TADH concentration had an impact on the interface, which is seen from the correlation of increasing dynamic surface pressure and TADH concentration

(Figure 2.4). This demonstrates that TADH is being adsorbed to the liquid-liquid interface, with the adsorption kinetics becoming faster with increasing TADH concentration.

### 2.4.3 Theoretical approach to predict TADH adsorption in drop tensiometry and within segmented flow

In the segmented flow microreactor, the loss of enzyme activity is influenced by the convective transport generated within the aqueous segments (Table 2.1), whereas, in the drop tensiometry experiments such effects could be excluded. To understand and compare the adsorption kinetics within the segmented flow microreactor and the tensiometry experiments, a theoretical approach to determine the rate constant for adsorption was developed. It is based on the simple theory of the Langmuir adsorption (Roach et al. 2005; Siegel et al. 1997). According to the Langmuir model, the rate of protein adsorption is proportional to its bulk concentration and to the available surface area. The equation is expressed as follows,

$$\frac{d\theta}{dt} = k_a c (1 - \theta_t) \quad (2.2)$$

Where,  $k_a$  [ $\text{mL } \mu\text{g}^{-1} \text{ s}^{-1}$ ] is the rate constant for adsorption,  $c$  [ $\mu\text{g mL}^{-1}$ ] is the bulk protein concentration and  $\theta$  is the fractional surface area covered by the proteins. Integrating and rearranging the above equation to resolve fractional surface coverage  $\theta$  is given as,

$$\theta_t = 1 - \exp(-k_a c t) \quad (2.3)$$

Equations 2.2 and 2.3 have been derived under the assumptions that protein adsorption is irreversible and that the solution contains excess amount of protein compared to the amount on surface.

### 2.4.4 TADH adsorption within segmented flow

To develop a relation between the loss in TADH activity (obtained experimentally, Figure 2.2) to the adsorption (Equation 2.3), it is assumed that the entire interfacial adsorbed enzyme loses its activity. Based on the Equation 2.1, the amount of TADH being inactivated is in the range of 3.4 to 3.6  $\mu\text{g mL}^{-1}$ , which correlates to the interfacial surface concentration of 2-3  $\text{mg}_{\text{Enzyme}} \text{ m}^{-2}$ . This surface concentration was sufficient to cover the entire interface area with a packed monolayer of enzyme (Baldascini and Janssen 2005; Beverung et al. 1999), corresponding to complete surface coverage  $\theta=1$ . Therefore, the fractional surface coverage ( $\theta$ ) is considered to be the ratio between TADH inactivated at time  $t$  to the maximum amount of TADH being inactivated.

$$\theta_t = \frac{E_{\text{inact.}}(t)}{E_{\text{inact. max}}} = 1 - \exp(-k_a c t) \quad (2.4)$$

Equation 2.4 was obtained by using several approximations: first a simple Langmuir model for TADH adsorption and second by correlating the amount of TADH being inactivated to the

amount adsorbed. The rate constant of adsorption  $k_a$  was adjusted to the experimental results to obtain an adequate fit according to the Equation 2.4. The obtained fits were in good agreement to the experimental values at  $k_a = 8 \times 10^{-3} \text{ mL } \mu\text{g}^{-1} \text{ s}^{-1}$  and  $k_a = 7 \times 10^{-3} \text{ mL } \mu\text{g}^{-1} \text{ s}^{-1}$  for  $c = 11 \text{ } \mu\text{g mL}^{-1}$  and  $c = 21 \text{ } \mu\text{g mL}^{-1}$ , respectively (Figure 2.5A and Table 2.2).

**Table 2.2: Comparison of rate constants for enzyme adsorption**

TADH <sup>a</sup> ( $\mu\text{g mL}^{-1}$ )	$k_a$ in drop tensiometry <sup>a</sup> [ $\text{mL } \mu\text{g}^{-1} \text{ s}^{-1}$ ]	TADH <sup>a</sup> ( $\mu\text{g mL}^{-1}$ )	$k_a$ in segmented flow <sup>a</sup> [ $\text{mL } \mu\text{g}^{-1} \text{ s}^{-1}$ ]	Fibrinogen <sup>b</sup> ( $\mu\text{g mL}^{-1}$ )	$k_a^b$ [ $\text{mL } \mu\text{g}^{-1} \text{ s}^{-1}$ ]
11	$6 \times 10^{-4}$	11	$8 \times 10^{-3}$	14	$3.66 \times 10^{-3}$
25	$5.5 \times 10^{-4}$	21	$7 \times 10^{-3}$	28	$2.60 \times 10^{-3}$

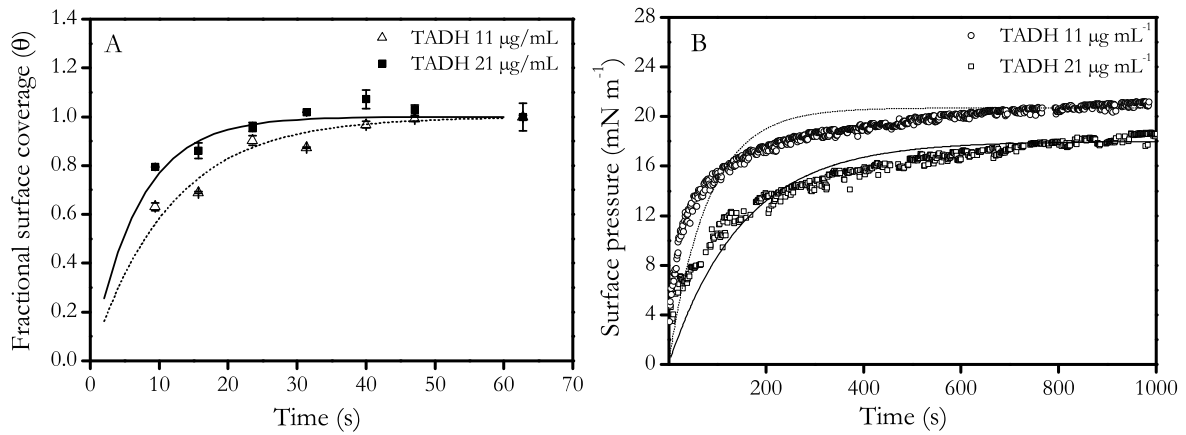
**a**-this work, obtained from Figure 2.5. **b**-adsorption of fibrinogen to a methyl-terminated alkanethiol self-assembled monolayer (SAM) from (Siegel et al. 1997).

#### 2.4.5 TADH adsorption in drop tensiometry

In order to relate surface pressure at time  $t$  to the fractional surface coverage (Equation 2.3), Equation 2.5 was applied.

$$\Pi(t) = \Pi_{\text{max}} \theta_t \quad (2.5)$$

When  $\theta_t = 0$ , surface pressure is equal to zero, it means that there is no effect of solute or protein on the interface. At  $\theta_t = 1$ , the surface area is completely covered by the solute or protein and surface pressure at time  $t$  is maximal.



**Figure 2.5: Comparison between experimental and theoretically fit calculated from Equation 2.4 and 2.5 at varying TADH concentrations. A) Fractional surface coverage with time for 11 and 21  $\mu\text{g/mL}$  of TADH, in the segmented flow system. B) Dynamic surface pressure at 11 and 25  $\mu\text{g/mL}$  of TADH concentration, obtained from drop tensiometry. The solid lines are numerical fits applied to obtain the rate constant for adsorption. The experimental data are also shown in figure 2.2 and 2.4**

Fitting the above equation to the experimental data at 11 and 25  $\mu\text{g mL}^{-1}$  (Figure 2.5B), yields the rate constants for adsorption  $k_a = 6 \times 10^{-4} \text{ mL } \mu\text{g}^{-1} \text{ s}^{-1}$  and  $k_a = 5.5 \times 10^{-4} \text{ mL } \mu\text{g}^{-1} \text{ s}^{-1}$ , respectively.

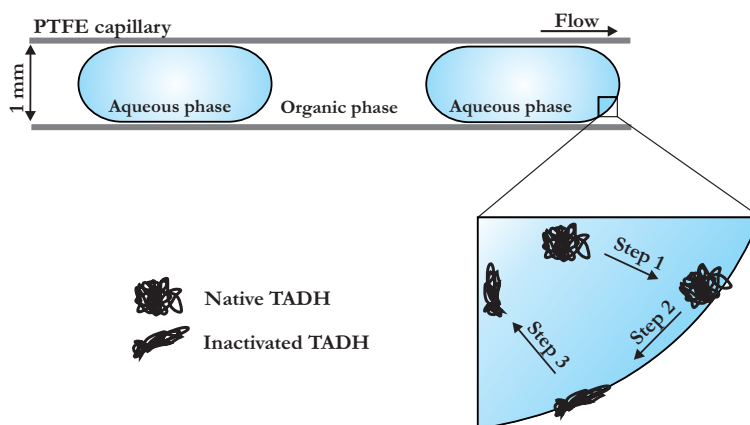
The adsorption rate constants in tensiometry were lower than in the segmented flow reactor which suggests the dominance of convective forces in the segmented flow reactor.

## 2.5 Discussion

### 2.5.1 TADH inactivation in a segmented flow system

There are a couple of mechanisms discussed in literature, describing the inactivation of enzymes due to liquid-liquid two phase systems (Baldascini and Janssen 2005; Ghatorae et al. 1994a). Ghatorae and co-workers proposed dissolved organic solvent molecules in the aqueous phase may interact with and inactivate the enzyme (Ghatorae et al. 1994b). However, the very low solubility of the organic liquid (hexadecane with a  $\text{Log}P_{\text{O/W}}$  value of 8.8 adapted from (Hickel et al. 1998)) in the aqueous phase makes this scenario very unlikely in our system. Another possibility that may lead to enzyme inactivation is the solid-liquid interface (Colombie et al. 2001; Tanaka et al. 2001). According to Nord and co-workers a thin film of organic solvent will stick to the tube wall throughout the tubing, due to the hydrophobicity of the tube material and the organic phase (Nord and Karlberg 1984). If we assume a thin film of hexadecane attached to the hydrophobic PTFE tubing, the enzyme interaction with the solid surface would be reduced, but the liquid-liquid interaction between the aqueous and the organic phase would increase.

On the basis of the experimental observations on the loss in TADH activity and the dynamic surface tension measurements, TADH inactivation in a segmented flow microreactor may occur in three consecutive steps as outlined in figure 2.6. A similar mechanism was described by Baldascini and Janssen for liquid-liquid stirred cell systems (Baldascini and Janssen 2005).



**Figure 2.6: Scheme showing TADH adsorption and inactivation mechanism in the liquid-liquid segmented flow system.** Step 1: irreversible adsorption of TADH to the interface; step 2: inactivation of TADH at the interface; step 3: desorption of TADH from the interface.

In the first step, TADH gets into contact with the interface between aqueous and organic phase either by convection and/or by diffusion, where it is irreversibly adsorbed. During the second step, the adsorbed TADH interacts with the exposed hydrophobic surface, which promotes the

loss of structural integrity of the protein. Finally in the third step, the attached inactivated TADH is desorbed. This is an energy consuming process as the attached TADH is desorbed from the interface and therefore seen only at a very high convective force. This inactivation mechanism is discussed in detail in the following paragraphs.

### **Step 1 and 2: Adsorption and inactivation of TADH**

An immiscible water-organic interface consists of molecules with imbalanced cohesive energy, which arises due to the uncompensated bonds between aqueous molecules and organic molecules. This excess free energy between both liquids is numerically equivalent to the interfacial tension (Donahue and Bartell 1952). An enzyme poses surface activity due to the presence of hydrophobic and hydrophilic amino acids (Eisenberg et al. 1984), and thus has the ability to interact with the interface molecules. This was confirmed by the outcome of the tensiometry experiments, where the dynamic surface pressure increased with TADH concentration (Figure 2.4). In addition, the adsorption rate constants in tensiometry were lower than in the segmented flow reactor (Table 2.2). These results conclude diffusion limitation in the drop tensiometry experiments and the dominance of convective forces in the segmented flow reactor. As the tensiometry experiments were performed at lower temperature compared to the segmented flow experiments, this temperature drop in the tensiometry experiments might also be the reason for a low TADH diffusion rate.

Roach and co-workers reported similar rate constants for RNase adsorption in a plug flow microreactor and in drop tensiometry (Roach et al. 2005). The similar rate constants for adsorption might come from the oversimplified equation used by the authors to relate the surface pressure from tensiometry to the fractional surface coverage. The dominance of convective forces within the segmented flow microreactor was also concluded from the initial TADH inactivation rate ( $6.3 \text{ mg m}^{-2} \text{ min}^{-1}$  from Figure 2.2), which was (approx.) 350 times faster than reported for epoxide hydrolase in a two-phase stirred reactor ( $1.8 \times 10^{-2} \text{ mg m}^{-2} \text{ min}^{-1}$  at 180 rpm in an octane-buffer system) (Baldascini and Janssen 2005). The amount of enzyme inactivated remained constant and was in the range of  $3.4 \text{ mg L}^{-1}$  to  $3.6 \text{ mg L}^{-1}$ . Based on the interfacial area of a single aqueous segment, inactivated TADH surface concentration reached was in the range of  $2\text{-}3 \text{ mg m}^{-2}$ . Ghatore and co-workers have found similar results for urease, lipase, chymotrypsin and ribonuclease in a liquid-liquid bubble column reactor (Ghatorae et al. 1994b). According to Baldascini et al., and Beverung et al., this concentration was sufficient to cover the interface area with a packed monolayer of enzyme (Baldascini and Janssen 2005; Beverung et al. 1999). The coverage of interface with the adsorbed enzyme led to a decrease in the inactivation rate similar to the effect observed for TADH in Figure 2.2.



### **Step 3: Desorption of TADH from the liquid-liquid interface**

As the interface is covered by TADH, further inactivation will only be possible by replacing the adsorbed protein with fresh enzyme. This process requires energy to desorb the enzyme from the interface (Baldascini and Janssen 2005). In liquid-liquid segmented flow, internal circulation generated within the segments is the only force available to break these bonds. This internal circulation is due to the shear stress generated by the solid wall on the moving segments pushing the liquid within the segments into a circulating flow (Burns and Ramshaw 2001) (Figure 2.1). It creates small eddies inside the segment and enhances the internal mixing. The segment length and flow velocity play an important role in developing internal circulations. This was reflected from the maximal loss in TADH activity in the 7 mm long segments at a residence time of 2.5 min. The corresponding very high Peclet number, which specifies the dominance of convective force within the segmented flow (Table 2.1), also confirmed this assumption. Interestingly, changing the residence from 2.5 to 8 min decreased the Peclet number and accordingly reduced the loss in TADH activity for the 7 mm segment length, whereas for the 3 mm and 1 mm the loss in TADH activity was slightly increased. Thus it could be concluded that the convective forces within the segment are dominant above a certain Peclet number and below this value the loss in TADH activity is mainly dependent on the residence time. Reducing the segment size to the micron range (1-100  $\mu\text{m}$ ) would decrease the phase ratio, which would not be beneficial for catalysis anymore (van der Vegt et al. 1996). Smaller droplets would significantly enhance the surface to volume ratio thus minimizing mass transfer barriers at the cost of higher inactivation rates. Such applications might target chip assay rather than production formats.

## 2.6 Conclusion

The present study investigated the influence of segmented flow microreactor process parameters on isolated enzymes activity. The loss in TADH activity was attributed to enzyme inactivation in the segmented flow microreactor due to non-specific interfacial adsorption which was confirmed by drop tensiometry experiments. The rate constant for adsorption suggests diffusion limitation in the drop tensiometry experiments, whereas TADH inactivation was highly influenced by the convective forces within the segments in the microreactor itself. Thus, the respective enzymes need to be stabilized in order to develop segmented flow microreactors as a tool to perform productive enzymatic catalysis. Approaches how to achieve this will be evaluated in the next chapter.

## Acknowledgments

We thank Patrick Degen (Lehrstuhl für Physikalische Chemie, Universität Dortmund) for his assistance during drop tensiometry experiments. This work was financially supported by the Zentrum für Angewandte Chemische Genomik, the European Union (EFRE) and by the Ministry of Innovation, Science, Research and Technology of North Rhine-Westphalia.

## Chapter 3

### Stabilizing Enzyme Activity in an Aqueous/Organic Segmented Flow

Rohan Karande, Andreas Schmid and Katja Buehler

Katja Buehler and Andreas Schmid coordinated and supervised the project and corrected the manuscript

Published in parts in *Langmuir*, 2010, 26 (11), 9152-9159.

### 3.1 Summary

A general and simple approach to stabilize enzyme activity in a segmented flow system is essential for the application of segmented flow microreactors for productive enzymatic synthesis. The enzyme inactivation in segmented flow reactors is mainly due to the large interfacial area and the strong convective forces within the segments. Addition of surfactant to the aqueous phase or enzyme immobilization prevented the biocatalyst from direct contact with the interface and thus stabilized enzyme activity. Almost 100 % of the enzyme activity could be recovered compared to 45 % without any enzyme or medium modification. Drop tensiometry measurements point to a mixed enzyme-surfactant interfacial adsorption. Above a certain surfactant concentration, the surfactant forms a protective layer between the interface and the biocatalyst and this optimal surfactant concentration was dependent on the aqueous-organic interfacial area. Comparing both approaches, addition of surfactant seems to be a simple and promising approach to recover maximum enzyme activity in the segmented flow, which could be used easily for the stabilization of different enzymes.

## 3.2 Introduction

The fast inactivation of enzymes limits the application of aqueous-organic segmented flow microreactors (chapter 2). A detailed understanding of the enzyme inactivation mechanism would aid to develop strategies to overcome this problem. The enzyme interaction with the aqueous-organic interface was studied by several authors using drop tensiometry (Hickel et al. 1998; Roach et al. 2005). For a hydroxynitrilelyase, a decrease in the interfacial tension due to interfacial contacts of hydrophobic parts of the enzyme resulted into the loss of the secondary protein structure. Similar results were observed using a thermophilic alcohol dehydrogenase (TADH) from *Thermus* species, where the interfacial surface tension decreased and the adsorption kinetic became faster with increasing TADH concentration, as described in chapter 2.

Moreover, the enzyme stability was also found to be dependent on the reactor geometry. For example, Colombie and co-workers studied the influence of liquid-solid and liquid-air interfaces on lysozyme stability in stirred tank reactors (Colombie et al. 2001). The inactivation rate was reported to be of first order and dependent on the type of interface, area of interface, and on the power conveyed by the impeller. In liquid-liquid bubble columns, the enzyme inactivation was observed to be proportional to the aqueous-organic interfacial area (Ross et al. 2000). In segmented flow microreactors, the strong internal convective forces within the segments not only enhanced the rate of enzyme inactivation but also increased the amount of enzyme being inactivated. Thus, the interfacial surface area and the convective forces within the segments thus both account for TADH inactivation (chapter 2).

The capability of segmented flow microreactors for enzymatic synthesis can only be realized if the interfacial adsorption and inactivation of enzymes is minimized. This may be done either by preventing the enzyme from driving towards the interface or by modifying the interface to reduce its detrimental effect. Enzyme immobilization is a general approach applied to improve enzyme stability (Buchholz et al. 2005). This might change enzyme characteristics and consequently lead to structural stability. In addition, depending on the surface properties immobilized biocatalyst can be attracted to or departed from the liquid-liquid interface. Moreover, application of the immobilized biocatalyst benefits from easy downstream separation and recycling of non-converted substrate (Rao et al. 2007).

Another approach to stabilize enzyme activity would be to change the surface properties of the interface by using surface active agents like surfactants (Kotsmar et al. 2008; Roach et al. 2005). For example, Roach and co-workers controlled enzyme adsorption to the interface in a drop flow system by using an aqueous insoluble surfactant (Roach et al. 2005). However, the downstream process to separate the surfactant from the organic phase would be a tedious task, as the product

formed during catalysis and the surfactants are dissolved in the organic phase. This problem could be circumvented by using an aqueous soluble surfactant.

In this work, we investigated the effect of enzyme immobilization as well as the addition of surfactant on TADH activity in the segmented flow system. Interestingly, both approaches were successful and maximum enzyme activity could be recovered after passing the enzyme through the segmented flow reactor. Additionally, the stability of formate dehydrogenase (FDH) used for cofactor regeneration of this NADH dependent reaction was investigated. The final aim of this work was to recover complete enzyme activity in liquid-liquid segment flow microreactors, and to set an experimental basis to perform demanding biocatalytic reactions.

### 3.3 Materials and methods

#### 3.3.1 Liquid-liquid segmented flow setup

The setup of the liquid-liquid segmented flow reactor was similar to the one introduced in chapter 2 (Figure 2.1). For the experiments performed with enzyme loaded beads, the setup was slightly modified by connecting an additional PTFE tubing (1 mm inner diameter and 200 mm long) to the end of the aqueous pump tube (between number 7 and 3 in figure 2.1). The beads (10 mg dry weight) containing immobilized TADH were initially pumped at a high flowrate (1 mL min<sup>-1</sup>) to fill up the additional tubing. As soon as the additional tube was filled with the beads, the respective residence time of the beads in the segmented flow was achieved by changing to the desired flowrate. All segmented flow experiments were conducted at 55°C.

The residence time of the segments was controlled either by varying the flow rates at a constant flow ratio or by changing the capillary length. TADH and FDH activity in the segmented flow was determined from the difference in enzyme activity before and after the segmented flow using a UV spectrophotometer based standard assay as described below, unless stated otherwise.

Information on the drop tensiometry experiments and purification of TADH can be found in chapter 2.3.3

#### 3.3.2 Preparation and purification of FDH

The formate dehydrogenase (FDH) C23S mutant from *Candida boidinii* was used for cofactor regeneration (Slusarczyk et al. 2000). It was purified from recombinant *E. coli* JM110 cultivated in a 3 L conical flask with baffles using 300 mL of Terrific Broth (Sambrook and Russell 2001) supplemented with ampicillin (100 µg mL<sup>-1</sup>). At an OD<sub>450</sub> nm of 0.5-0.6, cells were induced by the addition of 0.5 mM IPTG and the cultivation was continued for another 5 hours. Subsequently, cells were harvested by centrifugation at 4618×g, 4°C for 20 minutes in a Sorvall RC-5B centrifuge (Thermo Electron Corporation, Langensfeld, Germany) and stored at -20°C. Enzyme purification was performed by resuspension of the cell pellet to 30 % (w/v) in 10 mM phosphate buffer (pH 7.5 at room temperature) and passing it through a French press unit at 1050 psi for two times (Aminco SLM Instruments, Urbana, IL). Insoluble cell debris was removed by ultracentrifugation for 30 min at 91500 g. The supernatant was loaded onto an anion exchange XK 16/20 column filled with 24 mL of DEAE streamline material at a flow rate of 2 mL min<sup>-1</sup> in 10 mM phosphate buffer. Elution was performed at the same flow rate by applying a linear gradient of 2M NaCl min<sup>-1</sup> in 10 mM phosphate buffer pH 7.5. Fractions were concentrated 5-fold by filtration (Centricon, 10 KDa, Millipore Corporation, Schwalbach, Germany) at 3990 × g (4°C), aliquoted in 1 ml Eppendorf tubes and stored at -20°C. A final purity of 60 to 70% was reached (based on PAGE analysis) and no contaminating activities were

found in the control experiments. Information on the preparation of TADH are described in chapter 2.3.4

### 3.3.3 TADH immobilization on epoxy SEPABEADS® EC-EP

100 mg of epoxy SEPABEADS® EC-EP were added to 1.8 mL phosphate buffer (0.5 M, pH 7) containing 1.1 mg mL<sup>-1</sup> TADH in a 2 mL Eppendorf safe-lock tube. The tube was attached to a REAX 2 rotator (Heidolph, Schwabach, Germany) set to 30 rpm at room temperature. After 3 hours, the supernatant was discarded and the beads were suspended in 100 mM phosphate buffer pH 8.9 to a final volume of 2 mL. It was incubated in a thermo mixer (Eppendorf Thermomixer, Hamburg, Germany) at 25°C, 500 rpm for 24 hrs. Finally, the bead surface was hydrophilized in 1 M glycine solution (100 mM phosphate buffer, pH 8.9) at room temperature for 2 hours. After hydrophilization the supernatants were discarded and the beads were washed several times with immobilization buffer and stored at 4°C. In order to evaluate the stability of immobilized TADH, immobilized TADH activity was performed as described in next section, and after the activity assay the beads were washed at least 3 times by using immobilization buffer, and then reused for the next activity test.

### 3.3.4 Determination of immobilized TADH activity

Activity of immobilized TADH was determined by adding 5 mg of beads loaded with TADH to 950 µL of 100 mM KPi buffer (pH 6.6) containing 160 mM 3-methylcyclohexanone in a 1.5 mL Eppendorf tube. The mixture was incubated at 55°C for 2 minutes before the reaction was started by the addition of 5 mM NADH to a final volume of 1 mL and incubated for another 10 min in a thermo mixer (Eppendorf Thermomixer, Hamburg, Germany) at 55 °C, 900 rpm. Afterwards, 0.5 mL of supernatant containing substrate and product were extracted with 1 mL of ether and quantified by gas chromatography (Focus GC, Thermo Electron Corporation, Dreieich, Germany) using a chiral RT-βDex-sm column (30m×0.25mm×0.25 µm Restek GmbH, Bad Homburg, Germany) column according to the method reported by Höllrigl et al. (Höllrigl et al., 2008).

### 3.3.5 Spectrophotometric determination of soluble FDH activity

The assay mixture for FDH contained 200 mM ammonium formate and 0.5 mM NAD in 100 mM phosphate buffer pH 6.5 at 30°C to a total volume of 200 µL. This mixture was thermostated at 30°C and the reaction was started by adding FDH.

For FDH activity the increase of the NADH signal was monitored. Enzyme activities were calculated using a specific absorption coefficient of  $\epsilon = 6220 \text{ M}^{-1} \text{ cm}^{-1}$  for NADH at 340 nm. 1



unit of enzyme activity was defined as 1  $\mu$ mole of NADH consumed or produced per minute. Spectrometric determination of TADH activity was applied as described in chapter 2.3.5.

### 3.3.6 Analytics

Analytical methods were applied as described in chapter 2.3.

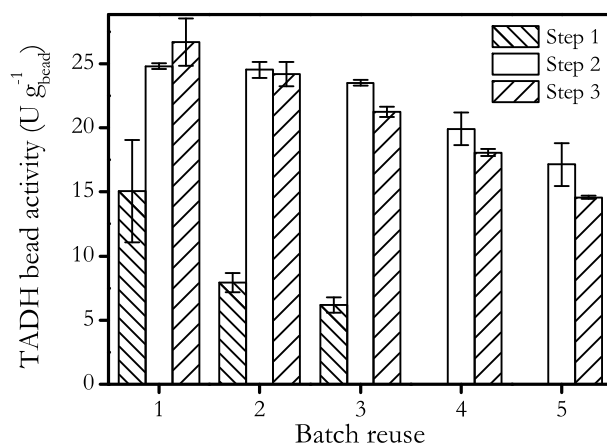
### 3.4 Results

Almost 20 to 55% of TADH activity was lost in the segmented flow, depending on the selected parameters and described in chapter 2. We investigated two approaches to stabilize TADH in the segmented flow reactor system. In the first approach, TADH was fixed on a matrix before introducing it into the segmented flow system. In the second approach, the interface was modified by adding surfactant, which formed a protective layer between the enzyme and the interface. The results of both methods are presented in the subsequent sections.

#### 3.4.1 Approach 1: Use of Immobilized TADH

The enzyme was immobilized on a solid surface to avoid the direct contact of TADH and the liquid-liquid interface. A spherical epoxy-functionalized polymethacrylate (SEPABEADS<sup>®</sup> EC-EP) carrier exhibiting a high porous structure which enhances the surface area was used to immobilize TADH. An optimal protocol to immobilize TADH covalently on the epoxy Sepabeads was developed on the basis of the recovered bead activity in several runs. The three step strategy for the covalent immobilization of TADH on the Epoxy SEPABEADS<sup>®</sup> EC-EP was similar to the protocol given by Ruinatscha and co-workers and described is described in methods section 3.3.3 (Ruinatscha 2009).

The enzyme stability on the beads after each immobilization step was determined by using repetitive batch mode activity tests (Figure 3.1), meaning that after each activity assay, the beads were washed several times and then reused for the next activity test.

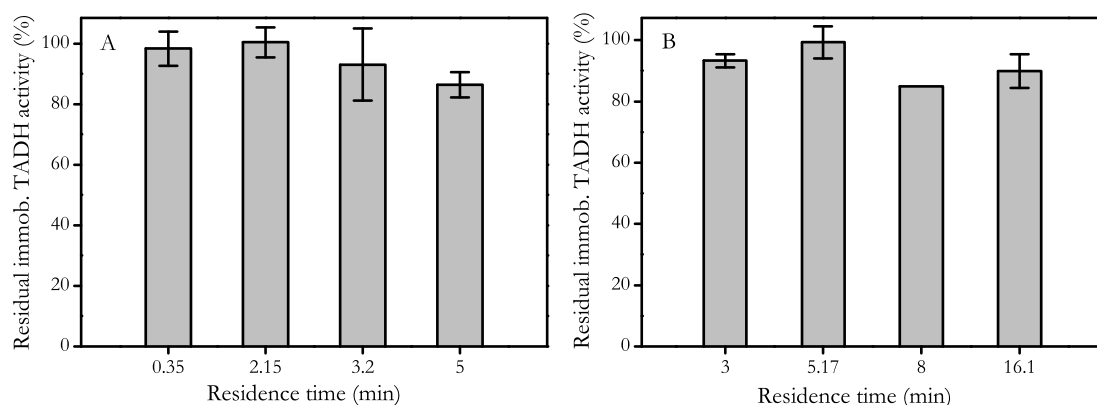


**Figure 3.1: Stability of immobilized TADH after each step of immobilization performed in a single phase batch system.** The dense hatched bars indicate immobilized TADH activity after the first step; plain bars indicate immobilized TADH activity after the second step; hatched bars indicate immobilized TADH activity after the third step.

After the first step of immobilization, the immobilized TADH activity decreased by 50 % in a single reuse. In comparison to the first step, the immobilized TADH activity in the second step is almost two-fold higher, and the beads could be reused for several runs. However, a slight

decrease in bead activity after each run was observed. After the final immobilization step, initial bead activity was slightly higher as compared to the second step, but the loss in the activity during the reuse was still persisting. These results indicate that two steps are sufficient for TADH immobilization on epoxy Sepabeads.

After immobilizing TADH on to the epoxy SEPABEADS carrier, the beads were tested for enzyme activity in the segmented flow system. Immobilization of TADH allowed for a recovery of 85 to 95 % of TADH activity regardless of the applied tube diameter (Figure 3.2). Compared to the experiments with non-immobilized TADH (chapter 2) in the segmented flow, the immobilized enzyme showed a significant enhanced half-life time indicating that the direct contact of TADH to the organic phase was successfully avoided, and the enzyme was less sensitive towards the convective force in the segments. However, technical problems like unequal distribution of beads in each aqueous segment, and difficulties in pumping the beads at low aqueous flow rates were observed.

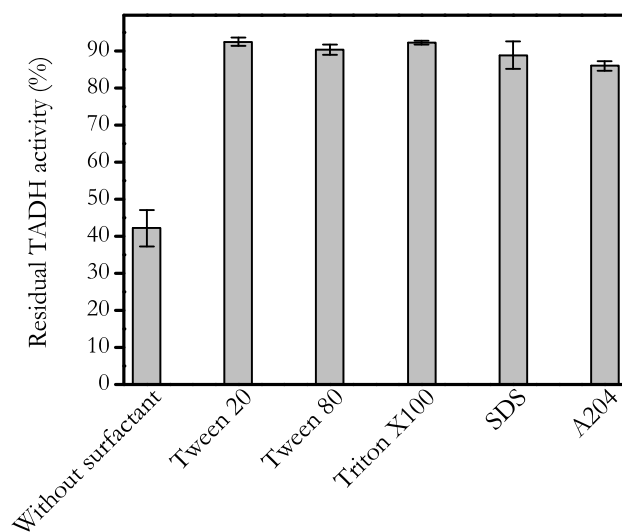


**Figure 3.2: Stability of immobilized TADH in the liquid-liquid segmented flow system. A) Experiment performed in a 2000 mm long, 1 mm i.d. PTFE capillary. B) Experiment performed in a 1000 mm long, 2.1 mm i.d. PTFE capillary.** In both capillaries, the aqueous to organic phase flow ratio was kept equal to 1 ( $Fr=1$ ) and the flow rates were adjusted from  $0.1 \text{ mL min}^{-1}$  to  $0.5 \text{ mL min}^{-1}$  to achieve the desired residence time. Immobilized TADH activity before and after the segmented flow was quantified as described in the material and methods section. 100 % relative activity corresponds to 30-40  $\text{U g}^{-1}$  bead TADH immobilized activity.

### 3.4.2 Approach 2: Stabilization of TADH activity in the segmented flow reactor by using surfactants

As an alternative to enzyme immobilization the influence of surfactant on TADH activity was evaluated. The use of surfactants to avoid enzyme adsorption on the liquid-liquid interface has been successfully applied by several authors (Kotsmar et al. 2008; Roach et al. 2005). In this work, surfactants dissolved in the aqueous phase were screened in the segmented flow reactor (Figure 3.3). For better comparison of TADH activity in different surfactant, the experiments were performed at equal flow rates ( $Fr=1$ ), and at constant residence times. All tested surfactants

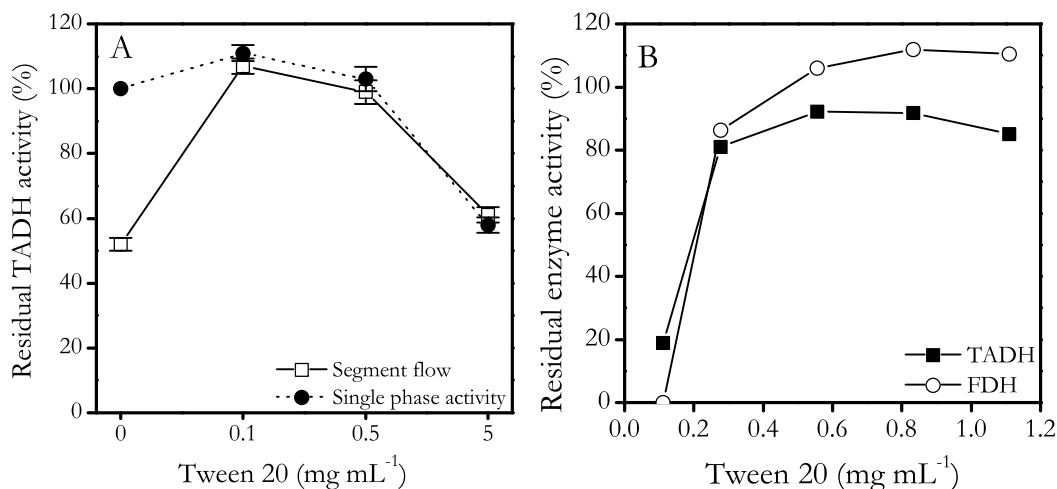
had a beneficial effect on enzyme activity (Figure 3.3), and a maximal of 15% TADH volumetric activity was lost during one run in the segmented flow system, compared to 55% in the absence of surfactant. For further studies Tween 20 was selected as a model compound.



**Figure 3.3: Loss in volumetric TADH activity by varying surfactants in the liquid-liquid segmented flow system.** The aqueous to organic phase flow ratio was kept equal and the flow rate was kept constant at  $0.075 \text{ mL min}^{-1}$ .

Apart from the stabilizing effect, Tween 20 had a dramatic impact on the catalytic activity of TADH (Figure 3.4A). In the standard spectrophotometer based activity assay the initial TADH activity was enhanced to 115% in the presence of  $0.1 \text{ mg mL}^{-1}$  Tween 20. Above this concentration TADH activity decreased again, in the single batch as well as in the segmented flow system. This indicates that TADH inactivation in presence of surfactant is due to the enzyme-surfactant interaction rather than the enzyme liquid/liquid interface interaction (Figure 3.4A). However, when reducing the capillary inner diameter from 1 mm to 0.5 mm, and increasing the residence time to 30 minutes, only 20% of TADH activity could be recovered using  $0.1 \text{ mg mL}^{-1}$  Tween 20 (Figure 3.4B). Further improvement in TADH activity was achieved by increasing the Tween 20 concentration to  $0.55 \text{ mg mL}^{-1}$ , which allowed a recovery of 90% TADH activity. By decreasing the capillary diameter the interfacial surface area becomes larger, which might lead to a higher degree of TADH inactivation. Therefore, higher surfactant concentrations were necessary to cover the interface and to avoid TADH-interface interactions. In similar set of experiments, activity of the NADH regeneration enzyme formate dehydrogenase (FDH) was investigated in the segmented flow system. Interestingly, a total loss in FDH activity was observed when applying  $0.1 \text{ mg mL}^{-1}$  of Tween 20 in the 0.5 mm capillary (Figure 3.4B). The subsequent increase in the surfactant concentration correlated with an increase in FDH activity

and finally almost 100 % could be recovered. Overall, by optimizing the Tween 20 concentration to the capillary diameter recovered 90 to 100% of TADH and FDH activities.

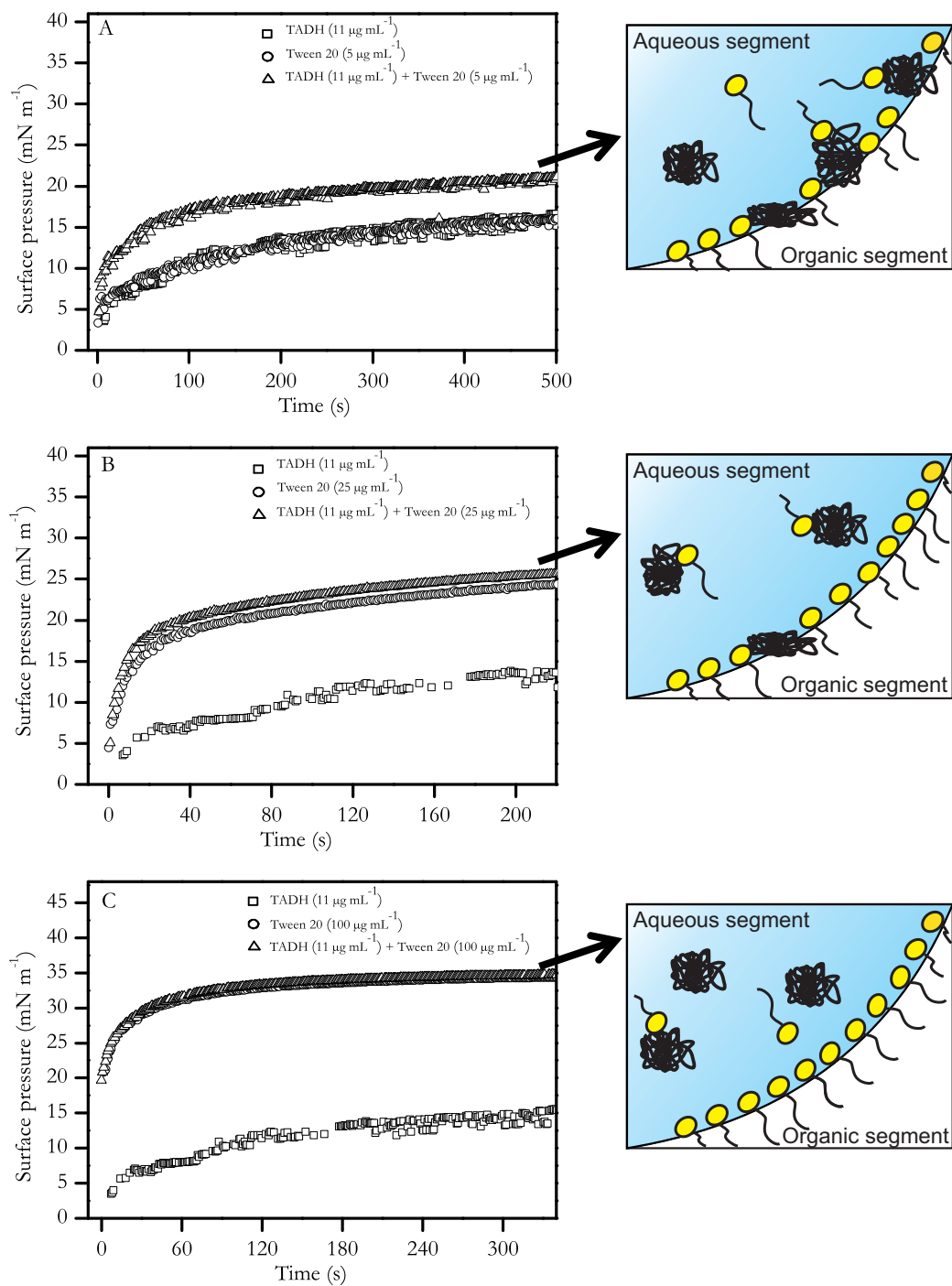


**Figure 3.4: A) Effect of Tween 20 concentration on TADH activity.** Dark circle represents TADH activity in presence of Tween 20 determined in a single phase batch system. TADH activity without surfactant corresponds to 100 % (0.5 U mL<sup>-1</sup>) and is related to the activities in presence of Tween 20. Open square represents TADH activity in the liquid-liquid segmented flow in the presence of Tween 20. The flow rates were constant at 0.2 mL min<sup>-1</sup> each in a 2500 mm long, 1 mm inner diameter capillary to achieve 4.9 minutes of residence time. **B) Effect of Tween 20 on the TADH and FDH stability using a 0.5 mm i.d. capillary.** Length 25 m, aqueous flow 82.5  $\mu$ L min<sup>-1</sup> and organic flow 82.5  $\mu$ L min<sup>-1</sup>, residence time of 30 min. Aqueous phase: FDH 2 U mL<sup>-1</sup>, TADH=4 U mL<sup>-1</sup>.

### 3.4.3 Drop tensiometry experiments to examine enzyme and/or surfactant adsorption

In order to investigate the role of the liquid-liquid interface on TADH and surfactant adsorption, drop tensiometry experiments were performed. The rates of mixed enzyme-surfactant adsorptions were determined by using dynamic surface pressure. At the lowest Tween 20 concentration studied (5  $\mu$ g mL<sup>-1</sup>), the mixed system (TADH + Tween 20) showed higher surface pressure as compared to the individual Tween 20 and TADH surface pressure curves (Figure 3.5A). This observation clearly points towards simultaneous adsorption of Tween 20 and TADH at the liquid-liquid interface. With an increase in the Tween 20 concentration to 20  $\mu$ g mL<sup>-1</sup>, the difference between the surface pressure of the mixed system and Tween 20 is reduced, indicating that Tween 20 is adsorbing faster to the interface than TADH (Figure 3.5B). At the highest concentration of Tween 20 (100  $\mu$ g mL<sup>-1</sup>), the surface pressure of the system containing TADH and surfactant and the one containing only Tween 20 are similar (Figure 3.5C), which indicates that Tween 20 is adsorbed to the interface rather than TADH.

These results demonstrate that at a certain Tween 20 concentration (0.1 mg mL<sup>-1</sup>), surfactant molecules dominate interfacial adsorption. However, to gain additional information on the adsorption layer formed by simultaneous or preferential adsorption of TADH and Tween 20, one can execute further investigation by ellipsometry or neutron reflection techniques.



**Figure 3.5: Dynamic surface pressure at the hexadecane-buffer interface.** Change of surface pressure for the hexadecane-buffer interface with time for TADH (A), Tween 20 (B) and with both (C), TADH and Tween 20, is shown. Schematic sketches describe possible mixed (enzyme and surfactant) interactions on the interface.

### 3.5 Discussion

On the basis of our hypothesis on enzyme inactivation, the direct contact of the enzyme with the interface should be avoided in order to stabilize enzyme activity. This is done either by reducing the surface free energy of the interface by using surface active molecules or by changing the surface activity of enzyme by immobilizing them onto a solid matrix (Mateo et al. 2002).

#### 3.5.1 Evaluation of the two approaches to stabilize TADH in the liquid-liquid segmented flow reactor

A three step enzyme immobilization protocol similar to the one published by Ruinatscha and co-workers for the covalent immobilization of a monooxygenase on epoxy-functionalized Sepabeads EC-EP (Ruinatscha 2009) was investigated for TADH immobilization. The reusability of immobilized TADH in a batch system was considered to be an important criterion for the success of the immobilization. After the first step of TADH adsorption, almost 50% of immobilized TADH activity was lost (Figure 3.1). This loss in activity is attributed to desorption of the enzyme from the carrier particles. Although bead activity after subsequent covalent attachment improved by two-fold which could be reused for several runs, a slight loss in immobilized enzyme activity after each run was observed (Figure 3.1). This could be the result of unbound epoxy functional groups on the beads, which react with the enzyme residues affecting the catalytic activity of TADH. To overcome the untreated epoxy functional groups and to obtain a chemically inert heterogeneous catalyst, the beads were post treated with a non-polar amino acid (Glycine). However, this treatment had no influence on bead performance.

Overall, TADH stability could be significantly improved by immobilization and only 5 to 15% of bead activity was lost in each cycle (Figure 3.2). This might be due to the hydrophobic nature of the Sepabeads (Srinivasulu and Rao 1993), which drives them towards the aqueous/organic interface where they attach. This interfacial adsorption would be beneficial to perform interfacial catalysis, but on the down side the enzymes present on the bead surface get exposed to the interface and might be inactivated. However, the main bottleneck of this system is of technical nature, which prevents the equal distribution of beads in each aqueous segment. We suggest using hydrophilic nano-beads with a lower specific gravity than the aqueous phase to overcome these challenges.

As an alternative approach, the surface free energy of the interface was reduced by adding molecules, which were more surface active than an enzyme such as surfactant. At low amounts of surfactant molecules present in the aqueous phase, both TADH and Tween 20 is adsorbed to the interface (Figure 3.5A). At higher concentrations of Tween 20, the adsorption of the surfactant to the interface was faster than in case of the protein. This becomes obvious from the surface

tension measurements, where the surface pressure approached the surfactant surface pressure (Figure 3.5B). With increasing Tween 20 concentrations the effect of TADH on interface was almost negligible (Figure 3.5C). These results suggest that Tween 20 prevents the interfacial adsorption of TADH, which might lead to an increase of TADH activity above 100% in the segmented flow system (Figure 3.4A).

This surface active molecule not only changed the surface free energy of the interface but also had an impact on enzyme activity. In the standardized spectrophotometric assay, the presence of  $0.1 \text{ mg mL}^{-1}$  Tween 20 had a positive impact on the initial TADH activity (enhancement to 115%). Also in the segmented flow system the addition of surfactant was beneficial for the recovery of enzyme activity (Figure 3.4A). According to Miller et al. and Kotsmar et al., the surfactant-enzyme interaction mechanism for the non-ionic surfactants is due to the hydrophobic interaction between the surfactant and the enzyme (Kotsmar et al. 2008; Miller et al. 2000). This hydrophobic interaction between Tween 20 and hydrophobic groups present on the TADH might lead to a better accessibility of the substrate to the binding pocket, indicated by a rise in TADH activity (Figure 3.4A). However, with increasing Tween 20 concentrations, the resulting hydrophobic interaction between surfactant and TADH might disrupt the entire structure of the protein and is therefore not beneficial for enzyme stability. Similar results of enhancement in the enzyme activity at low surfactant concentration and inhibition at higher surfactant concentration have been described by Srinivasulu and Rao (Srinivasulu and Rao 1993). Interestingly, a Tween 20 concentration of  $0.1 \text{ mg mL}^{-1}$  was observed not to be beneficial in the 0.5 mm capillary as almost 80% of TADH activity and 100% of FDH activity was lost (Figure 3.4B). The increase in the interfacial surface area by reducing the capillary diameter necessitates more surfactant to cover the interface. Due to the low amount of surfactant at  $0.1 \text{ mg mL}^{-1}$  subsequent adsorption of enzymes and loss in the activities was observed. However, with increase in the surfactant concentration, the recovery of TADH and FDH activity improved in the segmented flow system. Overall, the enzyme immobilization and the use of surfactant approaches tested here showed magnificent improvement in stability of TADH and FDH activity. This surfactant approach would also be an interesting option to control enzyme inactivation in liquid-liquid batch or semi batch systems. Now the stage is set to exploit the segmented flow technology for productive biocatalysis. The presented TADH/segmented flow system allows qualitative cause-effect studies with time dependent losses of enzyme activities as read-out parameters. System boundaries identified might include different inactivation rates of multienzyme reactions or the identification of optimal solvent/enzyme/reaction combinations.



### 3.6 Conclusions

The present study shows the successful stabilization of an isolated dehydrogenase in a segmented flow reaction system. Inactivation of TADH in the segmented flow microreactor was due to non-specific interfacial adsorption. The enzyme was stabilized either by immobilization or by the addition of surfactants. Drop tensiometry experiments helped to elucidate how the surfactant replaces the enzyme at the interface. The use of surfactants seems to be more attractive because of better activity yield, less complexity, and easier implementation into the liquid-liquid segmented flow reactor. At an optimal Tween 20 concentration, TADH and FDH activities in the segmented flow microreactor are stabilized. This simple solution can be applied to a variety of enzymes to stabilize their activity. The potential of this technique for biocatalysis will be evaluated in the next chapter.

### Acknowledgments

This work was financially supported by the Zentrum für Angewandte Chemische Genomik, the European Union (EFRE) and by the Ministry of Innovation, Science, Research and Technology of North Rhine-Westphalia.

## Chapter 4

### Miniaturizing Biocatalysis: Enzyme Catalyzed Reactions in an Aqueous/Organic Segmented Flow Capillary Microreactor

Rohan Karande, Andreas Schmid and Katja Buehler

Katja Buehler and Andreas Schmid coordinated and supervised the project and corrected the manuscript

Published in *Advanced Synthesis and Catalysis*, 2011, 353 (13), 2511-2521.

## 4.1 Summary

A segmented flow capillary microreactor was used to perform the enzyme catalysed conversion of 1-heptaldehyde to 1-heptanol in a two liquid-liquid phase system. These reactor formats are established for chemical reactions but so far data describing the relevant system parameters for enzymatic catalysis are missing. This work addresses the impact of important parameters such as capillary diameter, flow velocity, phase ratio, and enzyme as well as substrate concentration on the enzymatic reaction performance under segmented flow conditions. All key parameters governing reaction performance have been correlated in a novel operational window for an easy assessment of the various system constraints. Such systems are characterized by high productivities and easy phase separation facilitating downstream processing. This work underscores the importance of segmented flow systems as a promising tool to perform multiphasic enzymatic catalysis.

## 4.2 Introduction

The main objective of bioreactor design is to ensure high productivities and catalyst stabilities at low manufacturing and maintenance costs. In the last decades, considerable efforts have been made in this respect either by design of new reactors or by optimization of established systems. Especially, the concept of miniaturizing reaction formats has gained interest as productivities of chemical reactions are enhanced by orders of magnitude (Ehrfeld et al. 2000; Watts and Haswell 2005). Accordingly, microreactors have been successfully implemented in the chemical industry for the production of fine chemicals (Roberge et al. 2008; Wirth 2008).

Segmented flow capillary microreactors are especially suited for reactions comprising multiple liquid-liquid phases due to the improved mass transfer rates compared to the conventional batch systems (Kashid et al. 2007). A segmented flow is formed by the contact of immiscible fluids through a T or Y shaped mixer generating alternate fluid segments (Kashid et al. 2011b; Kashid et al. 2008; Kinkel and Tomlinson 1980). The high mass transfer rates are obtained from the enhanced surface area to volume ratio between the segments, while the shearing motion generates re-circulations or vortex motions and enhances mixing within the segments (Burns and Ramshaw 2001; Burns and Ramshaw 2002; Nord et al. 1987). Additionally, the power input necessary to obtain high mass transfer coefficients in the segmented flow are low compared to the conventional systems (Kashid et al. 2007). Moreover, these types of microreactors are simple in design, easy to construct and cheaper than conventional reactors.

Although well established for chemical reactions, segmented flow capillary microreactors are so far not used for enzymatic catalysis. One has to keep in mind that only fast reaction limited by mass and heat transfer profit from the advantages of miniaturization. Contrary to chemical reactions, biocatalytic conversions are relatively slow and are often not hampered by mass or heat transfer problems. Therefore just a limited number of multiphase enzymatic reactions which are depending on sufficient inter-phase transport will benefit from a microscale reaction system (Bolivar et al. 2011). However, high surface to volume ratios between the segments might lead to biocatalyst inactivation. In the chapter 2 and 3, the enzyme (TADH and FDH) inactivation in the segmented flow was investigated and successfully circumvented by addition of surfactant to the aqueous phase. This chapter presents our continuing effort for the development of segmented flow enzymatic microreactors (SFER).

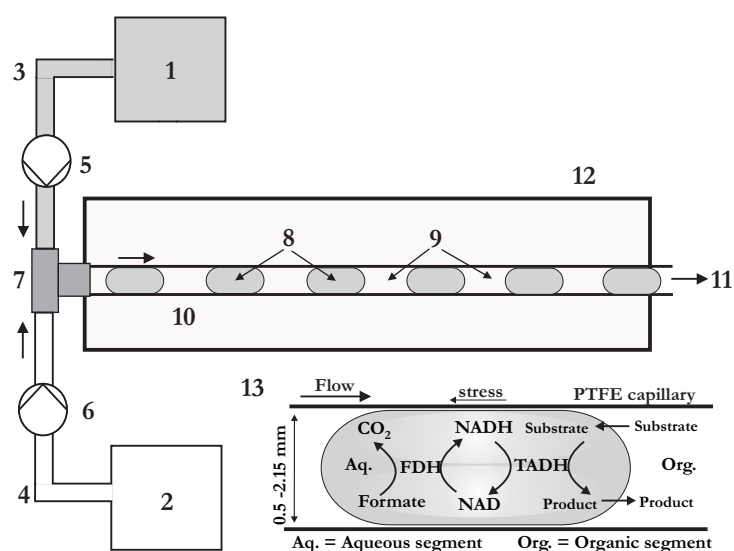
In the course of SFER development the impact of the mass transfer rates on the TADH reaction kinetics were pre-evaluated by using the Damköhler number. The reduction of 1-heptaldehyde to 1-heptanol was chosen as a model reaction. Important parameters governing the interplay between reaction rates and mass transfer rates were investigated and visualized in an operational

window for a systematic optimization of the SFER performance (Figure 4.5 and 4.6). An average productivity of  $10.4 \text{ g}_{\text{product}} \text{ L}_{\text{org}}^{-1} \text{ hr}^{-1}$  ( $90 \text{ mM h}^{-1}$ ) was obtained in the segmented flow system using a 0.5 mm inner diameter capillary. Phase separation, as well as product isolation, was straightforward.

## 4.3 Material and Methods

### 4.3.1 Segmented flow enzymatic microreactors (SFER) setup

The setup of the SFER was similar to that described previously (chapter 1), and shown in Figure 4.1. The PTFE capillaries were kept in a thermo bath to maintain the reaction temperature (45°C). Prior to starting the biotransformation, the flow was stabilized for 10 min at the desired flow rate. A standard experiment contained hexadecane as organic phase with 100 mM 1-heptaldehyde as substrate, and 100 mM Bis-Tris buffer as aqueous phase containing 0.5 mM NADH, 500 mM ammonium formate, and TADH as well as FDH for cofactor regeneration. The ratio of TADH:FDH was always 2:1. The Tween 20 concentration varied with the capillary diameter applied. For 2.15 and 1 mm i.d. capillaries 0.11 mg mL<sup>-1</sup>, and for 0.5 mm i.d. capillary 0.55 mg mL<sup>-1</sup> have been added to the aqueous phase.



**Figure 4.1: Schematic view of the liquid-liquid segmented flow setup.** 1: aqueous phase reservoir; 2: organic phase reservoir; 3, 4: solvent resistant tubing; 5, 6: two channel peristaltic pump; 7: T shaped mixer; 8: aqueous phase segments; 9: organic phase segments; 10: 0.5 mm, 1 mm or 2.15 mm inner diameter PTFE capillary; 11: samples collected for off line analysis; 12: water bath to control temperature; 13: magnified sketch of segment showing mass transfer and reaction scheme.

The reactions were started by contacting and passing organic phase containing the substrate and aqueous phase including the enzymes and cofactors through the capillaries. The residence time of the segments was controlled either by varying the flow rates or by changing the capillary length. The segments were collected from the tube outlet in an Eppendorf tube for every 2 minutes. Aqueous phase and organic phase were separated based on the density difference. Substrate consumption and product formation were analysed using gas chromatography (GC), while residual enzyme activity was determined via an UV spectrophotometer based assay.

#### 4.3.2 Preparation, purification and activity determination of TADH and FDH

Information on the preparation and purification of TADH and FDH can be found in chapter 2.3.4 and 3.3.2. Determination of TADH and FDH activities, protein concentration and analytical methods were applied as described in chapter 2.3.5 and 3.3.5.

#### 4.3.3 Product recovery

After the enzymatic transformation, phase separation was based on the density difference. 1-heptanol was purified by fractional distillation at 7 mbar at elevated temperature. The organic phase was heated to 180°C and the temperature of the distillate increased to 65°C. Two distillate fractions and the final residue were collected from the still. The first distillate fraction contained the major portion of 1-heptaldehyde (70% based on GC containing flame ionization detector), whereas the rest of the material was 1-heptanol. The second fraction contained 1-heptanol with a purity of 97-98% as determined by GC-FID, with small traces of 1-heptaldehyde. The final residue contained 1-hexadecane at a purity of 99.4% (GC-FID analysis) with minor amounts of 1-heptanol.

## 4.4 Results

### 4.4.1 Which enzymatic reactions profits from a microreactor system?

The true benefit of micro-scale systems are excellent mass transfer rates accomplished by the enhanced surface area to volume ratio (Janasek et al. 2006). Therefore, reactions limited by mass transfer rates benefit from the substantial transfer potential of micro-systems. Hence, knowing the rate limits of the mass transfer and the enzymatic reaction can be helpful to judge in suitability for the micro-systems. To evaluate the TADH reaction rate limit, the substrate mass transfer resistance was assumed to solely reside in the aqueous phase (based on the high substrate partition coefficients,  $K_{org./aq.}$ ) (Ramelmeier and Blanch 1989). The substrate mass transfer rate through the organic phase into the aqueous phase is thus:

$$m_A = k_L a (C_{Ae} - C_{AL}) \quad (4.1)$$

Where  $k_L$  is the mass transfer coefficient ( $m\ s^{-1}$ ),  $a$  is the interfacial area per volume ( $m^{-1}$ ),  $C_{Ae}$  is the equilibrium substrate concentration in the aqueous phase (mM),  $C_{AL}$  is the aqueous phase substrate concentration (mM). For the enzyme reactions following Michaelis-Menten kinetics, the reaction rate is:

$$r_A = \frac{V_{max} \times C_{AL}}{K_m + C_{AL}} \quad (4.2)$$

where,  $K_m$  is the Michelis constant (mM). At steady state the substrate mass transfer rate is in balance with the reaction rate ( $m_A = r_A$ ), hence equation 4.1 and 4.2 are equated as follows:

$$k_L a (C_{Ae} - C_{AL}) = \varphi \times \frac{V_{max} \times C_{AL}}{K_m + C_{AL}} \quad (4.3)$$

where,  $\varphi$  is the phase volume ratio ( $V_{aq}/V_{org}$ ). This equation is rearranged in terms of dimensionless quantities by putting:

$$x = \frac{C_{AL}}{C_{Ae}} \text{ and } \kappa = \frac{K_m}{C_{Ae}} \quad (4.4)$$

$$\frac{(\kappa + x)(1 - x)}{x} = \frac{V_{max} \times \varphi}{k_L a \times C_{Ae}}$$

The right side term can be reduced by introducing the dimensionless variable Damköhler number second (Da). Therefore equation 4.4 now becomes:

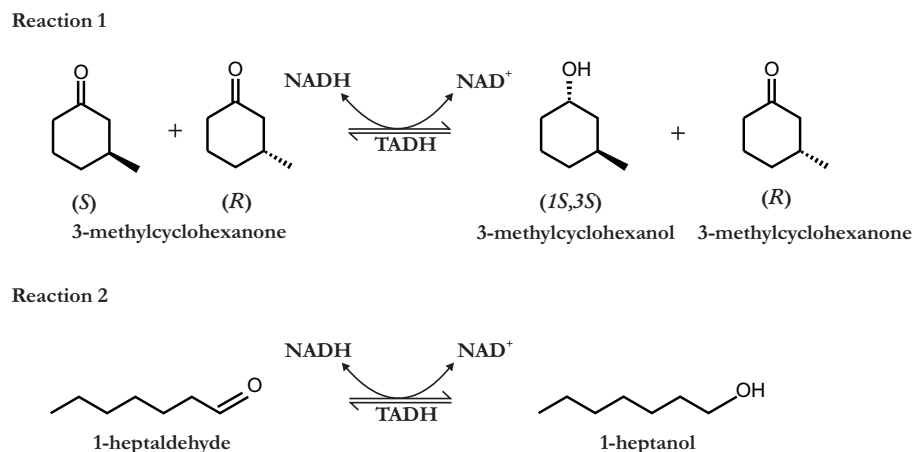
$$\frac{(\kappa + x)(1 - x)}{x} = Da \quad (4.5)$$

$$\text{and, } Da = \frac{V_{max} \times \varphi}{k_L a \times C_{Ae}} = \frac{k_{cat} \times e_0 \times \varphi}{k_L a \times C_{Ae}} \quad (4.6)$$

where,  $V_{max} = k_{cat} \times e_0$ ,  $k_{cat}$  is the turnover number ( $s^{-1}$ ) and  $e_0$  is the enzyme concentration (mM). This number parameterizes the reaction kinetics and mass transfer rates, similar to the



Hatta number or Thiele modulus (Samant and Ng 1998). A high Damköhler number represents a mass transfer controlled regime where the reaction rate is faster than the mass transfer rate, whereas a low Damköhler number indicates a reaction rate controlled regime since the reaction rate is much slower than the mass transfer.



**Scheme 1: Reactions catalyzed by TADH and used for pre-evaluation presented in Table 4.1.**

Table 4.1 illustrates two reactions catalyzed by TADH with a different turnover number: reduction of rac-3-methylcyclohexanone to (*1S,3S*)-3-methylcyclohexanol, and reduction of 1-heptaldehyde to 1-heptanol (Scheme 1). As the reaction rate equals the mass transfer rate at a Da number of 1 ( $Da=1$ ), it was possible to estimate the mass transfer coefficient ( $k_L a$ ) necessary in the reactor system to normalize the reaction speed. The respective mass transfer coefficient ( $k_L a$ ) differs for both reactions: for the conversion of 1-heptaldehyde a  $k_L a$  of  $0.25 \text{ s}^{-1}$  is obtained, whereas the conversion of 3-methyl-cyclohexanone gives a  $k_L a$  of  $0.0012 \text{ s}^{-1}$  (Table 4.1).

**Table 4.1: Pre-evaluation of reactions based on the Damköhler number**

	Reaction 1	Reaction 2
<b>k<sub>cat</sub></b>	$\sim 10 \text{ s}^{-1}$	$\sim 100 \text{ s}^{-1}$
<b>Enzyme</b>	0.025 mM	0.025 mM
<b>Substrate<sup>a)</sup></b>	200 mM	10 mM
<b>Damköhler number</b>	1	1
<b>Mass transfer coefficient</b>	$0.00125 \text{ s}^{-1}$	$0.25 \text{ s}^{-1}$

Mass transfer coefficients were determined by assuming Damköhler number = 1; <sup>a)</sup> solubility limit of the substrate in the aqueous phase.

This suggests a 200-fold higher mass transfer coefficient for the conversion of 1-heptaldehyde as compared to the conversion of 3-methylcyclohexanone. It indicates that the conversion of 1-heptaldehyde is mass transfer limited, if the reactor is not operated at a mass transfer coefficient equal to or above  $0.25 \text{ s}^{-1}$ . Kashid and co-workers investigated mass transfer in various aqueous organic segmented flow systems and compared those to traditional extraction formats (e.g.

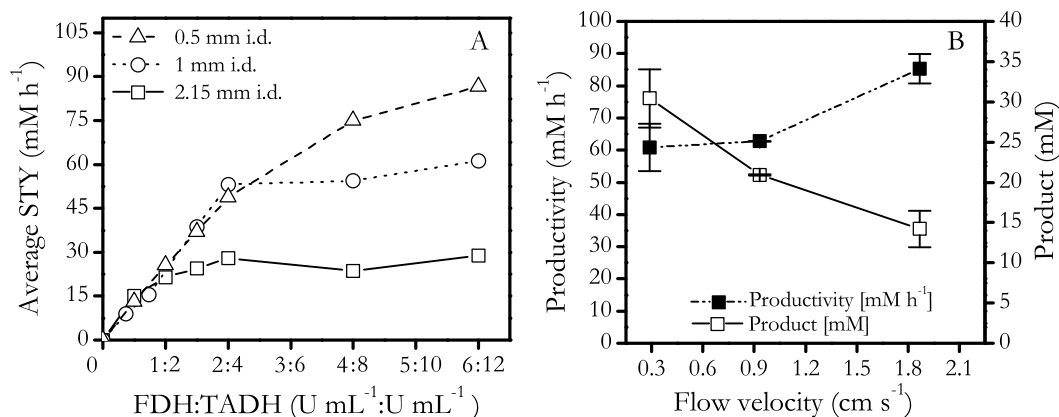
agitated vessels). The reported mass transfer coefficients for the segmented flow ( $k_L a$ ) have been in the range of 0.1 to 2 s<sup>-1</sup> (Kashid et al. 2007), which were higher than those obtained for the conventional units. As our predicted mass transfer coefficient based on the Da number (Da=1) for the conversion of 1-heptaldehyde lies within this range (Table 4.1,  $k_L a = 0.25$  s<sup>-1</sup>), the segmented flow system is highly attractive to perform this enzymatic transformation. Based on this pre-evaluation, 1-heptaldehyde was chosen as a model substrate for further investigation of the SFER.

#### 4.4.2 Which parameters influence the enzymatic reaction performance in a SFER?

Several authors have identified important parameters affecting mass transfer performance in segmented flow reactors, such as phase ratio, capillary diameter, and flow velocity (Burns and Ramshaw 2001; Burns and Ramshaw 2002; Jovanovic et al. 2010; Kashid et al. 2007; Nord et al. 1987). These parameters were studied in detail to understand their impact on TADH performance.

##### Trade-off between the enzyme concentration and the capillary diameter

The impact of enzyme concentration on the reaction performance in the segmented flow reactor was investigated in 0.5 mm, 1 mm, and 2.15 mm inner diameter PTFE (Polytetrafluoroethylene) capillaries. For all studied capillaries, the space time yield (STY) increased linearly with the enzyme concentration, until it reached a maximum before levelling off (Figure 4.2A). This point to a transition from a reaction rate limited regime to a mass transfer limited regime.



**Figure 4.2. A) Influence of enzyme concentration on the space time yield (STY) using capillaries of varying inner diameter (i.d.).** Flow rate and capillary length were adapted to achieve 30 min residence time for each capillary. Aqueous and organic phase flows were kept equal and constant during the experiment. 2.15 mm i.d.: length 4.9 m, total flow 0.58 mL min<sup>-1</sup> (0.26 cm s<sup>-1</sup>); 1 mm i.d.: length 11 m, total flow 0.29 mL min<sup>-1</sup> (0.61 cm s<sup>-1</sup>); 0.5 mm i.d.: length 25 m, total flow 0.165 mL min<sup>-1</sup> (1.40 cm s<sup>-1</sup>). For more information on enzyme stability (TADH / FDH) see supplemental information. **B) Impact of flow velocity on the product formation.** TADH = 8 U mL<sup>-1</sup>; 1 mm i.d. capillary 11 m long; total flow rate varied from 0.19 to 0.88 mL min<sup>-1</sup>.

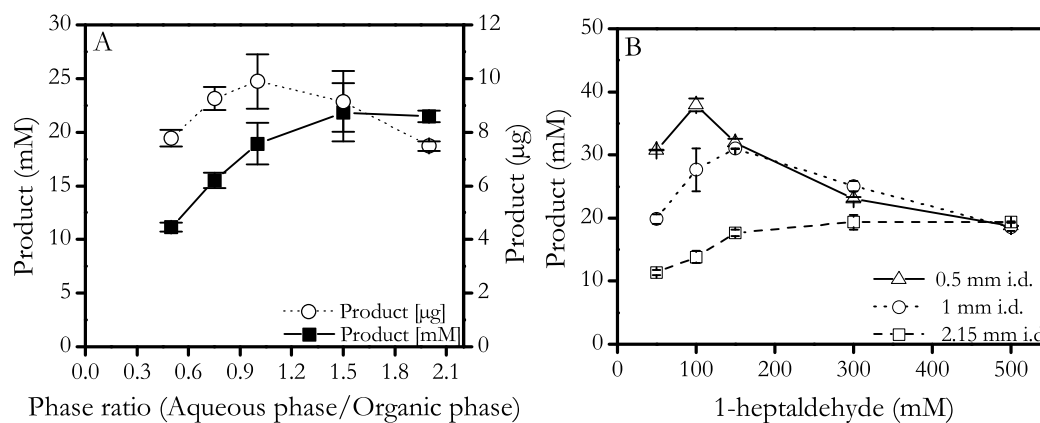
For 2.15 mm PTFE capillary, no significant increase in the reaction rate was seen at higher enzyme concentrations (2U FDH mL<sup>-1</sup> and 4U TADH mL<sup>-1</sup>). However, the reaction rate was further increased by reducing the capillary inner diameter to 1 mm or 0.5 mm. The maximum STY of 90 mM h<sup>-1</sup> was achieved for the smallest capillary (i.d. 0.5 mm), which illustrates an enhancement of mass transfer due to increase in the length of segments and flow velocity with decreasing capillary diameter. For the efficient usage of enzymes, it is thus essential to determine the optimal enzyme concentration for each capillary unit.

### **The impact of flow velocity on the product formation rate**

Segmented flow forms internal circulations or forced vortex within the segments which are developed from the shear forces implied by the capillary wall across a segment interface (Burns and Ramshaw 2001; Burns and Ramshaw 2002; Jovanovic et al. 2010; Kashid et al. 2007; Nord et al. 1987). These circulations improve mixing within the segments and are dependent on the flow velocity, length of segments and inner diameter of the tubing. Out of these parameters, flow velocity was varied in order to investigate the effect of higher internal circulations on the reaction performance while other parameters were kept constant. At high flow velocities and short residence times (1.86 cm s<sup>-1</sup>, 10 min), the space time yield was high (Figure 4.2B). Lowering the flow velocity to 0.91 cm s<sup>-1</sup> or 0.61 cm s<sup>-1</sup> (residence times of 20 or 30 min), increased the total product concentration on the expense of STY. This experiment shows the effects of flow velocity on the STY at varying residence times.

### **The impact of phase ratio on product formation**

In segmented flow reactors, the ratio of aqueous to organic phase (phase ratio) alters the segment sizes and is an important parameter influencing the mass transfer rates (Burns and Ramshaw 2001; Burns and Ramshaw 2002; Nord et al. 1987). The phase ratio was varied by changing the individual phase flow rate, while keeping the total flow rates constant to obtain a residence time of 20 min (Figure 4.3A). The product concentration in the organic phase increased up to a phase ratio of 1.5 and then remained constant. However, the maximal amount of product considering both phases was formed at a phase ratio of 1.0. Though, the optimal phase ratio of 1.0 was based on the total amount of product formed, a trade-off between the product concentration and the amount is necessary to meet downstream separation cost.



**Figure 4.3: A) The influence of phase ratio on the product formation.** TADH = 4 U mL<sup>-1</sup>, 1 mm i.d. capillary 11 m long; aqueous flow 0.15 to 0.3 mL min<sup>-1</sup> and organic flow 0.3 to 0.15 mL min<sup>-1</sup>; residence time 20 min. **B) Influence of substrate concentration on the product formation using capillaries of varying inner diameter (i.d.).** TADH = 6 U mL<sup>-1</sup>; residence time 30 min.; 2.15 mm i.d.: length 4.9 m, total flow 0.58 mL min<sup>-1</sup>; 1 mm i.d.: length 11 m, total flow 0.29 mL min<sup>-1</sup>; 0.5 mm i.d.: length 25 m, total flow 165 mL min<sup>-1</sup>.

### Trade-off between substrate concentration and capillary diameter

The effect of varying substrate concentrations on the enzymatic reaction performance in the SFER was analyzed in 0.5, 1, and 2.15 mm inner diameter PTFE capillaries. The maximum reaction rate was obtained in the smallest capillary (0.5 mm i.d.) at a substrate concentration of 100 mM 1-heptaldehyde in the organic phase (Figure 4.3B). A further increase of the substrate concentration was not beneficial as TADH was inhibited by substrate concentrations above 1 mM 1-heptaldehyde in the aqueous phase (100 mM in the organic phase, partition coefficient  $K_{\text{org/aq}}=100$ ). In capillaries with a larger inner diameter a lower conversion rate was obtained and the optimal substrate concentration shifted from 100 mM to 150 mM. Interestingly, similar amounts of product were converted at a substrate concentration of 500 mM, irrespective of the capillary inner diameter. This indicates that smaller capillaries are only beneficial for the mass transfer rate at lower substrate concentrations.

Based on the above findings, different reactor set-ups were considered for maximizing product formation. Utilizing small sized capillaries is not recommendable, because they have to be very long to achieve a sufficient residence time for the reaction. To achieve a residence time of 210 min, one would need a capillary of 175 m (0.5 mm i.d.), which leads to problems with high backpressure and is thus not attractive. Simply changing the flow rate to prolong the residence time is no option, as this will in turn change the operating region of the system and lower the overall reaction performance (Figure 4.2B). Instead, different sized capillaries have been combined (Figure 4.4), which reduced the overall capillary length to 41 m. The reaction was started in a 2.15 mm i.d. capillary with the organic segments containing 300 mM 1-heptaldehyde. With on-going conversion to 1-hetanol the inner capillary diameter was reduced to 1 mm and

finally to 0.5 mm, because at lower substrate concentrations smaller capillaries support higher reaction rates. In this combined system 85 mM of the product 1-heptanol could be gained in 105 min (Table 4.2). With the decrease in capillary inner diameter the flow velocity and the surface area to volume ratio increases, which contributes to the enhancement of the mass transfer rates and results in a higher product concentration. However, for the longer residence time (210 min) single 2.15 capillary turned out to be beneficial as TADH inactivation was more pronounced in the coupled capillaries.

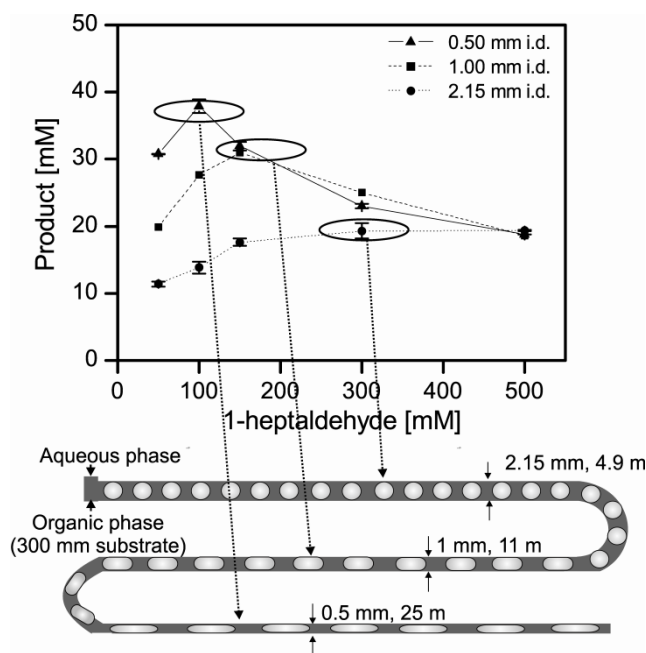


Figure 4.4: Coupled capillaries SFER set-up (experimental data shown in table 4.2 used to elaborate the coupled capillaries SFER set-up). SFER combining 2.15 mm, 1 mm and 0.5 mm capillaries in series.

Table 4.2: TADH catalyzed conversion of 1-heptaldehyde in different SFER configurations

System	Residence time (min)	Product (mM <sub>org.</sub> )	STY (mM <sub>org.</sub> hr <sup>-1</sup> )	TADH <sup>ⓐ</sup>
cSFER <sup>a)</sup>	105	85	48	50
SFER <sup>b)</sup>	105	64	36	88
cSFER <sup>a)</sup>	210	112	32	36
SFER <sup>b)</sup>	210	137	39	63

**General conditions:** Total flow<sub>105min</sub> 0.3 mL min<sup>-1</sup>; total flow<sub>210min</sub> 0.165 mL min<sup>-1</sup>. Aqueous phase: NADH = 0.5 mM, TADH = 15 U mL<sup>-1</sup>, ammonium formate = 1 M, Tween 20 = 0.11 mg mL<sup>-1</sup>. Organic phase: 300 mM 1-heptaldehyde.

<sup>a)</sup>cSFER: coupled SFER combining different sized capillaries: total capillary length 40.9 m (2.15 mm i.d. = 4.9 m, 1 mm i.d. = 11 m, 0.5 mm i.d. = 25 m).

<sup>b)</sup>SFER: standard set-up. Total capillary length 9 m (2.15 mm i.d. only).

<sup>ⓐ</sup> Recovered TADH activity; FDH activity was above 89% in all cases.

#### 4.4.3 Product isolation

Product isolation is crucial for the overall process design and very often neglected. Two phase systems tend to form stable emulsion in traditional stirred tank systems, which severely complicate downstream processing and the recycling of the organic phase due to difficulties in phase separation (Mathys et al. 1999). Applying two phase reaction systems to a SFER circumvents this problem, as no emulsions are formed and the phases may be easily separated based on their density difference. The maximum product concentration obtained in the organic phase of our SFER corresponds to 1.5 to 2 wt % of the total organic phase. For the practical application of 2-phase enzymatic reactions one of the key steps is to isolate the product and to recycle the organic phase. In preliminary experiments, fractional batch distillation of the organic phase at 7 mbar and 180°C recovered 410 mg of 1-heptanol (purity 97-98% based on GC analysis) as a clear liquid from the distillate. The bottom phase of distillation contained mainly hexadecane (99.45% based on GC analysis), which could be recycled in the 2-phasic enzymatic reactor. The isolated product yield was 40%, and further optimization to enhance the product yield will be of special interest in future works.

## 4.5 Discussion

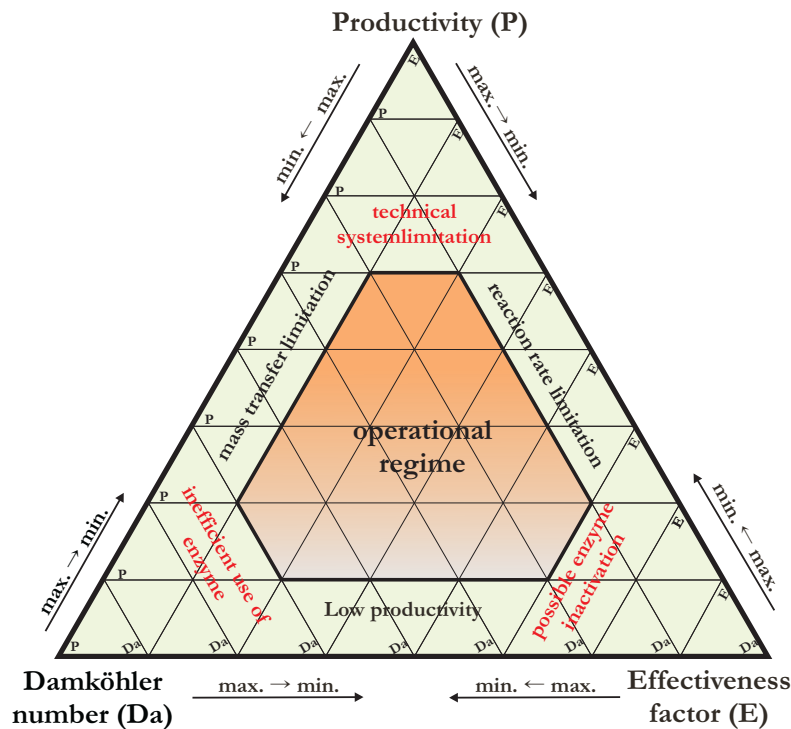
The missing information about the suitability of a given reaction for SFER systems hampers their broad application in biocatalysis. This was demonstrated by studies investigating the application of lyases and lipases in microscale systems (Koch et al. 2008; Swarts et al. 2008). These reactions were obviously not mass transfer limited and thus the outcome of the studies was that there was no benefit from applying those catalysts to a microscale system. The performance was comparable to a lab-scale batch system. The here presented work elaborates a simple approach to evaluate enzymatic reactions for application in a microreactor system. By analysing the Damköhler number (equation 4.6), it is possible to predict whether the enzymatic reaction would profit from the transfer potential of the microsystem. Pompano and co-workers have used the Damköhler number to predict the outcome of autocatalytic reactions in segmented flow systems (Pompano et al. 2008).

### 4.5.1 Tuning reaction, fluidic and system parameters to maximize product formation rates

In microreactor technology, the scale-up from laboratory to production level is achieved by the numbering up or scale out technique (Kashid et al. 2010; Mendorf and Agar 2011). Therefore, optimizing the operational parameters for a single unit is the most essential step to develop a large-scale system operating at maximal output. In this work, various parameters governing the SFER performance were investigated. For the optimal operation of SFER, it is not only important to study the impact of single parameters, but also to evaluate how these factors are interconnected with each other and influence the overall performance of the SFER. There are two approaches to recognize the collective process parameters in two phase systems with an aim to understand and optimize a bioprocess. A mathematical approach requiring numerical computations (Sayar et al. 2009a; Sayar et al. 2009b), or graphical representation referred to as windows of operation (Chen et al. 2007; Woodley and TitchenerHooker 1996). The later approach, has been demonstrated and applied to various examples in system and process development to identify key limitations using qualitative or quantitative windows of operation (Chen et al. 2007; Woodley and TitchenerHooker 1996). In this study, the window of operation approach was extended to a ternary diagram for the conceptual design of the SFER (Figure 4.5). The three variables that form the axes of the ternary diagram are the reaction efficiency or effectiveness factor ( $E$ ), the Damköhler number ( $Da$ ) and the productivity ( $P$ ).

The **effectiveness factor** is defined as the ratio of the actual reaction rate in the presence of mass transfer limitation to the maximum reaction rate possible (no mass transfer limitation). The second variable, the **Damköhler number** (equation 4.6), couples all of the important parameters in the SFER and is used in the ternary diagram as a measure of an individual or collective

parameter. For example, an increase in enzyme concentration, phase ratio and capillary diameter will lead to a rise in the Da number, whereas, the increase in flow velocity and substrate concentration will decrease it. Finally, the third variable on the ternary diagram is the productivity, which governs the system performance. These variables were used to plot a qualitative (Figure 4.5) and quantitative (Figure 4.6AB) ternary diagram correlating the findings of our experimental study. The feasible operational regime is indicated by the shaded region and determined by six factors as shown in Figure 4.5.

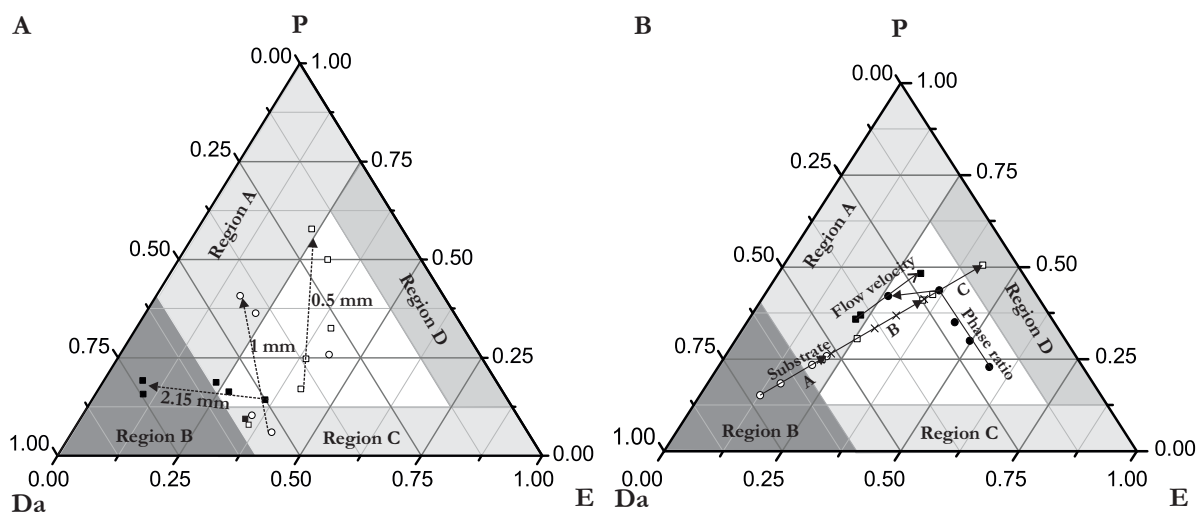


**Figure 4.5: Window of operation for qualitative representation of the Damköhler number (Da) and effectiveness factor (E) plotted as a function of productivity (P).** Each edge of the triangle represents 100% of the respective variable, and the percentage decreases as the variable moves towards the opposite side of the triangle, where it is 0%. Lines drawn show the impact of the individual parameter on Da, P and E. The shaded area indicates the feasible operational area.

Out of these six factors, mass transfer limitation, reaction rate limitation and low productivity regimes result from the very low values of the variable opposite of the respective factor. An enzyme inactivation regime occurs at a very high effectiveness factor combined with a low Da number and low productivity. This sounds contradictorily at first. A high E value means the enzyme is operating at  $V_{max}$ , but as the productivity is low, the amount of enzyme has to be low as well otherwise the productivity should be higher. The low Da number reflects a high mass transfer coefficient, which could be obtained by high velocities and/or a high surface area in a segmented flow system. As seen in chapter 2, these conditions will lead to enzyme inactivation (Karande et al. 2010). This has also been shown by Woodley and co-workers in a typical stirred tank batch reactor and was evaluated in a comparable operating window (Woodley and



TitchenerHooker 1996). A technical system limitation regime occurs at a very high productivity, combined with a low effectiveness factor and a low Da number. In this situation, the system operates at very high enzyme concentrations and necessitates high mass transfer rates to obtain high productivities, which is usually not possible due to the technical system constraints (e.g. stirring speed in batch formats and flow velocities in the segmented flow systems).



**Figure 4.6: Quantitative representation of the experimental data in the ternary plot for the here investigated SFER set-up. A)** Impact of the enzyme concentration in 2.15 mm, 1 mm and 0.5 mm inner diameter capillary as a function of P, Da and E. **B)** Impact of substrate concentration, flow velocity and phase ratio as a function of P, Da and E. The respective regions were plotted based on the experimental data. 1.00 corresponds to 100 %. Region A-Mass transfer limited regime; Region B-Inefficient use of enzymes; Region C-Low productivity regime; Region D-Reaction limited regime; P - Productivity, Da-Damköhler number, E-Effectiveness factor.

At a very high Da number, low effectiveness factor, and low productivity the enzyme is only used inefficiently. In this regime, the system is either operated at a very high enzyme concentration or phase ratio, but is strongly limited by the mass transfer rate. Therefore, most enzyme molecules are unable to perform a reaction because of the low amount of substrate. To enhance the reactor performance, it is essential to move towards the top variable (high productivity), but concurrently keeping the balance of the variables on right and left, and to operate within the shaded region.

For the quantitative representation of the ternary diagram the maximum productivity in the SFER was set to  $150 \text{ mM h}^{-1}$  by extrapolating the data obtained in Figure 4.2A. To achieve the **P-values** the measured productivities were then divided by this maximum of  $150 \text{ mM h}^{-1}$ . To determine the **E-values**, the observed reaction rate in an aqueous-organic 2-phase system was divided by the reaction rate in the single phase system. These two variables (effectiveness factor (E) and productivity (P)) were used to plot the experimental sample points in the ternary diagram. With increasing **enzyme concentration** the system moves towards a mass transfer limited regime (Figure 4.2A). In the ternary diagram, this shift is represented by dotted lines for 2.15 mm,

1 mm and 0.5 mm inner diameter capillaries (Figure 4.6A). At low enzyme concentrations, the system operates at very low productivity (Region C) irrespective of the capillary inner diameters. With increasing enzyme concentration in the 2.15 mm i.d. capillary, the system operation moves into region B where the enzymes are inefficiently used as the system is strongly limited by the substrate transfer from the organic into the aqueous phase. To overcome this situation, thinner capillaries have been used to improve the mass transfer rate and thus the productivity. The capillary inner diameter is directly influencing the segment size which controls the surface area to volume ratio and therefore the mass transfer rate. However, at very high enzyme concentrations the system performance again moves towards the mass transfer limited regime (Region A).

Our experimental results have shown an increase in the STY in parallel to the **flow velocity** (Figure 4.2B). The flow velocity mainly attributes to the internal circulations within the segments, which influences the mixing and enhances the mass transfer rates (Karande et al. 2010). This is well mirrored in the ternary diagram where the system operation moves from mass transfer limited regime (Region A) into the feasible operational area. Changing the **phase ratio** has an impact on both the mass transfer and the reaction rate. By increasing the phase ratio, the organic segments become shorter as compared to the aqueous segments which results in a higher surface area of the aqueous phase and an increase in the substrate transfer rate. However, the change in the aqueous segment is further compounded by the rise in the enzyme to substrate ratio, which in turn enhances the reaction rate and shifts the reaction towards a mass transfer limited regime. This is well reflected in the ternary diagram, where the productivity improves with the phase ratio at the cost of effectiveness factor. At a certain phase ratio (phase ratio 1.5, Figure 4.3A) the system operation moves towards mass transfer limited regime (Region A, Figure 4.7B) with an increasing Da number.

The **substrate concentration** in the organic segments has to be correlated to the respective capillary diameter (Figure 4.3B). The product formation rate is higher in the smaller capillaries as compared to the bigger ones at low substrate concentrations (Figure 4.3B). At 1-heptaldehyde concentrations above 1 mM, TADH is inhibited by the substrate in the single phase system (data not shown). In the segmented flow a substrate concentration of 100 mM in the organic phase corresponds to 1 mM in the aqueous phase at equilibrium (partition coefficient of 100), which is reached only in the smallest capillaries because of higher mass transfer rate. Therefore the product formation rate is higher in the smaller capillaries as compared to the bigger ones at 100 mM (Figure 4.3B). In the ternary diagram (Figure 4.6B); this enhancement is represented by lines A, B and C for 2.15 mm, 1 mm and 0.5 mm capillaries, respectively. Productivity and effectiveness factor are improved in the initial phase, whereas the Da number is lowered.

However, in the later stage, the observed reaction rate is reduced due to substrate inhibition for the 1 mm and 0.5 mm capillaries and the system operation follows the same line but in the reverse direction. Here the productivity and effectiveness factor are reduced, whereas the Da number is increased. As the Da number does not account for substrate inhibition of the enzyme further improvement to integrate this limit is necessary.

The interconnection between the experimental parameters studied and their impact on the overall performance of the SFER can now be visualized in the ternary diagram. As this figure defines the reactor operation, the windows of operation may be used as guidance for strategic improvement in reactor design. As an example a new reactor setup was developed to maximize the product formation at higher substrate concentration (Figure 4.4). This was based on the move from line A to B and from B to C the ternary diagram (Figure 4.6B). Technically this was obtained by assembling the 2.15 mm, 1 mm and 0.5 mm capillaries in series and starting the conversion at a substrate concentration of 300 mM. In this system it was possible to produce 85 mM of the product 1-heptanol in 105 min, which was 1.3 fold higher than the maximum reached in a SFER set-up using a 2.15 mm inner diameter single capillary (Table 4.2). One of the critical parameter during this approach was the adjustment of the optimal surfactant concentration. Tween 20 is necessary to stabilize the enzyme but it also decreases the surface tension and thus destabilizes the segmented flow at a certain concentration. The amount of surfactant added is depending on the surface area, which changes with the capillary inner diameter and thus is different throughout the reactor if using a coupled approach (Figure 4.4). Nevertheless, the surfactant concentration applied stays constant and cannot be adjusted to the different diameters. As a consequence the enzyme becomes inactivated at some point. If the system is running for a longer time, the inactivation of the enzyme is significant, leading to an overall lower production rate. In this case it is better to use a larger sized capillary, where the optimal surfactant concentration is present throughout the reactor reducing the enzyme inactivation (Table 4.2). For short residence times the coupled approach performs better.

## 4.6 Conclusion

The segmented flow system is a promising tool to enhance enzymatic reactions limited in rate by mass transfer. The results presented in this work point out the system boundaries that affect the product formation rates in the SFER. The segmented flow eliminates emulsion formation and thus significantly reduces workup and of downstream phase separation. The synthesis of 1-heptanol using TADH and FDH in the segmented flow system sets a benchmark to perform enzymatic transformations in segmented flow microsystems. The presented work is the basis for implementing enzymatic reactions in microsystems to a scalable level using the numbering technique.

## Acknowledgments

We thank Prof. Martina Pohl (Forschungszentrum Jülich) for the kind gift of plasmids containing formate dehydrogenase genes. Furthermore, we thank Dr. Jonathan Collins for his expert support during vacuum distillation. This work was financed by the ZACG (Zentrum für Angewandte Chemische Genomik), the European Union (EFRE) and by the Ministry of Innovation, Science, Research and Technology of North Rhine-Westphalia.

## Chapter 5

### The Segmented Flow Biofilm Microreactor- A Novel Reactor Concept

Rohan Karande, Katja Buehler and Andreas Schmid

Katja Buehler and Andreas Schmid coordinated and supervised the project and corrected the manuscript

Experimental basis for patent “Segmented flow biofilm reactor”  
(WO/2012/152337)

## 5.1 Summary

Biofilm reactors are very often mass transfer limited due to excessive biofilm growth which hampers overall reactor performance. This work aimed at developing a biofilm microreactor containing a very large surface area ( $2000\text{-}4000\text{ m}^2\text{ m}^{-3}$ ) to grow a compact and homogenous biofilm without clogging the capillary system. As fluidic conditions play a key role for the development of the biofilm structure, we investigated the effect of aqueous-air interfacial forces on biofilm morphology and reactor performance. A simple three step method was developed allowing stable biofilm formation under aqueous-air segmented flow conditions: i) development of a first-generation biofilm during single phase flow, ii) introduction of air segments which discarded most of the well grown biofilm, iii) development of a second-generation biofilm in the presence of air-aqueous segments. The application of segmented flow have several advantages on the biofilm development: enhanced biofilm growth rate, faster spatial distribution, and a significantly compact kind of biofilm in comparison to biofilms grown in single phase flow. Furthermore, the applicability of SFBMR was investigated for several biofilm catalyzed reactions such as octane and cyclohexane hydroxylation, and styrene epoxidation. For styrene epoxidation to (*S*)-styrene oxide (ee > 99%), oxygen transfer was the key limiting factor and the volumetric productivity ( $11\text{ to }46\text{ g L}_{\text{tube}}^{-1}\text{ day}^{-1}$ ) was enhanced by 4-fold by increasing the air flowrate. This work adds a new direction to engineer biofilm structure and to exploit them in microreactors which have the merits to form a suitable platform technology.

## 5.2 Introduction

Biofilms are ubiquitous life form in nature, around and within us (Hall-Stoodley et al. 2004). They are microbial communities embedded within a self-produced matrix, which grow at the interface of liquids and solids. Biofilms are very robust structures and can endure a wide range of physical, chemical and biological stresses (Hall-Stoodley et al., 2004; Nicolella et al., 2000; Qureshi et al., 2005). Their unique features of self-immobilization, regeneration, and high biomass retention have driven research towards application of biofilms as biocatalysts for chemical synthesis (Halan et al., 2012). Biofilms can circumvent classical pitfalls of planktonic cell based bioprocesses such as short term operational stability, toxicity associated issues, and low volumetric productivities (Halan et al., 2011; Nicolella et al., 2000). To fully exploit biofilm potential, novel reactor configurations have been developed on the laboratory and pilot scales (Halan et al., 2012; Qureshi et al., 2005).

Key parameters essential for biofilm reactor design are (i) a large solid-liquid surface area for biofilm growth, (ii) a solution to cope with excess biomass and (iii) high oxygen transfer in case of aerobic biofilms. In the last decade, continuous miniaturized reactors have emerged as a potent technology due to high surface area to volume ratios, which are typically in the range of 2000-4000  $\text{m}^2 \text{m}^{-3}$ , and easy scale-up using parallelization of units (Roberge et al., 2008). Typically, the catalysts are deposited on the large surface of such reactors resulting in a reactive coating, and are applied for fine chemical synthesis, enzymatic transformations (chapter 4), and energy generation (Kreutzer et al., 2005). Gross and co-workers utilized the large surface area of capillary microreactors to maximize biofilm growth and thereby volumetric productivities for a biotransformation (Gross et al., 2007). Despite higher biomass ( $45 \text{ Kg m}^{-3}$ ), the overall reactor performance was reported to be mass transfer limited and oxygen was identified as the key limiting compound (Gross et al., 2010). Strikingly, more biomass leading to a thick biofilm will not contribute to the improved reactor performance because oxygen will be completely consumed within the upper layers of a biofilm (depth of 100 to 200  $\mu\text{m}$ ) (chapter 1 section 1.3.1), but may lead to a high risk of system clogging. Thus, excessive biofilm growth restricts the applicability of biofilm microreactors, calling for a good mechanism to remove excess biomass and thereby to achieve a high amount of active biofilm. Biofilm growth and structure are associated with the growth conditions, and are strongly affected by the fluidic conditions. High shear stress accomplished by turbulent flow usually leads to compact and dense biofilms, while bulgy and patchy biofilms develop under a moderate or low shear stress attained by laminar flow (Picioreanu et al., 2000).

This work introduces a segmented flow biofilm microreactor, with a novel strategy to apply aqueous-air segmented type of flow to overcome excessive biofilm growth and oxygen limitation. The (aqueous-air) segmented flow impose fluidic forces such as interfacial forces which becomes highly dominant at miniaturized scale, and shear forces caused by the axial movement of air segments and the wall (Burn et al., 2001 and Burn et al., 2002). These forces strongly influence biofilm development. Continuous injection of air segments showed a positive impact on the biofilm growth, spatial distribution, and biofilm compactness without any clogging issues in comparison to the biofilm grown under single phase flow. The performance of the segmented flow biofilm membrane reactor (SFBMR) was evaluated with *Pseudomonas. putida* PpS81 pBT10 biofilms, which employed the hydroxylation of octane to n-octanol. Further, the versatility of SFBMR was shown using the long term biocatalytic hydroxylation of cyclohexane to cyclohexanol by *Pseudomonas sp.* KT2440 pCom8-PFR1500 biofilms and the epoxidation of styrene by *Pseudomonas sp.* Strain VLB120 $\Delta$ C biofilms. Overall, this work reports the development of the SFBMR concept for continuous biocatalytic production of chemicals.



### 5.3 Materials and Methods

The strain and plasmids used in this study are listed in Table 5.1. All organisms used have been cultivated in Luria-Bertani (LB) medium or M9-medium supplemented with 0.5% (w/v) glucose as a carbon source, US\* trace elements (Emmerling et al. 2002), and the appropriate antibiotics (streptomycin 100  $\mu\text{g mL}^{-1}$ ; tetracycline 100  $\mu\text{g mL}^{-1}$ ; kanamycin 100  $\mu\text{g mL}^{-1}$ ).

*Pre-culture cultivation:* Pre-cultures of *P. putida* PpS81 pBT10, *Pseudomonas* sp. VLB120 $\Delta$ C and *P. putida* KT2440 pCom8-PFR1500 were grown overnight in 5 mL LB-medium using baffled 50 mL Erlenmeyer flasks in a horizontal shaker (30°C and 200 rpm, Multitron, Infors HT, Bottmingen, Switzerland).

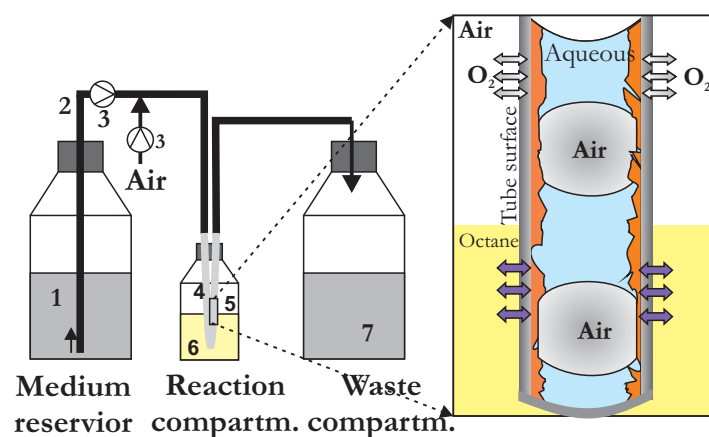
**Table 5.1: Strains and plasmids used in this study**

Strain	Remarks	References
<i>Pseudomonas</i> sp. Strain VLB120	biofilm forming strain isolated from a styrene degrading biofilter	(Panke et al. 1998) (Gross 2010)
<i>Pseudomonas putida</i> PpS81	chromosomal knockout mutant of <i>P.putida</i> GPo1 lacking a medium chain-length alcohol	(Grund et al. 1975)
<i>Pseudomonas putida</i> KT2440	<i>P.putida</i> mt-2 cured of the TOL plasmid, solvent sensitive	(Bagdasarian et al. 1981)
Plasmids	Remarks	References
pBT10	pCom10 derivative, with <i>alkBFG</i> , <i>alkST</i> genes from pGEc47	(Gross 2010)
pCom8-PFR1500	Contains genes for CYP153A6, ferredoxin, and ferredoxin reductase from <i>Mycobacterium</i> sp. Strain HXN-1500 in broad host-range vector pCom8 under control of the <i>alk</i> regulatory system; Gm <sup>r</sup>	(van Beilen et al. 2005)

#### 5.3.1 (Aqueous-air) segmented flow biofilm membrane microreactor (SFBMR): setup and operation

A schematic view of this set-up is shown in Figure 5.1. The system can be divided into three sections: the medium reservoir, the reaction compartment, and the waste outlet. A four channel peristaltic pump (Ismatec, Glattbrugg, Switzerland) was fitted with two 1.5 mm inner diameter pump tubing (Ismatec Tygon MHLL, Glattbrugg, Switzerland) to pump M9 minimal medium and filtered air through the reaction compartment. The reaction compartment consisted of silicone tubing with different dimensions depending on the catalyst used. The system was heat sterilized (Table 5.2) and inserted into a closed 100 mL glass bottle submerged in biotransformation substrate. The inner tube surface served as growth surface for the biocatalyst.

The reaction compartment was placed in a thermo-bath to maintain the reaction temperature of 30°C. The reactor was inoculated by filling the silicone tubes with an overnight culture of the respective biofilm forming strain as given in Table 5.2. The flow was turned off for 2 h to allow the organisms to attach to the inner tube surface. Thereafter, the medium flow was turned on again and after 3-4 days the filtered air flow was started.



**Figure 5.1: Scheme of the aqueous-air SFBMR for the production of octanol, cyclohexanol or styrene oxide with biofilm forming organisms.** 1: medium reservoir; 2: 1.5/2 mm silicone tubing; 3: peristaltic pump; 4: silicone tubing as growth surface; 5: air phase; 6: octane phase; 7: waste. The magnified sketch of aqueous-air segments describes the mass transfer scheme of substrates in to the biofilm.

**Table 5.2: Parameters applied in the SFBMR setup**

Strain	Silicone tube (i.d. × length)	Reaction	Organic phase (mL)	Air flow (aqueous flow)	Biofilm tube in the organic phase (%)
<i>P. putida</i> PpS81 pBT10	2 mm × 250 mm	Octane to octanol	Octane (20 ml)	0.05 mL min <sup>-1</sup> (0.05 mL min <sup>-1</sup> )	20%
<i>Pseudomonas</i> sp. KT2440 pCom8- PFR1500	2 mm × 1000 mm	Cyclohexane to cyclohexanol	50%(v/v) cyclohexane and 50%(v/v) BEHP (40 to 100 mL)	0.1 mL min <sup>-1</sup> (0.1 mL min <sup>-1</sup> )	0 to 100%
<i>Pseudomonas</i> sp. Strain VLB120ΔC	2 mm × 2000 mm	Styrene oxide	Styrene (80 mL)	0.25 - 4 mL min <sup>-1</sup> (0.25 mL min <sup>-1</sup> )	80%

BEHP-Bis(2-ethylhexyl)phthalate

### 5.3.2 Sample preparation and analysis

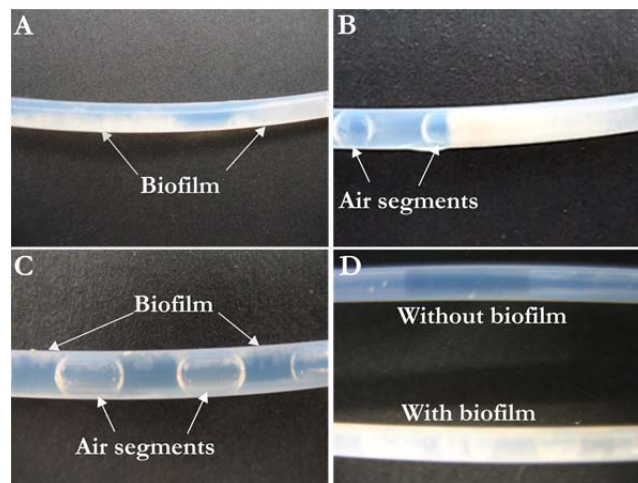
Aqueous phase samples were extracted with an equal amount of ice cold diethyl ether containing 0.2 mM of dodecane or decane as an internal standard, and mixed in an thermo mixer (1400 rpm, 10°C) for 2 min to extract the compounds into the ether phase. After quick spinning the samples in a micro-centrifuge (Thermo Electron Corporation, Langensfeld, Germany), the ether phase was separated and dried by adding sodium sulphate prior to gas chromatography (Focus GC, Thermo Electron Corporation, Dreieich, Germany) using a chiral RT-βDex-sm column (30m×0.25 mm×0.25μm; Restek GmbH, Bad Homburg, Germany). The organic phase samples

were diluted 1:10 times in ice cold diethyl ether, dried with sodium sulphate, and analyzed as described above.

## 5.4 Results

### 5.4.1 Biofilm development in the presence of segmented flow – a crucial task

In order to exploit the potential of biofilms in the segmented flow set-up, conditions that allow biofilm growth in the presence of segmented flow had to be identified. Two parallel experiments were performed to investigate biofilm development under segmented flow conditions. In both approaches, tubings were filled with an overnight culture of *P. putida* PpS81 pBT10 and kept idle for 2 h to seed the cells on to the inner surface of the tubing. Biofilm formation was either initiated by feeding nutrients via a fixed single phase flowrate or by starting an aqueous-air segmented flow. After 3 days, biofilm was visible under single phase flow conditions (Figure 5.2A), while no biofilm was observed in the air-aqueous segmented flow mode. This effect might result from the high fluidic stress implied by the segmented flow on the capillary wall, which obviously detaches the adhered cells and prevents biofilm formation at this initial stage. In contrast, the single aqueous phase flow implied low fluidic stress on the capillary walls enabling biofilm establishment.



**Figure 5.2: Biofilm grown under single aqueous phase flow and aqueous-air segmented flow conditions.** (A) Biofilm grown on the PTFE surface after 3 days of continuous medium flow. (B) Biofilm detached from the surface of PTFE tubing after the injection of air segments. (C) Recolonization of the biofilm on to the surface of PTFE tubing after 1 day of continuous injection of air segments. (D) After 8 to 10 days, PTFE tube without biofilm (above for comparison) and mature biofilm grown on to the surface of PTFE tubing (below). Biofilm adaptation in the presence of segmented flow was similar in silicone and PTFE tubings, but due to high transparency of PTFE tubing we have displayed their images.

In the next step, air segments were injected into the well-grown biofilm capillary. As soon as the air segments were injected, the biofilm trashed and was flushed out of the capillary tubing (Figure 5.2B). Surprisingly, by continuing the segmented flow for 1 day, the biofilm seemed to adapt to the segmented flow conditions and was able to recover on the surface of the capillary wall (Figure 5.2C). In the next 3 days, distinct biofilm growth was clearly visible on the complete surface of the silicone tube in the presence of aqueous-air segmented flow (Figure 5.2D). Overall, three

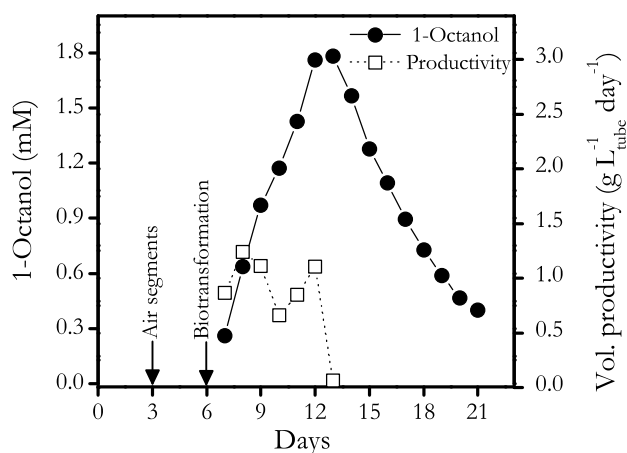
steps are necessary to allow biofilm growth in the presence of segmented flow: predevelopment of biofilm during single phase flow (first generation biofilm), detachment of cells and biofilm during aqueous-air segmented flow, and adaptation and regrowth of biofilm under segmented flow conditions (second generation biofilm).

#### 5.4.2 Performance of segmented flow biofilm membrane reactors

After successfully developing a biofilm under segmented flow conditions, the applicability of SFBMRs was evaluated for octanol, cyclohexanol and styrene oxide synthesis.

##### SFBMR for octanol synthesis

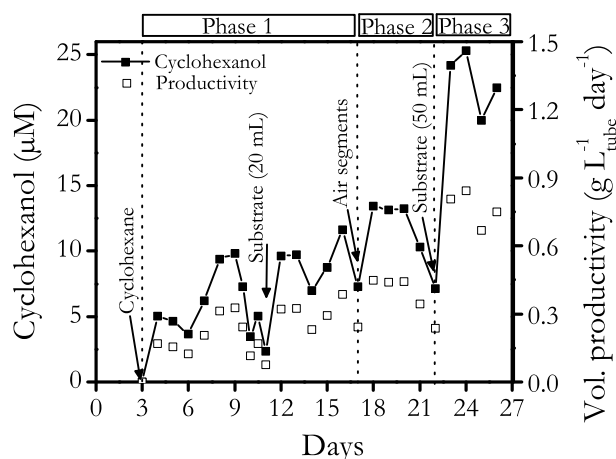
In this set-up, oxygen supply was ensured by directly inserting air segments into the aqueous flow as well as by diffusion through an oxygen permeable silicone tubing as depicted in Figure 5.1. The biotransformation was initiated by inserting tubing containing well grown biofilm into a closed compartment with (approx.) 20% of the tube being directly submerged in octane. Octane diffused through the silicone membrane into the biofilm, where it was converted to octanol, which was then extracted back into the octane phase. Nearly 1.8 mM octanol could be accumulated in 20 mL organic phase during 7 days of biotransformation, which corresponds to an average volumetric productivity of  $1 \text{ g}_{\text{octanol}} \text{ L}_{\text{tube}}^{-1} \text{ day}^{-1}$  (Figure 5.3). After 7 days of biotransformation, the octanol concentration declined to 0.3 mM, probably because of product degradation by the host intrinsic dehydrogenases. However, during the first 7 days of biotransformation the volumetric productivity in the segmented batch mode was two-fold higher than the non-segmented batch mode (data not shown here), indicating a positive effect of the additional air supply.



**Figure 5.3: Octanol production and volumetric productivity in the air-aqueous segmented flow biofilm reactor for octane reduction using silicone tubing.** Air segments were added to the aqueous flow after 3 days; after 6 days the biotransformation was started by the addition of octane into the reaction compartment.

### SFBMR for cyclohexanol synthesis

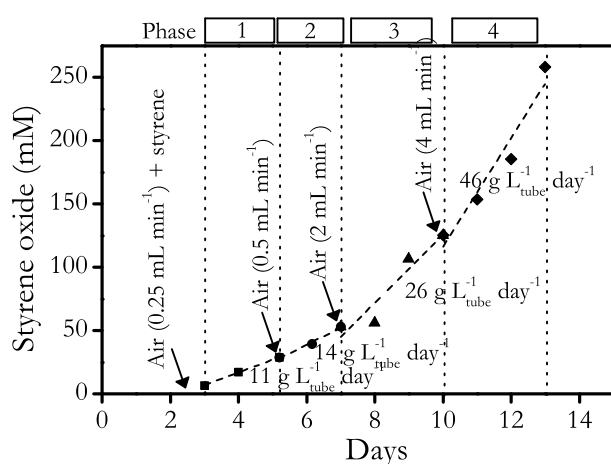
Cyclohexanol synthesis was initiated by inserting tubing containing *Pseudomonas sp.* KT2440 pCom8-PFR1500 biofilm into a compartment where (approx.) 40 % of the tube was directly submerged in an 50 % (v/v) cyclohexane–BEHP phase. While the organic substrate (cyclohexane) diffused through the silicone membrane into the biofilm, the product cyclohexanol was continuously stripped through the aqueous phase and was not extracted into the organic phase. The reactor operation can be distributed into three phases. First the reactor performance was evaluated under aqueous flow conditions. Approximately 10  $\mu\text{M}$  cyclohexanol could be stripped into the aqueous phase after 5 days of biotransformation, which corresponds to an average volumetric productivity of  $0.3 \text{ g}_{\text{cyclohexanol}} \text{ L}_{\text{tube}}^{-1} \text{ day}^{-1}$  (Figure 5.4; Phase 1). After 8 days of biotransformation, the cyclohexanol concentration in the aqueous phase declined to 2  $\mu\text{M}$ . This was most probably due to substrate limitation as cyclohexane easily evaporated out of the system. Upon addition of 20 mL cyclohexane to the organic phase, the cyclohexanol synthesis rate increased again to the average volumetric productivity of  $0.3 \text{ g}_{\text{cyclohexanol}} \text{ L}_{\text{tube}}^{-1} \text{ day}^{-1}$ . After 17 days air segments were injected into the aqueous flow. This resulted in only a slight improvement in the cyclohexanol product formation and after 3 days of stable cyclohexanol synthesis (13  $\mu\text{M}$ ), the product concentration declined (Figure 5.4; Phase 2). Completely submerging the tube containing biofilm in the organic phase resulted in a significant increase in the product concentration in the outlet stream, which corresponds to an increase in the volumetric productivity by 2 fold (Figure 5.4; Phase 3).



**Figure 5.4: Cyclohexanol production and volumetric productivity in the air-aqueous segmented flow biofilm reactor for cyclohexane reduction using silicone tubing.** The biotransformation was started by the addition of cyclohexane into the reaction compartment on the 3rd day and air segments were added to the aqueous flow after 17 days.

### SFBMR for styrene oxide synthesis

In this set-up, the biotransformation was initiated by inserting silicone tubing containing *Pseudomonas sp.* Strain VLB120 $\Delta$ C biofilm into a closed compartment with approx. 80 % of the tube being submerged in styrene (Figure 5.1). Styrene diffused through the silicone membrane into the biofilm, and most of the product formed was extracted back into the styrene phase while a very small fraction was stripped into the aqueous phase. The reactor operation is divided in four phases depending on the increment in air flow rates (Figure 5.5). In phase I, the system was operated with an equal air to aqueous flow at 0.25 mL min<sup>-1</sup> and a dilution rate of 4.8 h<sup>-1</sup>. The product concentration in the organic phase increased linearly at an average volumetric productivity of 11 g<sub>sty. oxid.</sub> L<sub>tube</sub><sup>-1</sup> day<sup>-1</sup>, which corresponds to 14 mmol L<sub>tube</sub><sup>-1</sup> h<sup>-1</sup> of oxygen (based on stoichiometric amounts) being consumed in the epoxidation reaction. In the next phase, the air flow was increased to 0.5 mL min<sup>-1</sup> while the aqueous flow was kept constant at 0.25 mL min<sup>-1</sup>, which resulted in an improved volumetric productivity of 14 g<sub>sty. oxid.</sub> L<sub>tube</sub><sup>-1</sup> day<sup>-1</sup>. Although the air flow was doubled the volumetric productivity only increased by 1.4 fold, probably because the oxygen is channelized for the endogenous respiration and epoxidation reaction. In phase 3, the air flow was increased by 4-fold attaining 2 mL min<sup>-1</sup> and a dilution rate of 21.5 h<sup>-1</sup>. Thereby styrene oxide concentration in the organic phase reached 125 mM with an average volumetric productivity of 30 g<sub>sty. oxid.</sub> L<sub>tube</sub><sup>-1</sup> day<sup>-1</sup>, which correspond to 1.85 fold increase in productivity. In the final phase (4), the air flow was further increased to 4 mL min<sup>-1</sup> with a dilution rate of 40.6 h<sup>-1</sup>. A total of 250 mM styrene oxide could be accumulated in 80 mL organic phase with the average volumetric productivity of 46 g<sub>sty. oxid.</sub> L<sub>tube</sub><sup>-1</sup> day<sup>-1</sup>. Overall, this result clearly shows that the increase in air flow from 0.25 to 4 mL min<sup>-1</sup> improved the volumetric productivity by 4 fold.



**Figure 5.5: Styrene oxide accumulation and the corresponding volumetric productivity in the air-aqueous segmented flow biofilm reactor using silicone tubing (basic setup shown in Figure 5.1). After 2 days the biotransformation was started by the addition of styrene into the reaction compartment. At the same time the air flow was started.**

## 5.5 Discussion

Conventional biofilm reactors can be classified as fixed bed reactors, where the biofilm attached to a surface does not move with respect to a fixed reference frame, and expanded bed reactors, where the feed stream flowing upwards through the catalyst bed expands the bed and maintains it in a fluidized state (Cheng et al. 2010; Qureshi and Maddox 1988). The most important advantage of fixed bed biofilm reactors is the high surface area for biofilm growth. In such reactor formats, the production rates increase with biofilm thickness and reach a maximal level when mass transfer of nutrients, oxygen and substrate become limiting factors due to undefined fluid flow and the absence of mixing. The expanded bed reactors benefit from good mixing, but suffer from their increased size, low gas dissolution rates and high energy costs (Nicolella et al. 2000). For the organic components having low water solubility biofilm reactor design requires a higher degree of complexity. Additionally, the  $\log P_{O/W}$  values of these substrates and products are in the range of 1 to 4, which typically is considered toxic to whole cells (Laane et al. 1987). The application of an organic phase in addition to the aqueous phase, which serves as substrate reservoir and product sink, is a straight forward solution to overcome substrate low solubility issue and to obtain efficient biomass utilization. However, multiphase biofilm reactors, which consist of organic-aqueous-air phases together with the biofilm makes the design fairly complex. Major issues in reactor design are substrate supply, proper phase ratios, and high interfacial mass transfer to attain maximum reactor performance. The development of segmented flow biofilm microreactor configurations was based on addressing these issues.

### 5.5.1 Biofilm establishment in the presence of segmented flow

Biofilm formation can be divided into three main steps; initial cell attachment, micro- and macrocolonies formation and growth (Cheng et al. 2010). During initial cell attachment, living cells anchor to a solid surface at the aqueous-solid phase boundary. The process of cell attachment is dependent on several parameters such as surface conditioning, nature of substratum, medium, and cell properties. If the conditions are favorable, the attached cells will start to grow microcolonies, which will develop to macrocolonies and excretion of EPS. Nevertheless, if cells anchored on a surface experience high shear force of fluid, which is larger than the adsorption energy holding the cells, then cells will no longer remain bound to the surface. Such observation of cell detachment by shear stress arising from bulk fluid motion has been confirmed by several authors (Korber et al. 1989; Lawrence and Caldwell 1987). In case of air-aqueous segmented flow, air segments are stretched to fit inside the capillary, and a thin film of liquid remains intact between the segment and the capillary wall (Burns and Ramshaw 2001). The interfacial forces are highly dominant in this type of flow which causes shear stress between



the wall surface and the segment axis (Burns and Ramshaw 2001; Burns and Ramshaw 2002). These forces might have been higher than the characteristic shear stress, which detach adhered cells and avoid biofilm formation. A similar observation of bacterial detachment by the addition of micro-bubbles to the continuous flow was reported by (Sharma et al. 2005a; Sharma et al. 2005b).

To overcome cell detachment by segmented flow, the attached cells should gain additional mechanical stability before switching the flow mode to segmented flow. This was accomplished by allowing the biofilm to mature before injecting the air segments into the system. Although the air segments dislodged a significant part of biofilm from the tubing, a certain amount of cells stayed attached to the inner capillary wall and started to develop a biofilm during 24 h (Figure 5.2B and C). Similar observations of biofilm recolonization after dislodging well grown biofilm by applying dynamic fluidic stress through single phase flow or by using laser irradiation have been reported (Korber et al. 1989; Nandakumar et al. 2003; Rittmann 1982). The biofilm grew much more homogeneously and compact under segmented flow conditions, eventually covering a larger area of the capillary tubing after the organisms adapted to the high shear stress (comparison Figure 5.2A and D). The recolonization of the biofilm is the key event to develop a stable biofilm under high shear stress of segmented flow, allowing for an improvement in the catalytic surface area.

### 5.5.2 Versatility and applicability of SFBMR

Regardless of the exceptional potential of biochemical hydroxylation reactions for industrial applications, only a few biocatalytic processes have been implemented on industrial scale. The major limitations are either on the side of biocatalyst or on the technical side regarding reactor configurations. Efficient oxygen transfer is one of the key design bottlenecks that limit the overall performance of such bioprocess. Membrane attached biofilms are a promising concept to maximize the oxygen transfer in biofilm reactors. The oxygen transfer rate over the silicone membrane was estimated to be  $30 \text{ g m}^{-2} \text{ day}^{-1}$  (Gross et al. 2010), which corresponds to  $60 \text{ g L}^{-1} \text{ day}^{-1}$  for 2 mm inner diameter silicone tube (surface to volume ratio of  $2000 \text{ m}^{-1}$ ). This oxygen transfer rate resembles  $350 \text{ U L}_{(\text{aq})}^{-1}$  which would allow an average biofilm oxygenase activity of  $115 \text{ U L}_{(\text{aq})}^{-1}$  assuming an endogenous respiration of  $235 \text{ U L}_{(\text{aq})}^{-1}$  (van Beilen et al. 2003). This estimation clearly indicate that there is an upper limit ( $115 \text{ U L}_{(\text{aq})}^{-1}$  biofilm oxygenase activity) and above this limit the membrane biofilm reactor is primarily constrained by oxygen transfer.

One of the solutions to maximize the oxygen transfer is to apply smaller diameter tubes with high surface area to volume ratios. The downside of this approach is the increased risk of reactor clogging due to biofilm growth. The aqueous-air segmented flow is a technical solution to

maximize the oxygen transfer. However, if the reactions are not oxygen transfer limited then there is no major benefit in applying segmented flow. Looking at octanol and cyclohexanol synthesis, the maximum volumetric activities achieved have been in the range of 5 to 7 U L<sub>(aq)</sub><sup>-1</sup> (Table 5.3). This is well below the membrane transfer limits. Thus, such reactions are primarily constrained by the biocatalyst rather than the mass transfer over the membrane. Although the activities are very low, slight improvements in volumetric productivities were observed after applying segmented flow in the case of cyclohexanol synthesis (Figure 5.4). The homogenous and compact reestablishment of the biofilm in the presence of segmented flow might result in larger biofilm surface area and improved volumetric activity. Nevertheless, the true benefit of aqueous-air segmented flow was accomplished for the reaction which is oxygen limited (Figure 5.5). In this case, the styrene oxide volumetric activity was enhanced by simply increasing the flow rates (Table 5.3). Higher volumetric productivities with increased flow rates may be caused by the improvement in air/oxygen supply. Another reason could be the enhanced oxygen transfer rates because of the longer air segments sizes which led to high interfacial area between the air-liquid surfaces. Overall, optimization of air flow shifted the mass transfer boundaries, but what are the limits of oxygen transfer in such segmented flow systems?

Kreutzer *et al.*, 2001 studied the physical absorption of oxygen in water for aqueous-air segmented flow and calculated the oxygen transfer coefficients in the range of 0.1 to 1 s<sup>-1</sup> (Kreutzer et al. 2001). By assuming the oxygen concentration in the aqueous phase to be 200 μm and an oxygen mass transfer coefficient of 0.1 s<sup>-1</sup>, the oxygen transfer rate corresponds to 1200 U L<sub>(aq)</sub><sup>-1</sup>, which is 3.5 fold higher than the membrane oxygen transfer rate. These figures equal the oxygenase activity of 400 U L<sub>(aq)</sub><sup>-1</sup> (while endogenous respiration is assumed to be 800 U L<sub>(aq)</sub><sup>-1</sup>), which is close to the experimental value (320 U L<sub>(aq)</sub><sup>-1</sup> oxygenase activity) achieved in phase 4. These figures are based on the assumption of 0.1 s<sup>-1</sup> oxygen mass transfer coefficient, and by the improvement in the mass transfer coefficients up to 1 s<sup>-1</sup> high volumetric activities are still attainable, which elaborates the potential of SFBMR.

Other most important aspects of these aqueous-air SFBMR are: I) Long term biotransformation due to self-immobilization and self-renewal capability of biofilms. II) Encapsulation of microorganisms in an EPS matrix enabling continuous biotransformation in the presence of toxic substrates and fluidic shear stress. III) Flow conditions can be easily tuned to adjust phase ratios and segment sizes. IV) Biofilm growth can be controlled by regulating shear stress implied through flow velocity.

**Table 5.3: Performance comparison of SFBMRs studied**

Product (reactor dimension)	Strain	Reactor operation	Air flow mL min <sup>-1</sup> (air/aqueous)	Activity U L <sup>-1</sup> (g L <sup>-1</sup> h <sup>-1</sup> )	Membrane O <sub>2</sub> transfer U L <sup>-1</sup>	Remarks
Octanol (2 mm × 250 mm)	<i>P. putida</i> PpS81 pBT10		0.05 (1:1)	5 (1)	68	Limitation on biocatalyst level (low activity)
Cyclohexanol (2 mm × 1000 mm)	<i>Pseudomonas sp.</i> KT2440	Phase 1	0 (0:1)	2 (0.3)	45	Limitation on biocatalyst level
		Phase 2	0.1 (1:1)	3.5 (0.5)	45	Improvement in mass transfer due to segmented flow
		Phase 3	0.1 (1:1)	7 (1)	16	High contact between the biofilm tube with organic phase led to improved volumetric productivity
Styrene oxide (2 mm × 2000 mm)	<i>Pseudomonas sp.</i> VLB120ΔC	Phase 1	0.25 (1:1)	76 (11)	32	Oxygen transfer limited
		Phase 2	0.5 (2:1)	97 (15)	32	Oxygen transfer limited
		Phase 3	2 (8:1)	180 (30)	32	Oxygen transfer limited
		Phase 4	4 (16:1)	320 (46)	32	Upper limit of oxygen transfer based on the k <sub>l</sub> a of 0.1 s <sup>-1</sup> in aqueous-air segmented flow

Oxygen transfer rate through silicone membrane 80 U L<sup>-1</sup> (Gross et al. 2010).

## 5.6 Conclusions

A three step method was developed to maintain constant biofilm growth under segmented flow conditions. The SFBMR system is rather flexible to adopt new biofilm transformations. The styrene oxide volumetric productivity was enhanced four-fold by maximizing the air segment flow rates. Thus, SFMBR is a promising alternative for the conventional biofilm reactors and it has the merits to form a suitable platform technology for several biofilm catalyzed reactions. This now sets the basis for executing biofilm catalysed reactions in membrane based microreactors to a higher scale using the numbering technique.

## Acknowledgments

This work was financially supported by the Deutsche Bundesstiftung Umwelt (DBU) and by the Ministry of Innovation, Science, Research and Technology of North Rhine-Westphalia.

## Chapter 6

### (Aqueous-Air-Organic) Three-Phase Segmented Flow Biofilm Microreactor

Rohan Karande, Katja Buehler and Andreas Schmid

Katja Buehler and Andreas Schmid coordinated and supervised the project and corrected the manuscript

Experimental basis for patent “Segmented flow biofilm reactor”  
(WO/2012/152337)

## 6.1 Summary

In the present study, the concept of a three-phase (aqueous-air-organic) biofilm microreactor was developed and evaluated. The contacting pattern between the biofilm and the other phases (aqueous-air-organic phases) was ensured by using a segmented type of flow. Different biotransformation reactions were evaluated in the aqueous-air-organic-biofilm microreactor system. Biofilms were observed to be stable and active over long periods (15 to 30 day), irrespective of the solvent stress and the fluidic stress. Other advantages of SFBRs include compact size, and maximum utilization of biofilm coverage as the biofilm and the liquid/gaseous phases (aqueous, air, and organic) are in direct contact. For octane hydroxylation, the application of a segmented flow biofilm reactor (SFBR) showed 2-fold improved productivities as compared to the segmented flow biofilm membrane reactor (SFBMR) described in chapter 5. Nevertheless, very low conversion rates observed due to short residence time is the key bottleneck that limits the applicability of such SFBR in comparison to SFBMR (chapter 5).

## 6.2 Introduction

In nature most microorganisms have the ability to attach on a surface, develop colonies, secret extracellular polymeric matrix (EPS) and subsequently get embedded in the EPS to form biofilms (Hall-Stoodley et al. 2004). This adaptation protects microorganisms against harsh environmental conditions such as fluidic stress, toxic chemicals, temperature and pH stress (Korber et al. 1989; Lawrence and Caldwell 1987). Biofilms are commonly found at the phase boundaries of rivers, water falls, hot springs, and also in glaciers. Their establishment on ship hulls, water cooling systems, and surface of plants can cause deleterious effects on the system performance. Nevertheless, their unique characteristics to self-immobilize and renew allow biomass accumulation and retention which in a technically context can be harnessed for constructive measure (Rosche et al. 2009). For example, biofilms are applied in waste water plants, bioremediation and in microbial leaching of mine spoils (Sand et al. 1995). Additionally, biofilms are also tuned as industrial workhorses for the production of value added chemicals like ethanol, lactic acid and acetic acid using fermentative process (Gross et al. 2010; Halan et al. 2010; Rosche et al. 2009).

One of the potential advantages of biofilm reactors is the high volumetric reaction rate accomplished due to the high biomass concentration (Qureshi et al., 2005). However, very few biofilm reactors exploit this advantage because of mass transfer limitation in the biofilm reactors (Syron and Casey 2008). Typically, this problem is observed in aerobic biofilms where the sparingly soluble oxygen must be transferred from the air phase in to the biofilms. Several different reactor configurations such as packed bed, trickle bed, expanded bed, bubble column etc., have been investigated to maximize the air transfer rates (Nicoletta et al. 2000). The complexity in the biofilm reactor design further increases with the application of badly soluble organic substrates. Organic substrates may be added as an additional water immiscible phase and either consists of a pure substrate phase or as a mixture of the substrate and a carrier phase. In such multiphasic biofilm processes, both oxygen and organic substrate must be transferred from the respective phases to the biofilms. This multi-component mass transfer is dependent on several parameters such as the specific surface area between the biofilm and the different phases, the ratio of different phases and the mixing pattern implied within the reactor.

Novel biofilm reactors are designed to maximize the multi-component mass transfer. Most of these reactor configurations have applied a membrane to partition the biofilm and different phases. For example, Gross *et al.*, 2007 have applied a silicone membrane to partition biofilm from the air and organic phase to perform styrene epoxidation using *Pseudomonas sp.* Strain VLB120 $\Delta$ C biofilms (Gross et al. 2007). By optimizing the air to aqueous phase ratios (127:1) and the organic

to aqueous phase ratio (32:1), average styrene oxide volumetric productivity of  $16 \text{ g L}_{\text{aq}}^{-1} \text{ day}^{-1}$  were reported. In order to shrink the air phase volume (or to reduce air to aqueous ratio) the reactor set-up was modified and continuous aeration was applied by using air-aqueous segmented flow (described in chapter 5). The oxygen transfer rate was optimized by varying the air-aqueous phase ratios from 1:1 to 16:1, which enhanced the average styrene oxide volumetric productivity from 11 to 46 to  $\text{g L}_{\text{aq}}^{-1} \text{ day}^{-1}$ . However, the membrane transfer might contribute to an additional mass transfer barrier and lower the reactor performance.

To overcome membrane mass transfer, we aimed at developing a biofilm reactor in which the biofilm and the rest of the phases (aqueous, air, and organic) are in direct contact. Such a system emphasis several challenges, the major one being the establishment of a stable biofilm under the impact of continuous organic phase and fluidic stresses. This was successfully solved by using a simple four step method to develop biofilm under three-phase segmented flow. As a proof of concept, the newly developed reactor performance was evaluated for biochemical hydroxylation of octane to n-octanol using the biofilm forming strain *P. putida* PpS81 pBT10. Further, the flexibility of SFBR was verified for long term biocatalytic epoxidation of styrene by using *Pseudomonas sp.* Strain VLB120 $\Delta$ C biofilm as a catalyst.



## 6.3 Materials and Methods

*P. putida* PpS81 pBT10 and *Pseudomonas* sp. Strain VLB120ΔC have been cultivated in Luria-Bertani (LB) medium or M9-medium supplemented with 0.5% (w/v) glucose as a carbon source, US\* trace elements (Emmerling et al., 2002), and the appropriate antibiotics (streptomycin 100 μg mL<sup>-1</sup>; tetracycline 100 μg mL<sup>-1</sup>; kanamycin 100 μg mL<sup>-1</sup>).

### 6.3.1 Pre-culture cultivation

Precultures of *P. putida* PpS81 pBT10 and *Pseudomonas* sp. VLB120ΔC were grown overnight in 5 mL LB-medium using baffled 50 or 100 mL Erlenmeyer flasks in a horizontal shaker (30°C and 200 rpm, Multitron, Infors HT, Bottmingen, Switzerland).

### 6.3.2 (Aqueous-air-organic) Segmented flow biofilm reactor (SFBR)

A schematic view of this set-up is shown in Figure 6.1. A four channel peristaltic pump (Ismatec, Glattbrugg, Switzerland) fitted with two 1.5 mm inner diameter pump tubing (Ismatec Tygon MHLL, Glattbrugg, Switzerland) was used to pump M9 minimal medium and air through the reaction compartments. Organic liquid (octane or styrene) was supplied by means of a two-channel peristaltic pump (Ismatec REGLO, Glattbrugg, Switzerland) fitted with 1 mm inner diameter solvent resistant pump tubing (Ismatec Tygon MHLL, Glattbrugg, Switzerland). The reaction compartment consisted of PTFE tubing with 2.15 mm i.d., and 250 mm length. This tube was placed in a thermo-bath to maintain a reaction temperature of 30°C. The reactor was inoculated by filling the PTFE capillary with an overnight culture of *P. putida* PpS81 pBT10 and to allow the organisms to attach to the tubing surface for 2 hrs. Thereafter, the medium flow was turned on at a rate of 0.075 mL min<sup>-1</sup>, and after 3-4 days the filtered air flow of 0.075 mL min<sup>-1</sup> was started. After 7 days, organic substrate was added at a flow rate of 0.06 mL min<sup>-1</sup>. For styrene epoxidation, PTFE tubings with 2.15 mm i.d., 500 mm and 1000 mm length capillaries were inoculated with an overnight culture of *Pseudomonas* sp. Strain VLB120ΔC and all consecutive steps were carried out accordingly. Medium flow and air were set to 0.05 mL min<sup>-1</sup> while organic phase was added at a flow rate of 0.06 mL min<sup>-1</sup>.

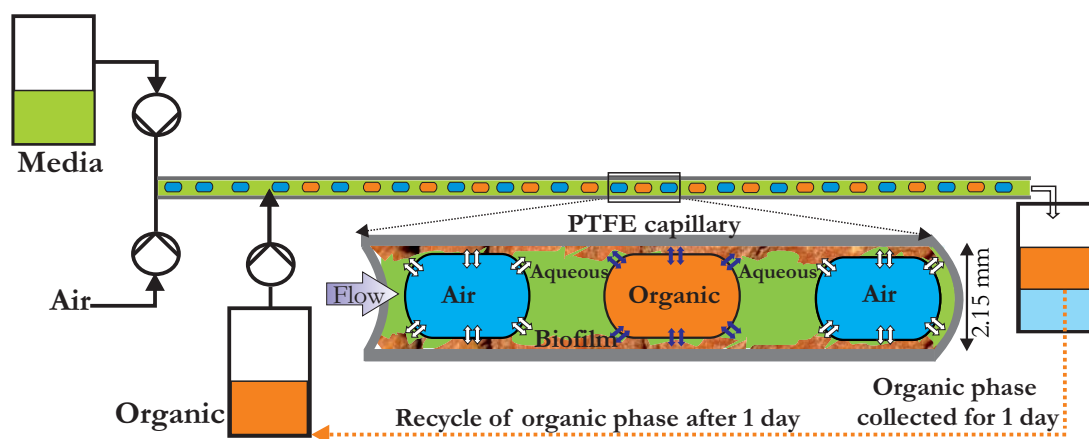


Figure 6.1: Scheme of aqueous-air SFBR for the production of either octanol from octane using a biofilm of *P. putida* Pps81 pBT10 or for the production of (*S*)-styrene oxide from styrene, using a biofilm of *Pseudomonas sp.* VLB120ΔC.

### Sample preparation and analysis

Details about the sample preparation and analytical methods are described in chapter 5.

**Table 6.1: Strains and plasmids used in this study**

Strain	Remarks	References
<i>Pseudomonas sp.</i> Strain VLB120	biofilm forming (styrene degrading) strain isolated from a biofilter	(Gross et al. 2007; Panke et al. 1998)
<i>Pseudomonas putida</i> PpS81	chromosomal knockout mutant of <i>P. putida</i> GPo1 lacking a medium chain-length alcohol dehydrogenase	(Grund et al. 1975)
<b>Plasmid</b>		
pBT10	pCom10 derivative, with <i>alkBFG</i> , <i>alkST</i> genes from pGEc47	(Gross 2010; Schrewe et al. 2011)

## 6.4 Results and discussion

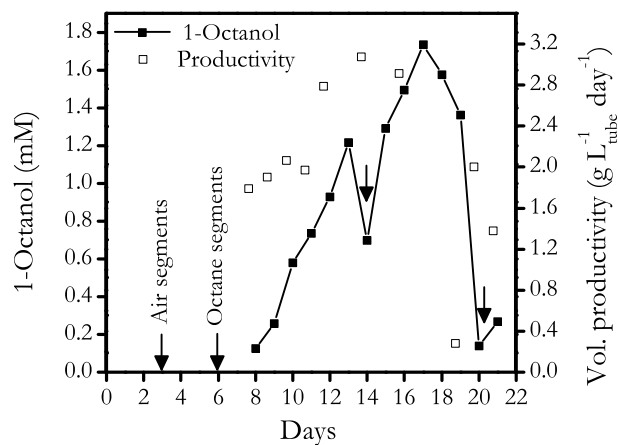
### 6.4.1 Biofilm establishment in the presence of an aqueous-air-organic segmented flow

To establish a biofilm under an aqueous-air-organic segmented flow, we followed the similar strategy developed in the previous chapter of growing biofilm in a single phase and then adapting them to the segmented flow (chapter 5). The three steps are necessary to establish biofilm in the presence of aqueous-air segmented flow: (i) development of a first-stage biofilm during single phase flow, (ii) start of aqueous-air segmented flow and subsequent detachment of a major biofilm part, and (iii) adaptation and regrowth of a second stage biofilm under aqueous-air segmented flow conditions. In this work, we had an additional step of injecting organic segments along with the aqueous-air segments. Two different organic solvents, octane and styrene with a  $\log P_{O/W}$  of 4.5 and 3 respectively, were applied. Typically, organic compounds with a  $\log P_{O/W}$  below 4 are considered to be toxic for microorganisms, while compounds with a  $\log P_{O/W}$  between 4 and 5 are considered as intermediate toxic (Laane et al. 1987). Upon organic phase injection only minor detachment of biomass was observed. However, the biofilm retain biofilms established in the presence of toxic organic solvents and showed stable activity for 20 to 30 days (results shown in the subsequent sections).

#### **(Aqueous-air-organic) SFBR for octanol synthesis**

Octane hydroxylation applying *P. putida* PpS81 pBT10 biofilms as catalysts was investigated in this three-phase segmented flow biofilm reactor. In order to increase the product titer in the organic phase, the organic phase (residence time of 4.31 min) was collected for 24 h and recycled. A maximum octanol concentration of 1.7 mM was accumulated in the 60 mL organic phase after 10 days of biotransformation, and thereafter the product concentration declined (Figure 6.2). The average volumetric activity for the first 10 days of biotransformation was  $2 \text{ g}_{\text{octanol}} \text{ L}_{\text{tube}}^{-1} \text{ day}^{-1}$ , which was two-fold higher than in the aqueous-air SFBMR applied in chapter 5. The substrate (octane) availability might be a probable explanation for the difference in the productivities of the two setups. As the solubility of octane in the aqueous phase is very low ( $0.7 \text{ mg L}^{-1}$  at  $20^\circ\text{C}$ ), the amount of octane available for the conversion by the biofilm catalyst is dependent on the octane mass transfer rate into the biofilm. In the aqueous-air SFBMR, octane had to diffuse through the silicone membrane, which contributes as an additional barrier to mass transfer. In contrast, octane was supplied directly into the biofilm grown tube in the three phase segmented flow. The presence of octane segments in the capillary enhanced the mass transfer rate and thus the octane availability for the conversion to octanol, which might have resulted in higher reaction rates. In addition, only 20% of the biofilm grown tube is immersed in the organic phase using the previous set-up, which could lead to an inefficient use of the available catalyst surface. In

aqueous-air-organic segmented flow, the organic phase is injected into the biofilm grown tube which improves biocatalyst utilization and might result in better productivities.



**Figure 6.2: Productivity of octanol production in the organic-air-aqueous segmented flow biofilm reactor (setup shown in Figure 6.1).** The arrows (without label) symbolize addition of octane phase.

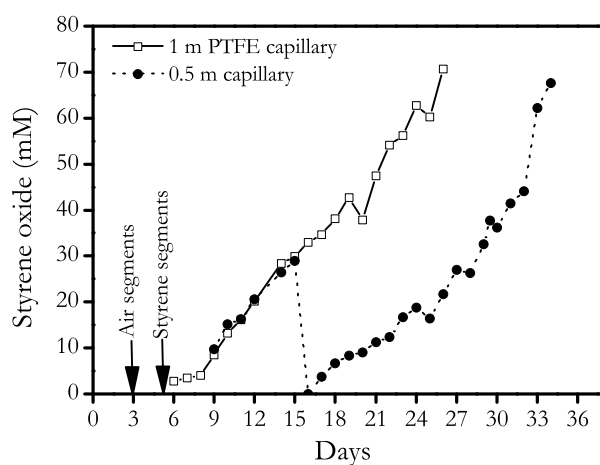
Nevertheless, octanol degradation and formation of unwanted products like octanal was observed at 1.7 mM of product in the octane phase. A similar pattern of octanol degradation by this strain being cultivated in a two-liquid phase bioreactors was also described by Bosetti and co-workers (Bosetti et al. 1992). The exact reason for this has not been fully elucidated, but several reasons are possible. This phenomenon could be due to the induction of intrinsic alcohol dehydrogenases, which are degrading the octanol much faster than it is synthesized. Also some kind of kinetic control mechanism is possible. Product inhibition or biocatalyst toxification, which slows down the alcohol production rate and consequently leads to extraction and loss of the octanol in to the aqueous phase, might be one of the reasons for product degradation. Further investigation is necessary to clarify this phenomenon. However, this is a catalyst based problem, which will be overcome by strain engineering or application of a different host strain.

### **(Aqueous-air-organic) SFBR for styrene epoxidation**

To evaluate the system versatility, the (aqueous-air-organic) SFBR performance was investigated with a *Pseudomonas sp.* Strain VLB120ΔC biofilm synthesizing (*S*)-styrene oxide from styrene. This epoxidation reaction using the same strain is well studied in various reactor formats such as fed-batch (Park et al. 2007), continuous (Park et al. 2007), and membrane reactors (Gross et al. 2010; Halan et al. 2010).

The performance of the SFBR regarding styrene epoxidation was explored in 0.5 m and 1 m long capillaries. A biofilm of *Pseudomonas sp.* Strain VLB120ΔC was grown under aqueous-air segmented flow conditions before the biotransformation was started by injecting styrene segments into the aqueous-air flow. Similar to the previous three-phase SFBR setup using octane,

the organic phase (styrene) was collected for 24 h and then recycled to improve the product titer. Interestingly, the styrene oxide concentration in the organic phase in both capillaries increased in similar rates, and the longer capillary did not result in a higher product concentration (Figure 6.3). A maximum product concentration of 70 mM<sub>org</sub> was achieved in the 1 m long capillary during 19 days of biotransformation. Whereas, in the 0.5 m long capillary a maximal product titer of 68 mM was reached in the styrene phase. This corresponds to an average volumetric productivity of 15 to 20 g<sub>sty.oxid.</sub> L<sub>tube</sub><sup>-1</sup> day<sup>-1</sup> of the 0.5 m capillary and 7 to 10 g<sub>sty.oxid.</sub> L<sub>tube</sub><sup>-1</sup> day<sup>-1</sup> of the 1 m capillary, respectively. Similar product formation pattern reveals that the system is under certain limitation and oxygen might be the possible substrate that limits the reactor performance. In both set-ups, the total flow rate was kept constant at 160 μL min<sup>-1</sup> with an air flow of 50 μL min<sup>-1</sup>. Thus, based on the mass balance, the amount of oxygen supplied in both setups was 25 mg day<sup>-1</sup>. According to the productivities achieved, the amount of oxygen utilized in the epoxidation reaction was estimated to be 24 mg day<sup>-1</sup>. As the oxygen supply rate and the oxygen consumption rate are almost similar, we conclude that the system becomes primarily constrained by the oxygen availability rather than the oxygen transfer. Technical solutions to enhance oxygen availability in SFBRs include use of oxygen enriched air or increase of the air throughput.



**Figure 6.3: Productivity of 0.5 m and 1 m long SFBRs harboring *Pseudomonas* sp. Strain VLB120ΔC as biocatalyst (setup shown in Figure 6.1).** The arrows indicate the addition of air segments after three days, addition of styrene segments and thus start of the biotransformation after 6 days, and the arrow without label on the 16 day represents exchange of the styrene phase for the 0.5 m long capillary.

## 6.5 Perspectives of the (aqueous-air-organic) SFBR concept

The present study shows the successful development of a three-phase segmented flow biofilm reactor. The application of such novel biofilm reactor for octane hydroxylation showed improved productivities as compared to the membrane based segmented flow biofilm approach. Other advantages of this system include compact reactor size, long term biocatalyst stability and activity, and maximum utilization of biofilm coverage as the biofilm and the liquid/gaseous phases (aqueous, air, and organic) are in direct contact. Additionally, the system is rather versatile to adapt to other biotransformation reactions.

Although the aqueous-air-organic segmented flow biofilm reactor has the potential to form a suitable platform technology several challenges still exist. The short residence time resulted into low product titers because of low conversion rates. Only (approx.) 0.004 % of octane and 0.04 % of styrene have been converted into the respective product after each run. To improve the residence time a longer capillary was applied for the biotransformation, but no improvement in product concentration was observed (Figure 6.3) because the system was strongly oxygen limited. Increase in air segment size analog to the approach introduced in the previous chapter could overcome such limitation. However, in this situation the cost of high flowrate or even lower residence time might directly have a negative impact on the productivity. Thus, comparing the three-phase SFBR to the optimized two-phase SFBMR (introduced in the chapter 5) one could conclude that three-phase SFBR is not the best solution for such reactions and the aqueous-air SFBMR is superior at least for reactions evaluated in this work.

## Acknowledgments

This work was financially supported by the Deutsche Bundesstiftung Umwelt (DBU) and by the Ministry of Innovation, Science, Research and Technology of North Rhine-Westphalia.

## Chapter 7

### General Discussion

Rohan Karande, Katja Buehler and Andreas Schmid

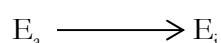
Katja Buehler and Andreas Schmid coordinated and supervised the project and corrected the manuscript

Microreactors are a potent technology for enhancing reaction rates of mass transfer limited reactions with simplified scale-up issues. Although frequently used for chemical reactions, this technology is not yet implemented on a broad basis in biocatalysis. The primary goal of this thesis was the development and application of multiphasic microreactors for biocatalytic reactions. The potential of microreactors were evaluated for both enzyme catalysed reactions and whole cells catalysed reactions in the form of biofilm. There are several microreactor formats available to perform biological reactions (chapter 1). Understanding the biocatalysts performance in specific microreactor formats at an early stage of process design allows for developing the most appropriate or ideal reactor configuration (chapter 1).

An ideal bioreactor configuration is one which explores maximum activity of the biocatalyst continuously over a longer time period. This necessitates a stable biocatalyst under process conditions. The stability of an enzyme is dependent on multiple parameters such as temperature, shear stress, organic solvents, interfacial surface area etc. In chapter 2, the influence of various process parameters on isolated enzyme activity in the segmented flow microreactor was evaluated, and will be discussed in the following section.

### I. Enzyme stability in the aqueous-organic segmented flow ---- kinetic perspective

The TADH exposure to the aqueous-organic interface combined with the shear stress generated from the moving segments and the capillary wall caused substantial TADH inactivation. The TADH inactivation was dependent on enzyme concentrations, segment length and capillary diameter (chapter 2). The inactivation rate was first order with the enzyme concentration. To determine the inactivation constant a simple model is considered,



Where,  $E_a$  is the active form of the enzyme and  $E_i$  is an inactivated form of the enzyme. For the first order enzyme inactivation, the rate of inactivation is given as,

$$r_d = k_D e_a \quad (7.1)$$

where,  $r_d$  is the volumetric rate of inactivation,  $k_D$  is the inactivation coefficient and  $e_a$  is the active enzyme concentration.

$$\frac{d(e_a)}{dt} = -k_D e_a \quad (7.2)$$

Integrating the above equation gives,

$$e_a = e_{a0} e^{-k_D t} \quad (7.3)$$

where,  $e_{a0}$  is the active enzyme at time zero. The inactivation of the enzyme directly affects the reaction performance as it reduces the reaction rate.

$$v_{\max} = k_{\text{cat}} e_a = k_{\text{cat}} e_{a0} e^{-k_D t} \quad (7.4)$$



Thus, the decline of the active enzymes by inactivation exponentially lowers the maximum reaction rate. The inactivation rate constant  $k_D$  was determined by plotting the logarithmic loss in enzyme activity versus time. The inactivation coefficient ( $k_D$ ) in the segmented flow was higher than the enzyme inactivation in other reactor configurations (Table 7.1). As stated earlier, the high interfacial area combined with the shear stress might result in a higher inactivation coefficient in the segmented flow.

In the aqueous-organic segmented flow microreactor, TADH inactivation occurs through three consecutive steps: enzyme adsorption, inactivation and desorption. In the first step, the adsorption rate constants in the segmented flow were found to be 10-fold higher than the adsorption in the drop tensiometry measurements (chapter 2). This again points to the dominance of convective forces in the segmented flow reactor compared to the slow diffusion in the drop tensiometry experiments.

In the second step, the adsorbed TADH interacts with the exposed hydrophobic surface which promotes the loss of structural integrity of the protein. While in the final step the attached inactivated TADH is desorbed from the interface. Although, we have estimated the overall inactivation coefficient, we were not able to distinguish the individual rate constants for the second and third step. Therefore in-depth study to determine these rate constants is essential. These rate constants will indicate which of the three steps has the maximum influence on the enzyme inactivation process. To improve enzyme stability, further strategies to reduce the inactivation coefficients of the dominating step must be examined.

**Table 7.1: Inactivation coefficients ( $k_D$ ) in different reactor formats**

System	Phases	Enzyme	Inactivation coefficient ( $k_D$ ) s <sup>-1</sup>	Interface coverage	Reference
<i>Segmented flow microreactor</i>	<i>hexadecane-aqueous</i>	<i>TADH</i>	$2.5 \times 10^{-3}$ to $9.6 \times 10^{-3}$	$2-3 \text{ mg m}^{-2}$	<i>This work</i>
Bubble column reactor	octan-2-one-aqueous	urease	$2.5 \times 10^{-5}$	$1 \text{ mg m}^{-2}$	(Ghatorae et al. 1994a)
Stirred tank reactor	air-aqueous	lysozyme	$0.7 \times 10^{-3}$ to $1.4 \times 10^{-3}$	ND	(Ghadge et al. 2003)
Falling film reactor (incline plane)	air-aqueous	lysozyme	$0.1 \times 10^{-3}$ to $0.5 \times 10^{-3}$	ND	(Ghadge et al. 2003)

ND-not determined

## II. Stabilizing enzyme activity in an aqueous-organic segmented flow

The key reason for TADH inactivation in the segmented flow system was the aqueous-organic interface. The interface consists of molecules with imbalanced cohesive energy, arising from the

uncompensated bonds between aqueous and organic molecules. In nature, every system is prone to reduce its free energy. An enzyme poses surface activity due to the presence of hydrophobic and hydrophilic amino acids (Eisenberg et al. 1984), and therefore has the ability to interact with the interface molecules to reduce the surface free energy. The excess free energy between both liquids is numerically equivalent to the interfacial tension (Donahue and Bartell 1952). Thus, the equation for surface excess energy can be expressed as:

$$\Gamma = \frac{1}{RT} \left[ \frac{d(\sigma)}{d(\ln C)} \right] \quad (7.5)$$

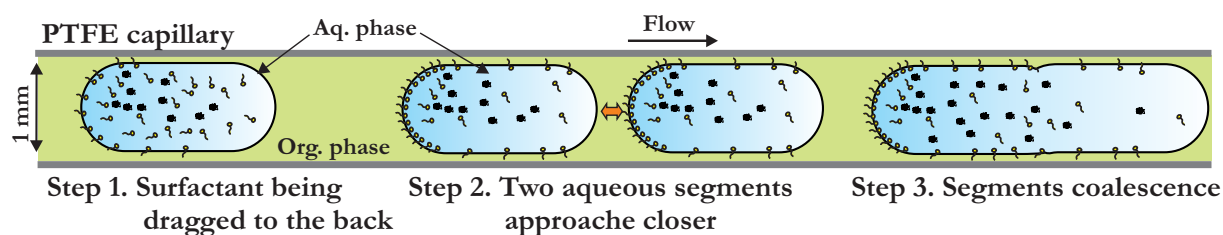
Where,  $\Gamma$  denotes the surface excess energy,  $C$  is the enzyme concentration and  $\sigma$  is the interfacial tension.

Two techniques were investigated in chapter 3, to recover maximum enzyme activity from the segmented flow. By immobilizing the enzyme on to a solid matrix, its surface activity was changed and consequently additional structural stability was gained. Upon covalent immobilization of TADH on (Epoxy)-Sepabeads, almost 85 to 95 % of TADH bead activity was recovered after one segmented flow cycle. For the suspended enzyme only 55% could be recovered (chapter 2). However, the main bottleneck of this mechanism is of technical nature, as it is difficult to distribute beads equally in each aqueous segment. A possible solution would be to immobilize TADH on hydrophilic nano-beads with a lower specific gravity than the aqueous phase to overcome this problem.

Another approach was the application of surface active molecules like surfactants to reduce the interfacial free energy. A competitive type of interfacial adsorption between the enzyme and the surfactant molecules was revealed from the drop tensiometry experiments. Above a certain surfactant concentration, the competitive adsorption was mainly dominant by surfactant molecules, which form a protective layer between the interface and the biocatalyst in the aqueous compartments. Overall, this mechanism recovered almost 100% of TADH activity in the segmented flow. The amount of surfactant necessary to form a protective layer was dependent on the interfacial surface area. In comparison to the first protective mechanism, the application of surfactants seems to be more attractive because of better activity yield, less complexity, and easier implementation into the liquid-liquid segmented flow reactor.

The main limitation of this approach comes from the coalescence of segments after a certain residence time. Typically, coalescence of segments is a thermodynamic thrust to minimize the interfacial area and is dependent on the surface tension. By adding the surfactants, the interfacial tension is reduced and coalescence is typically prevented, as the surfactant acts as a physical barrier and repels the adjacent droplet. However, in our setup the coalescence of segments was pronounced after addition of surfactants in comparison to the system without surfactants. It has

been observed that the adsorbed surface active agents like surfactants on the interface are swept to the back of the aqueous segments (Ratulowski and Chang 1990). This generates Marangoni effects due to the gradient in surface tension on the interface, which drags the liquid back with the surfactant. As the continuous phase in our system is highly viscous (hexadecane) compared to the dispersed phase (aqueous phase), the surfactant present in the aqueous phase requires a certain period of time to carry the viscous phase. Once the viscous liquid is dragged back two aqueous segments approaches closer. The rear end of the forward-facing droplet is highly concentrated with surfactant as compared to the front side of the backward-facing droplet. This difference between the two interacting droplets facilitates fusion and coalescence of the segments. The schematic representation of the segment coalescence mechanism is shown in the Figure 7.1. Other ways for coalescence of surfactant-stabilized droplets was observed by heating with a laser, electro-coalescence and changing the geometry of the microchannel (Mazutis et al. 2009; Mazutis and Griffiths 2012). Possible solutions to control the coalescence and to guarantee a stable segmented flow over a longer time period should be investigated.



**Figure 7.1: Schematic view of possible aqueous segment coalescence.**

### III. Enzyme catalysis in the aqueous-organic segmented flow microreactors---kinetic perspective

After stabilizing TADH activity, the reaction performance in the segmented flow was investigated. The reduction of 1-heptaldehyde to 1-heptanol was chosen as a model reaction based on the pre-evaluation by using the Damköhler number. Important parameters governing the interplay between reaction rates and mass transfer rates are reported in chapter 4. The enzymatic reaction performance under segmented flow conditions was found to be dependent on capillary diameter, flow velocity, phase ratio, and enzyme as well as substrate concentration (chapter 4).

The interaction of substrate mass transfer and the reaction of two enzymes are explored using a modelling approach. A detailed kinetic study of both enzymes TADH and FDH were performed and rate laws were established (Equation 7.6 and 7.7). The kinetic parameters are given in Table 7.2. TADH is non-competitively inhibited by the substrate heptaldehyde and competitively inhibited by  $\text{NAD}^+$ . Formate dehydrogenase was seen to be affected by competitive inhibition of NADH. In comparison to TADH, FDH shows lower affinity to its substrates.

$$r_{\text{TADH}} = \frac{V_{\text{maxTADH}} \times C_{\text{S}}}{K_{\text{mTADH}} + \left(1 + \frac{C_{\text{S}}}{K_{\text{iS}}}\right) \times C_{\text{S}}} \times \frac{C_{\text{NADH}}}{C_{\text{NADH}} + K_{\text{mNADH}} \left(1 + \frac{C_{\text{NAD}}}{K_{\text{iNAD}}}\right)} \quad (7.6)$$

$$r_{\text{FDH}} = \frac{V_{\text{maxFDH}} \times C_{\text{S,For}}}{C_{\text{For.}} + K_{\text{mFor.}}} \times \frac{C_{\text{NAD}}}{C_{\text{NAD}} + \left(1 + \frac{C_{\text{NADH}}}{K_{\text{iNADH}}}\right) \times K_{\text{mNAD}}} \quad (7.7)$$

**Table 7.2: Kinetic parameters of TADH and FDH**

TADH		FDH	
$K_{\text{mTADH}}$	0.786 mM	$K_{\text{mFor.}}$	22 mM
$K_{\text{mNADH}}$	0.025 mM	$K_{\text{mNAD}}$	0.316 mM
$K_{\text{iNAD}}$	0.25 mM	$K_{\text{iNADH}}$	0.06 mM
$K_{\text{is}}$	1.5 mM		

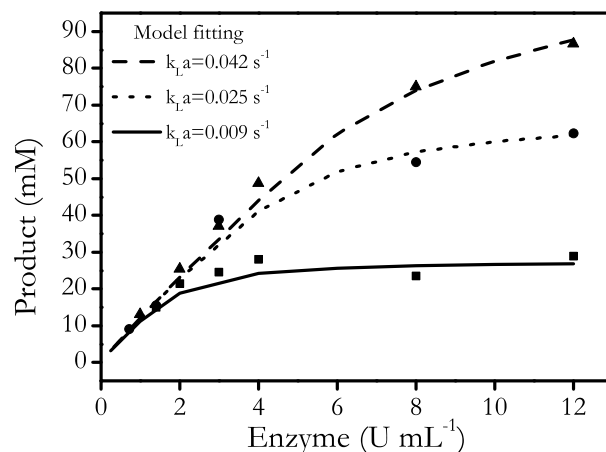
The mass balance was performed for the aqueous phase by considering the film model and assuming that the organic side mass transfer resistance is negligible. This assumption is valid due to the very high partition coefficient of the substrate ( $K_{\text{org/aq}}=100$ ). The mass transfer and the reaction then becomes,

$$\frac{d[\text{Substrate}_{\text{TADH}}]}{dt} = k_{\text{L}} a \left( K C_{\text{org.}} - C_{\text{aq.}} \right) - r_{\text{TADH}} \quad (7.8)$$

$$\frac{d[\text{NADH}]}{dt} = r_{\text{FDH}} - r_{\text{TADH}} \quad (7.9)$$

Equations 7.8 and 7.9 were solved by using a simple Euler's one step method and by linearizing the rate equations over a small time interval (1 to 5 s). The model suitability was verified by comparing measured and computed product formation at the assumed mass transfer coefficients. The model shows a good fit to the experimental results reported in chapter 4 at the mass transfer coefficients of 0.5, 1.4 and 2.5  $\text{min}^{-1}$  for the 2.15, 1 and 0.5 mm capillary diameter, respectively (Figure 7.2; Table 7.3). The mass transfer coefficients for the 1 mm diameter capillary predicted by the model are in good range of experimentally determined values reported by Kashid and co-workers (Kashid et al. 2007). However, for the smallest capillary diameter (0.5 mm) there seems to be some discrepancy between the model predicted and experimental determined values. Such difference might come from the high coalescence seen at smaller capillary diameters. The fusion of droplets reduces the surface area by volume ratio, which ultimately affects the mass transfer rates. Therefore, such undesired coalescence within the capillary microreactor should be avoided to maximize the mass transfer performance. However, it is interesting to note here that by using cationic surfactant like cetyl-trimethyl-ammonium-bromide (CATB), the mass transfer rates and consequently the mass transfer coefficients were reported to be higher compared to system

without surfactant addition (Kashid et al. 2010). The stabilization of the segments depends on the type and amount of surfactant, the properties of the phases, and the micro-device geometry. An in-depth study of each individual parameter is necessary to guarantee a stable coalescence free segmented flow.



**Figure 7.2: Modeled and experimental values of mass transfer and reaction with increasing enzyme concentration.** The solid lines represent modeled values and the dotted lines experimental values shown in Figure 4.2A.

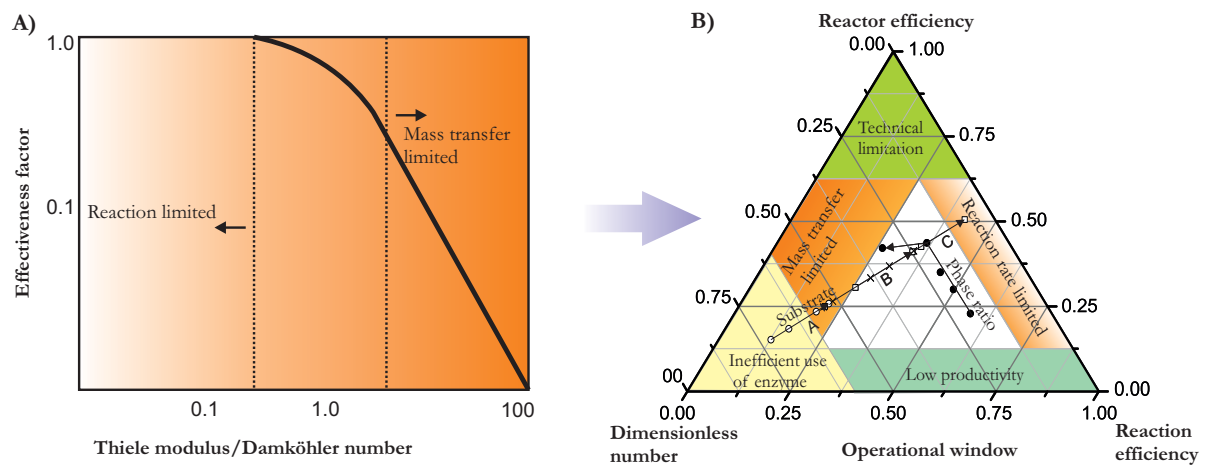
**Table 7.3: Mass transfer coefficients ( $k_{La}$ ) in different liquid-liquid segmented flow**

System	Phases	Operation mode	Reactors dimensions	Mass transfer coefficients ( $k_{La}$ )	Reference
<i>Segmented flow microreactor</i>	<i>hexadecane-aqueous (heptaldehyde)</i>	<i>Enzyme reactions</i>	<i>d= 0.5 mm</i>	<i>0.042 s<sup>-1</sup></i>	<i>This work</i>
			<i>d= 1 mm</i>	<i>0.025 s<sup>-1</sup></i>	<i>(estimated from model)</i>
			<i>d= 2.15 mm</i>	<i>0.009 s<sup>-1</sup></i>	<i>(estimated from model)</i>
Segmented flow (extractor)	n-butanol-aqueous (succinic acid)	Non-reacting system	d= 0.5 mm d= 0.75 mm d= 1 mm	0.12-0.31 s <sup>-1</sup> 0.07-0.15 s <sup>-1</sup> 0.02-0.09 s <sup>-1</sup>	(Kashid et al. 2007)
Segmented flow microreactor	kerosene-aqueous	Acid base reaction	d= 0.38 mm	0.5 s <sup>-1</sup>	(Burns and Ramshaw 2001)
Segmented flow (extractor)	n-butyformate-aqueous	Non-reacting system	d= 1 mm	0.7-1.57 s <sup>-1</sup>	(Ghaini et al. 2010)

#### IV. Operational window approach:

Another approach to understand the impact of mass transfer of molecules on the reaction rates is to plot dimensionless numbers (Thiele modulus or Damköhler number) against effectiveness factor (Figure 7.3A). At lower dimensionless numbers the system is operated in a reaction rate limited regime, while at higher dimensionless numbers the system runs in to a mass transfer limited regime. Although such plots clearly point to the regime where the system is being operated and allow judging the reaction efficiency in the reactor, it is not possible to deduce how

efficient the system operates. Therefore, this approach was executed (introduced in chapter 4) to a ternary diagram connecting dimensionless number, and the effectiveness factor to the reactor efficiency (Figure 7.3B).



**Figure 7.3: Effectiveness factor as a function of the dimensionless number (A), and ternary diagram (B, applied in chapter 4).**

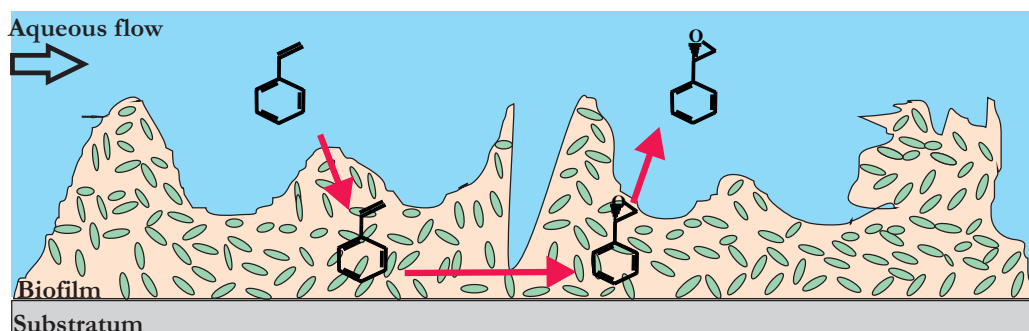
The reactor efficiency is the ratio of the volumetric productivity to the maximum volumetric productivity that could be theoretically achieved within the given reactor volume. The maximum value sets an upper limit and remains fixed to all reactor configurations for specific reactor volume. This allows not only characterization of the reactor performance but also comparison with other reactor configurations. This ternary diagram applied in chapter 4 visualizes the impact of single parameters and how these parameters are interconnected and influence the overall performance of the SFER. Noteworthy, the operational window was used as guidance for strategic improvement of the key parameters that limited the reactor performance (chapter 4).

The performance of enzymatic reactions in the segmented flow microreactor can be evaluated using both modelling and operational window approaches as outlined in the above section. Both approaches have certain advantages and disadvantages. In order to get to a faster understanding on the system performance it is recommended to integrate both approaches.

## V. Segmented flow biofilm microreactors---kinetic perspective

The application framework of the segmented flow was extended to whole cell biocatalysis in the form of biofilms (chapter 5 and 6). The aim was to integrate the advantages of *catalytic biofilm* such as self-immobilization, robustness and high turnover rates, to the benefits of *segmented flow systems*, such as high mass transfer rates and easy scalability. Within the biofilm, mass transfer of substrates is mostly based on molecular diffusion. The substrate that limits the reaction performance should be addressed by comparing the relative substrate diffusion and reaction rates within the biofilm. Once this is known, specific approaches to maximize the respective substrate

flux and thus the reaction performance can be undertaken. Based on the available reactor configurations in literature and the reactor developed in this thesis, a microreactor assessment for the conversion of styrene to (*S*)-styrene oxide using *Pseudomonas* sp. Strain VLB120ΔC biofilm (Figure 7.4) is described in the following section. The objective was to identify critical parameters that influence the overall reactor performance.



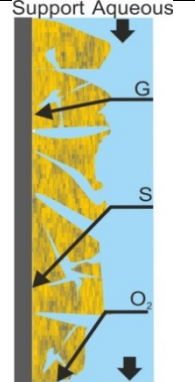
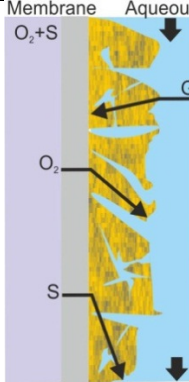
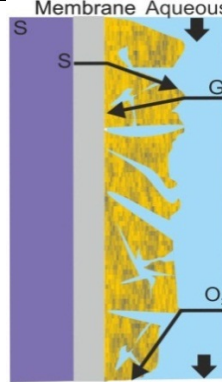
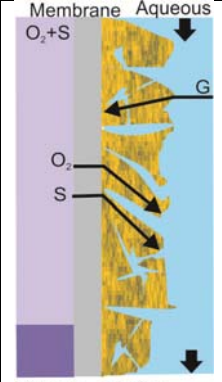
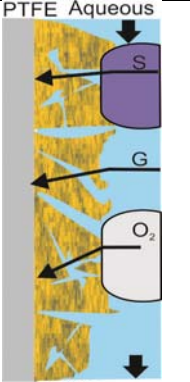
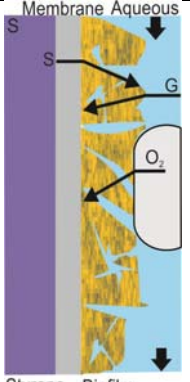
**Figure 7.4: Schematic view of styrene epoxidation in the biofilm**

In order to elucidate the substrate that limits the reactor performance the characteristic time scales of three most important substrates (glucose, styrene, and oxygen) have been estimated. This approach is based on the estimation of dimensionless numbers like the Thiele modulus or the Damköhler number to predict the biofilm reactor performance and its constraining factors. Gross and co-workers have reported the oxygen, glucose, and styrene substrate uptake rate for *Pseudomonas* VLB120ΔC to be 1.1, 0.2, and 0.07 mmol  $g_{BDW}^{-1}h^{-1}$ , respectively. Although, these rates were reported for a particular membrane biofilm microreactor setup, they showed the maximum styrene oxide volumetric productivities achieved by *Pseudomonas* sp. Strain VLB120ΔC. Therefore, these rates were taken as upper limit for the calculations of the dimensionless numbers.

#### Two-phase biofilm microreactor----oxygen availability as the rate limiting step

This reactor setup is mainly implemented in the flow cell format for analytical measures. The biofilm is grown on a non-permeable substratum and the aqueous flow is supplied with all substrates, namely styrene, oxygen, and glucose to the biofilm (Table 7.4; #1). The substrate concentrations at the inlet of the aqueous flow were estimated to be 0.2, 3 and 27 mM for oxygen, styrene, and glucose, respectively. Based on the assumed reaction rates for oxygen, styrene, and glucose, the reaction times for complete conversion of these substrates are 0.2, 5.3, and 185 min, respectively. This clearly shows that oxygen and styrene are consumed much faster as compared to the glucose and are therefore the substrates that might limit the performance of the system.

**Table 7.4: Contacting patterns and design criteria for the selection of biofilm microreactors setups**

 <p>Support Aqueous Biofilm</p>	 <p>Membrane Aqueous Air Biofilm</p>	 <p>Membrane Aqueous Styrene Biofilm</p>	 <p>Membrane Aqueous Styrene Biofilm</p>	 <p>PTFE Aqueous Biofilm</p>	 <p>Membrane Aqueous Styrene Biofilm</p>
<p><b>#1: Two phase (aq-bf)</b> Biofilm is grown on an impermeable surface and all substrates (styrene, glucose, oxygen) are supplied through the aqueous phase to the biofilm.</p>	<p><b>#2: Three phase (aq-bf-air)</b> Biofilm is grown on a silicone membrane surface, and oxygen and styrene are supplied through the membrane to the biofilm.</p>	<p><b>#3: Three phase (aq-bf-org)</b> Biofilm is grown on a silicone membrane surface, and styrene enters through the membrane, while oxygen and glucose are supplied directly by the aqueous phase.</p>	<p><b>#4: Four phase (aq-bf-org-air)</b> Biofilm is grown on a silicone membrane surface, of which 20 % is submerged in a styrene phase, while 80 % is in the air phase. See also set-up #2.</p>	<p><b>#5: Four phase (aq-bf-org-air)</b> Biofilm is grown on a PTFE surface. The substrates, oxygen and styrene enter the biofilm through the biofilm side in the form of segments.</p>	<p><b>#6: Four phase (aq-bf-org-air)</b> Biofilm is grown on a silicone membrane surface. While oxygen enters the biofilm through the biofilm side and styrene are supplied through the membrane to the biofilm.</p>
<p><math>S_o</math> 6 mg/L <math>S_s</math> 312 mg/L <math>S_g</math> 5000 mg/L <math>D_o</math> <math>1.5 \times 10^{-9}</math> m<sup>2</sup>/s <math>D_s</math> <math>0.24 \times 10^{-10}</math> m<sup>2</sup>/s <math>D_g</math> <math>2 \times 10^{-10}</math> m<sup>2</sup>/s</p>	<p><math>S_o</math> 6 mg/L <math>S_s</math> 45 mg/L <math>D_o</math> <math>1.5 \times 10^{-9}</math> m<sup>2</sup>/s <math>D_s</math> <math>0.24 \times 10^{-10}</math> m<sup>2</sup>/s</p>	<p><math>S_o</math> 6 mg/L <math>S_s</math> 312 mg/L <math>D_o</math> <math>1.5 \times 10^{-9}</math> m<sup>2</sup>/s <math>D_s</math> <math>0.24 \times 10^{-10}</math> m<sup>2</sup>/s</p>	<p><math>S_o</math> 6 mg/L <math>S_s</math> 312 mg/L <math>D_o</math> <math>1.5 \times 10^{-9}</math> m<sup>2</sup>/s <math>D_s</math> <math>0.24 \times 10^{-10}</math> m<sup>2</sup>/s</p>	<p><math>S_o</math> 6 mg/L <math>S_s</math> 312 mg/L <math>D_o</math> <math>1.5 \times 10^{-9}</math> m<sup>2</sup>/s <math>D_s</math> <math>0.24 \times 10^{-10}</math> m<sup>2</sup>/s</p>	<p><math>S_o</math> 250 mg/L <math>S_s</math> 312 mg/L <math>D_o</math> <math>1.5 \times 10^{-9}</math> m<sup>2</sup>/s <math>D_s</math> <math>0.24 \times 10^{-10}</math> m<sup>2</sup>/s</p>
<p><math>t_{o,r}</math> 0.22 min <math>t_{s,r}</math> 5.35 min <math>t_{g,r}</math> 185 min <math>\tau</math> 6.28 min</p>	<p><math>t_{o,r}</math> 0.22 min <math>t_{s,r}</math> 0.77 min <math>\tau</math> 6.28 min</p>	<p><math>t_{o,r}</math> 0.22 min <math>t_{s,r}</math> 5.35 min <math>\tau</math> 6.28 min</p>	<p><math>t_{o,r}</math> 0.22 min <math>t_{s,r}</math> 5.35 min <math>\tau</math> 6.28 min</p>	<p><math>t_{o,r}</math> 12.6-1.4 min <math>t_{s,r}</math> 5.35 min <math>\tau</math> 6.28 min</p>	<p><math>t_{o,r}</math> 12.6-1.4 min <math>t_{s,r}</math> 5.35 min <math>\tau</math> 6.28 min</p>
<p><math>\Phi_o</math> 12, <math>Da_{1,o}</math> 27 <math>\Phi_s</math> 1, <math>Da_{1,s}</math> 1.17 <math>\Phi_g</math> 0.1, <math>Da_{1,g}</math> 0.03</p>	<p><math>\Phi_o</math> 7 <math>\Phi_s</math> 22</p>	<p><math>\Phi_o</math> 12, <math>Da_{1,o}</math> 27 <math>\Phi_s</math> 3</p>	<p><math>\Phi_o</math> 9 <math>\Phi_s</math> 16</p>	<p><math>Da_{1,o}</math> 22; <math>A=0.05</math> mL min<sup>-1</sup></p>	<p><math>Da_{1,o}</math> 9, <math>A=0.25</math> mL min<sup>-1</sup>; <math>Da_{1,s}</math> 3.5; <math>A=0.5</math> mL min<sup>-1</sup>; <math>Da_{1,o}</math> 0.8; <math>A=2</math> mL min<sup>-1</sup>; <math>Da_{1,o}</math> 0.31; <math>A=4</math> mL min<sup>-1</sup> <math>A</math>=air flow</p>
<p>High Da number for oxygen suggest <b>oxygen availability</b> to be the rate limiting step</p>	<p>High Thiele modulus for styrene suggest <b>styrene mass transfer</b> to be the rate limiting step</p>	<p>High Da number for oxygen suggest <b>oxygen availability</b> to be the rate limiting step</p>	<p>High Thiele number for styrene compared to oxygen suggest <b>styrene transfer</b> to be the rate limiting step</p>	<p>High Da number for oxygen suggests <b>oxygen availability</b> to be the rate limiting step.</p>	<p>Decrease in Da number with air flow overcomes <b>oxygen availability</b></p>
<p>Flow cell reactor; Halan et al., 2011</p>	<p>Tubular membrane reactor; Gross et al., 2007</p>	<p>Tubular membrane reactor; Gross et al., 2007</p>	<p>Tubular membrane reactor; Gross et al., 2007</p>	<p>Aq.-air-org. SFBR; This work, chapter 6</p>	<p>Aq.-air. SFBMR; This work, chapter 5</p>



**Abbreviations:** aq- aqueous phase, bf-biofilm phase, org-organic phase, S-styrene, O<sub>2</sub>-oxygen, G-glucose

**Reaction time** ( $t_r$ ) is the *time necessary* for the catalyst to convert the substrate supplied.

$t_r = c/r$ , where  $c$  is the substrate concentration and  $r$  is the rate of reaction.

**Residence time** ( $\tau$ ) is the *time available* for the reaction and is dependent on the reactor volume ( $V$ ) and volumetric flow rate ( $v_r$ ).

$$\tau = V/v_r,$$

**Mass transfer time** ( $t_{m}$ ) is the *time necessary* for the substrate to penetrate the biofilm.

$t_{m} = (\text{thickness})^2/D$ , where  $D$  is the diffusion coefficient.

**First Damköhler number** ( $Da_1$ ) is the ratio of the residence time to the respective reaction time.

$$Da_1 = \tau/t_r$$

**Observable Thiele modulus or Weisz modulus** ( $\Phi$ ) is the ratio of the substrate mass transfer time to the respective reaction time.

$$\Phi = t_{m}/t_r$$

This is an important measure for substrate conversion within the continuous flow reactor. If the reaction time is very low than the residence time ( $Da_1 \gg 1$ ), substrate conversion would be fast and the system is limited by substrate availability. As a rule of thumb the residence time should be at least in the same order of magnitude as the reaction time in order to obtain high conversion in continuous flow reactors.

Noteworthy, the reaction time for glucose was several fold higher than the residence time in the microreactor (Reactor #1, Table 7.4), therefore the biofilm is not glucose limited. As the flow conditions in reactor #1 are similar to the other reactor formats (reactor #2, #3, #4, #5), prediction for glucose limitation was not performed for the other reactor setups.

The reaction time for oxygen is the same in all reactor formats (0.22 min). However, it has to be noted that in reactor #1 and #3, oxygen is delivered to the biofilm through the aqueous phase. Whereas in reactors #2 and #4, oxygen is delivered through the membrane and is transferred perpendicularly to the biofilm substratum. In such reactor setups, the diffusion distance has to be estimated based on the reaction time (0.22 min). This diffusion distance can be compared with the biofilm thickness to ensure that the oxygen is not the limiting substrate.

According to the first Damköhler number, which analysed the comparison of the flow residence time with the reaction time, the reactor performance was clearly oxygen availability limited. Oxygen is important in biofilm for two purposes: cell growth (influencing production by lower biocatalyst concentration) and reaction rate (oxygen is a substrate for the epoxidation reaction). As oxygen is a key substrate for biofilm growth, its limitation means a lower biomass in the reactor and a limited styrene conversion rate. Therefore, improvement of oxygen transfer is absolutely crucial for maximizing the reaction and reactor performance in such setups.

Three-phase membrane based biofilm microreactor----substrate mass transfer as the rate limiting step

A tubular membrane biofilm microreactor was designed by Gross and co-workers to improve oxygen transfer to the biofilm (Gross et al. 2007). Here, the silicon tube offers a dual function, on one side it acts as substratum for biofilm growth and on the other side it supplies oxygen radially over the membrane to the biofilm (Table 7.4; #2). The biofilm containing silicone tube is kept in contact with the gas phase saturated with styrene allowing simultaneous diffusion of both, styrene and oxygen. In this setup, an average styrene oxide volumetric productivity of  $4.3 \text{ g L}_{\text{tube}}^{-1} \text{ day}^{-1}$  was reported for 30 days of reactor operation. Detailed analysis of the experimental results was performed by calculation of the Thiele modulus in order to determine the limiting substrate. As the Thiele modulus for styrene is approximately 3 times higher than for oxygen, the styrene mass

transfer was limiting the reaction performance. Substrate mass transfer is a function of substrate concentration, consumption rate, and its diffusivity in the biofilm. As the styrene concentration in the air phase is very low (0.44 mM), the mass transfer limitation originates from the very low styrene concentration in the gaseous phase. Therefore, an additional modification is essential to improve styrene mass transfer and the catalytic performance in this setup.

By immersing the tube containing the biofilm into a pure styrene phase, the styrene transfer by permeation through the tube wall was improved, whereas oxygen was available for the biofilm via the aqueous phase (Table 7.4; #3) (Gross et al. 2007). However, the styrene oxide productivity ( $2.2 \text{ g L}_{\text{tube}}^{-1} \text{ day}^{-1}$ ) in this reactor (Table 7.4; #3) was found to be two fold lower than the previous discussed example ( $4.3 \text{ g L}_{\text{tube}}^{-1} \text{ day}^{-1}$ ; Table 7.4; #2)). The high Thiele modulus and the first Damköhler number for oxygen in comparison to styrene indicate that oxygen availability becomes critical in this set-up, which hampers biofilm formation and the styrene conversion rate. Overall, it could be concluded that the volumetric productivity in such three phase reactor formats is likely to be limited by the missing fourth phase (in this example air).

#### Four-phase membrane based biofilm microreactor----scale up a crucial factor

In this format, 20% of the biofilm containing tube is immersed in a pure styrene phase while the remaining 80% are located in the air phase (Table 7.4; #4). This enhanced the styrene and oxygen transfer rates into the biofilm, which resulted in elevated productivities ( $16 \text{ g L}_{\text{tube}}^{-1} \text{ day}^{-1}$ ), compared to the previous setups (Gross et al. 2007) (Gross et al. 2007). Although promising results have been achieved within this reactor format, the very high air phase volume necessary would lead to an unacceptably high reactor volume at production scale. For example, a reactor comprising 1 litre of aqueous phase one would require 80 and 20 litres of air phase and organic phase volume, respectively.

#### Four-phase segmented flow microreactor (SFBR) ---- low conversion a big problem

To overcome the oxygen limitation, a concept of continuous aeration within the biofilm grown membrane was developed and applied in chapter 6 (Table 7.4; #5). Realizing such a concept need to overcome several challenges. The major challenge was the establishment of a stable biofilm under the impact of organic phase, fluidic (organic and/or aqueous) flow and air flow stresses, which was successfully solved by using a simple three step method described in chapter 6. A product concentration of 70 mM was achieved in the 1 m long capillary during 19 days of biotransformation, which corresponds to an average volumetric productivity of 15 to 20  $\text{g}_{\text{sty oxid.}} \text{ L}_{\text{tube}}^{-1} \text{ day}^{-1}$ .

Although this system overcomes aeration limitation, challenges still prevail like a short residence time leading to very low conversion rates. Only, 0.04 % of styrene gets converted into the

respective product after each run. Therefore, this study demonstrates that the contacting pattern of substrate to the biofilm needs to be modified in this specific set-up.

#### Four-phase segmented flow membrane microreactor (SFMBR) ---- an optimal choice

To overcome lower styrene conversion problem, the approach of using a membrane for styrene supply and extraction was evaluated in chapter 5. To ensure a high oxygen transfer rate, an aqueous-air segmented type of flow system similar to the previous setup was selected. The challenges of aeration and low substrate conversion were overcome by modifying the microreactor system and applying the concept of a membrane biofilm microreactor introduced in chapter 5. The operation for styrene conversion is divided into four phases. In the first phases, the high first Damköhler number points to the fact that the oxygen availability was the rate limiting step (Table 7.4; #6). As this system was flexible to maximize the air flowrate, the oxygen transfer could be easily altered. Therefore, the air flow was increased from 0.25 to 4 mL min<sup>-1</sup>, which shortened the residence time from 12.6 to 1.8 min, and consequently the first Damköhler number from 9 to 0.31. This ensured a high oxygen transfer which is well reflected by the enhanced styrene formation rate from 11 to 46 g<sub>sty oxid.</sub> L<sub>tube</sub><sup>-1</sup> day<sup>-1</sup> (4 fold).

Thus, after advocating existing reactor configurations and understanding the key limitations we designed the reactor configuration that could overcome several limitations and to improve the process performance significantly. For an easy assessment of microreactor technologies from laboratory to technical scale, the scale-up of such a system which is dependent on the numbering of tubes, needs to be guaranteed. Such concept of applying (liquid-gas) segmented flow on monoliths deposited with chemical catalysts are well studied in chemical engineering and even applied on the industrial scale (Kreutzer et al., 2005). Examples include segmented flow monolithic reactors applied for large scale hydrogen peroxide production in Akzo-Nobel and nitro-aromatic hydrogenations in Air Products and Chemicals. Thus, future work should concentrate on executing biofilm catalysed reactions in monoliths to a higher scale.

## Outlook

This thesis focussed on integrating the concept of microreactors into biocatalysis. Novel reactor designs were explored by combining multiphasic microfluidics, biocatalysis and membrane technology. New interesting insights were gained and the applicability of microreactors was extended to enzyme and biofilm based catalysis. Nevertheless, for practical implementation of such designs on industrial scale several questions still need to be addressed. (i) Selection of **membrane material**. This should be solvent resistant, highly permeable for the desired compounds, non-toxic for the applied biocatalysts, reusable, and cheap. (ii) Selection of **design geometry**. This needs a maximum surface area in a compact size. (iii) **Scale up** based on numbering-up. Here a single unit related issues like flow distribution, clogging and fouling in the single reactor units needs to be taken in to account.

Interestingly, nature evolved designs have applied the concept of microfluidics and miniaturized design in biological systems and solved most of these questions. For example, the size of a single cell balances the surface area to volume ratio such that the surface area is maximized while the diffusion distance is minimized. Thus, according to Fick's first law the mass transfer rate is enhanced, as it is proportional to the area through which diffusion occurs and inversely dependent on the diffusion distance.

With increasing organism size, the average size of cells remains constant, while the number of cells increases and the mass transfer of nutrients to the cells are provided by continuous fluidic transport. Examples include capillary suction in plants to transport water containing nutrients from the roots to the leaves through the xylem conduits (Tyree and Ewers 1991), while in animals the fluid (blood) is transported in a circulatory fashion from the heart throughout the body (Labarbera 1990). The adaptation of fractal geometry in these designs, combining an increased number of micro and nano-sized capillaries, boost the surface area and minimize the diffusion distance, which leads to an efficient mass transfer (Emerson et al. 2006; Murray 1926). The best example is the human lung, where the air flow is distributed from a single trachea to  $8.3 \times 10^6$  alveolar sacs, which typically reduce the diameter from 15 mm to 0.8 mm, and thus enhance the surface area 4720-fold (Johnson et al. 2000). This fractal geometry or hierarchical branching networks have bridged the macroscopic and microscopic world in nature and facilitated transport mechanisms.

Thus, understanding nature's solutions might motivate to work around microsystem design bottlenecks currently faced in industry.

## References

- Al-Rawashdeh M, Cantu-Perez A, Ziegenbalg D, Lob P, Gavriilidis A, Hessel V, Schonfeld F. 2012. Microstructure-based intensification of a falling film microreactor through optimal film setting with realistic profiles and in-channel induced mixing. *Chemical Engineering Journal* 179:318-329.
- Bagdasarian M, Lurz R, Ruckert B, Franklin FCH, Bagdasarian MM, Frey J, Timmis KN. 1981. Specific-Purpose Plasmid Cloning Vectors .2. Broad Host Range, High Copy Number, Rsf1010-Derived Vectors, and a Host-Vector System for Gene Cloning in *Pseudomonas*. *Gene* 16(1-3):237-247.
- Baldascini H, Janssen DB. 2005. Interfacial inactivation of epoxide hydrolase in a two-liquid-phase system. *Enzyme and Microbial Technology* 36(2-3):285-293.
- Baret JC, Kleinschmidt F, El Harrak A, Griffiths AD. 2009. Kinetic Aspects of Emulsion Stabilization by Surfactants: A Microfluidic Analysis. *Langmuir* 25(11):6088-6093.
- Beverung CJ, Radke CJ, Blanch HW. 1999. Protein adsorption at the oil/water interface: characterization of adsorption kinetics by dynamic interfacial tension measurements. *Biophysical Chemistry* 81(1):59-80.
- Bolivar JM, Wiesbauer J, Nidetzky B. 2011. Biotransformations in microstructured reactors: more than flowing with the stream? *Trends in Biotechnology* 29(7):333-342.
- Bosetti A, Vanbeilen JB, Preusting H, Lageveen RG, Witholt B. 1992. Production of Primary Aliphatic-Alcohols with a Recombinant *Pseudomonas* Strain, Encoding the Alkane Hydroxylase Enzyme-System. *Enzyme and Microbial Technology* 14(9):702-708.
- Bradford MM. 1976. A rapid and sensitive method for the quantitation of microgram quantities of protein utilizing the principle of protein-dye binding. *Anal Biochem* 72:248-54.
- Buchholz K, Kasche V, Bornscheuer UT. 2005. *Biocatalysts and enzyme technology*. Weinheim: WILEY-VCH.
- Burns JR, Ramshaw C. 2001. The intensification of rapid reactions in multiphase systems using slug flow in capillaries. *Lab on a Chip* 1(1):10-15.
- Burns JR, Ramshaw C. 2002. A microreactor for the nitration of benzene and toluene. *Chemical Engineering Communications* 189(12):1611-1628.
- Cao. L. 2005. *Carrier-bound immobilized enzymes*. Weinheim: WILEY-VCH. 551 p.
- Chen DLL, Li L, Reyes S, Adamson DN, Ismagilov RF. 2007. Using three-phase flow of immiscible liquids to prevent coalescence of droplets in microfluidic channels: Criteria to identify the third liquid and validation with protein crystallization. *Langmuir* 23(4):2255-2260.
- Chen YZ, Wu MH, Wang KY, Chen B, Yao SZ, Zou HF, Nie LH. 2011. Vinyl functionalized silica hybrid monolith-based trypsin microreactor for on line digestion and separation via thiol-ene "click" strategy. *Journal of Chromatography A* 1218(44):7982-7988.
- Cheng KC, Demirci A, Catchmark JM. 2010. Advances in biofilm reactors for production of value-added products. *Applied Microbiology and Biotechnology* 87(2):445-456.
- Colombie S, Gaunand A, Lindet B. 2001. Lysozyme inactivation under mechanical stirring: effect of physical and molecular interfaces. *Enzyme Microb Technol* 28(9-10):820-826.
- Costantini F, Benetti EM, Reinhoudt DN, Huskens J, Vancso GJ, Verboom W. 2010. Enzyme-functionalized polymer brush films on the inner wall of silicon-glass microreactors with tunable biocatalytic activity. *Lab on a chip* 10(24):3407-12.
- Cremonesi P, Carrea G, Ferrara L, Antonini E. 1975. Enzymatic preparation of 20 beta-hydroxysteroids in a two-phase system. *Biotechnol Bioeng* 17(8):1101-8.
- Dabir B, Riazi MR, Davoudirad HR. 1996. Modelling of falling film reactors. *Chemical Engineering Science* 51(11):2553-2558.

- Dencic I, Meuldijk J, Croon M, Hessel V. 2011. From a review of noble metal versus enzyme catalysts for glucose oxidation under conventional conditions towards a process design analysis for continuous-flow operation. *Journal of flow chemistry* 1(1):13-23.
- Donahue JR, Bartell FE. 1952 The Boundary Tension at Water-Organic Liquid Interfaces. *The Journal of Physical Chemistry* 56(4):480-484.
- Doraiswamy LK, Sharma MM. 1984. *Heterogeneous Reactions: Analysis, Examples, and Reactor Design : Volume 2 : Fluid-Fluid-Solid Reactions*. New York: John Wiley & Sons.
- Doran P. 2004. *Bioprocess engineering principles*. Oxford: Elsevier Academic Press. 439 p.
- Dummann G, Quittmann U, Groschel L, Agar DW, Worz O, Morgenschweis K. 2003. The capillary-microreactor: a new reactor concept for the intensification of heat and mass transfer in liquid-liquid reactions. *Catalysis Today* 79(1-4):433-439.
- Ehrfeld W, Hessel V, Löwe H. 2000. *Microreactors*. Weinheim: Wiley-VCH.
- Eisenberg D, Schwarz E, Komaromy M, Wall R. 1984. Analysis of membrane and surface protein sequences with the hydrophobic moment plot. *J Mol Biol* 179(1):125-42.
- Emerson DR, Cieslicki K, Gu X, Barber RW. 2006. Biomimetic design of microfluidic manifolds based on a generalised Murray's law. *Lab on a chip* 6(3):447-54.
- Emmerling M, Dauner M, Ponti A, Fiaux J, Hochuli M, Szyperski T, Wuthrich K, Bailey JE, Sauer U. 2002. Metabolic flux responses to pyruvate kinase knockout in *Escherichia coli*. *Journal of bacteriology* 184(1):152-164.
- Faber K. 2004. *Biotransformations in organic chemistry*: Springer-Verlag Berlin Heidelberg.
- Garcia-Ochoa F, Gomez E. 2009. Bioreactor scale-up and oxygen transfer rate in microbial processes: An overview. *Biotechnology Advances* 27(2):153-176.
- Ghadge RS, Sawant SB, Joshi JB. 2003. Enzyme deactivation in a bubble column, a stirred vessel and an inclined plane. *Chemical Engineering Science* 58(23-24):5125-5134.
- Ghaini A, Kashid MN, Agar DW. 2010. Effective interfacial area for mass transfer in the liquid-liquid slug flow capillary microreactors. *Chemical Engineering and Processing* 49(4):358-366.
- Ghatorae AS, Bell G, Halling PJ. 1994a. Inactivation of enzymes by organic solvents: New technique with well-defined interfacial area. *Biotechnol Bioeng* 43(4):331-6.
- Ghatorae AS, Guerra MJ, Bell G, Halling PJ. 1994b. Immiscible Organic-Solvent Inactivation of Urease, Chymotrypsin, Lipase, and Ribonuclease - Separation of Dissolved Solvent and Interfacial Effects. *Biotechnology and Bioengineering* 44(11):1355-1361.
- Gross R. 2010. *Catalytic biofilms in membrane reactors: continuous asymmetric epoxidation of styrene and regioselective hydroxylation of alkanes*. Dortmund: Technischen Universität Dortmund. 201 p.
- Gross R, Hauer B, Otto K, Schmid A. 2007. Microbial biofilms: New catalysts for maximizing productivity of long-term biotransformations. *Biotechnology and bioengineering* 98(6):1123-1134.
- Gross R, Lang K, Buehler K, Schmid A. 2010. Characterization of a biofilm membrane reactor and its prospects for fine chemical synthesis. *Biotechnology and bioengineering* 105(4):705-17.
- Grund A, Shapiro J, Fennewald M, Bacha P, Leahy J, Markbreiter K, Nieder M, Toepfer M. 1975. Regulation of Alkane Oxidation in *Pseudomonas-Putida*. *Journal of bacteriology* 123(2):546-556.
- Halan B, Buehler K, Schmid A. 2012. Biofilms as living catalysts in continuous chemical syntheses. *Trends in Biotechnology* 30(9):453-65.
- Halan B, Schmid A, Buehler K. 2010. Maximizing the productivity of catalytic biofilms on solid supports in membrane aerated reactors. *Biotechnol Bioeng* 106(4):516-27.
- Halan B, Schmid A, Buehler K. 2011. Real-Time Solvent Tolerance Analysis of *Pseudomonas sp* Strain LB120 Delta C Catalytic Biofilms. *Applied and Environmental Microbiology* 77(5):1563-1571.

- Hall-Stoodley L, Costerton JW, Stoodley P. 2004. Bacterial biofilms: From the natural environment to infectious diseases. *Nature Reviews Microbiology* 2(2):95-108.
- Harries N, Burns JR, Barrow DA, Ramshaw C. 2003. A numerical model for segmented flow in a microreactor. *International Journal of Heat and Mass Transfer* 46(17):3313-3322.
- Hessel V, Angeli P, Gavriilidis A, Lowe H. 2005. Gas-liquid and gas-liquid-solid microstructured reactors: Contacting principles and applications. *Industrial & Engineering Chemistry Research* 44(25):9750-9769.
- Hessel V, Renken A, Schouten JC, Yoshida JI. 2009. *Micro Process Engineering A comprehensive handbook*: WILEY-VCH.
- Heydorn A, Nielsen AT, Hentzer M, Sternberg C, Givskov M, Ersboll BK, Molin S. 2000. Quantification of biofilm structures by the novel computer program COMSTAT. *Microbiology* 146 ( Pt 10):2395-407.
- Hickel A, Radke CJ, Blanch HW. 1998. Hydroxynitrile lyase adsorption at liquid/liquid interfaces. *Journal of Molecular Catalysis B-Enzymatic* 5(1-4):349-354.
- Höllrigel V, Hollmann F, Kleeb AC, Buehler K, Schmid A. 2008. TADH, the thermostable alcohol dehydrogenase from *Thermus sp ATN1*: a versatile new biocatalyst for organic synthesis. *Applied Microbiology and Biotechnology* 81(2):263-273.
- Honda T, Miyazaki M, Nakamura H, Maeda H. 2006. Facile preparation of an enzyme-immobilized microreactor using a cross-linking enzyme membrane on a microchannel surface. *Advanced Synthesis & Catalysis* 348(15):2163-2171.
- Horvath C, Sardi A, Woods JS. 1973. L-Asparaginase Tubes - Kinetic Behavior and Application in Physiological Studies. *Journal of Applied Physiology* 34(2):181-187.
- Horvath C, Solomon BA. 1972. Open tubular heterogeneous enzyme reactors: preparation and kinetic behavior. *Biotechnology and bioengineering* 14(6):885-914.
- Janasek D, Franzke J, Manz A. 2006. Scaling and the design of miniaturized chemical-analysis systems. *Nature* 442(7101):374-380.
- Johansson PA, Karlberg B, Thelander S. 1980. Extraction Based on the Flow-Injection Principle .4. Determination of Extraction Constants. *Analytica Chimica Acta* 114(Feb):215-226.
- Johnson AT, Lausted CG, Bronzino JD. 2000. Respiratory system. In: Bronzino JD, editor. *The biomedical engineering handbook: second edition*. Boca Raton: CRC press LLC.
- Jovanovic J, Rebrov EV, Nijhuis TA, Hessel V, Schouten JC. 2010. Phase-Transfer Catalysis in Segmented Flow in a Microchannel: Fluidic Control of Selectivity and Productivity. *Industrial & Engineering Chemistry Research* 49(6):2681-2687.
- Karande R, Schmid A, Buehler K. 2010. Enzyme catalysis in an aqueous/organic segment flow microreactor: ways to stabilize enzyme activity. *Langmuir* 26(11):9152-9.
- Karande R, Schmid A, Buehler K. 2011. Miniaturizing Biocatalysis: Enzyme-Catalyzed Reactions in an Aqueous/Organic Segmented Flow Capillary Microreactor. *Advanced Synthesis & Catalysis* 353(13):2511-2521.
- Karimi G, Kawaji M. 1998. An experimental study of freely falling films in a vertical tube. *Chemical Engineering Science* 53(20):3501-3512.
- Kasche V, Kuhlmann G. 1980. Direct Measurement of the Thickness of the Unstirred Diffusion Layer Outside Immobilized Biocatalysts. *Enzyme and Microbial Technology* 2(4):309-312.
- Kashid MN, Agar DW. 2007. Hydrodynamics of liquid-liquid slug flow capillary microreactor: Flow regimes, slug size and pressure drop. *Chemical Engineering Journal* 131(1-3):1-13.
- Kashid MN, Gupta A, Renken A, Kiwi-Minsker L. 2010. Numbering-up and mass transfer studies of liquid-liquid two-phase microstructured reactors. *Chemical Engineering Journal* 158(2):233-240.
- Kashid MN, Harshe YM, Agar DW. 2007. Liquid-liquid slug flow in a capillary: An alternative to suspended drop or film contactors. *Industrial & Engineering Chemistry Research* 46(25):8420-8430.

- Kashid MN, Renken A, Kiwi-Minsker L. 2011a. Gas-liquid and liquid-liquid mass transfer in microstructured reactors. *Chemical Engineering Science* 66(17):3876-3897.
- Kashid MN, Renken A, Kiwi-Minsker L. 2011b. Microstructured reactors and supports for ionic liquids. *Chemical Engineering Science* 66(7):1480-1489.
- Kashid MN, Rivas DF, Agar DW, Turek S. 2008. On the hydrodynamics of liquid-liquid slug flow capillary microreactors. *Asia-Pacific Journal of Chemical Engineering* 3(2):151-160.
- Kerby MB, Legge RS, Tripathi A. 2006. Measurements of kinetic parameters in a microfluidic reactor. *Analytical chemistry* 78(24):8273-80.
- Kinkel JFM, Tomlinson E. 1980. Drug Liquid-Liquid Distribution Based on the Fundamentals of Segmented Flow. *International Journal of Pharmaceutics* 6(3-4):261-275.
- Koch K, van den Berg RJF, Nieuwland PJ, Wijtmans R, Schoemaker HE, van Hest JCM, Rutjes FPJT. 2008. Enzymatic enantioselective C-C-bond formation in microreactors. *Biotechnology and Bioengineering* 99(4):1028-1033.
- Kockmann N. 2006. *Micro Process Engineering - Fundamentals, Devices, Fabrication, and Applications*. O. von Brand GK, Fedder C, Hierold JG, Korvink OT, editors. Weinheim Wiley-VCH.
- Korber DR, Lawrence JR, Sutton B, Caldwell DE. 1989. Effect of Laminar-Flow Velocity on the Kinetics of Surface Recolonization by Mot<sup>+</sup> and Mot<sup>-</sup> Pseudomonas-Fluorescens. *Microbial Ecology* 18(1):1-19.
- Kotsmar C, Grigoriev DO, Xu F, Aksenenko EV, Fainerman VB, Leser ME, Miller R. 2008. Equilibrium of adsorption of mixed milk protein/surfactant solutions at the water/air interface. *Langmuir* 24(24):13977-84.
- Kreutzer MT, Du P, Heiszwolf JJ, Kapteijn F, Moulijn JA. 2001. Mass transfer characteristics of three-phase monolith reactors. *Chemical Engineering Science* 56(21-22):6015-6023.
- Kreutzer MT, Kapteijn F, Moulijn JA. 2005. Monoliths as biocatalytic reactors: Smart gas-liquid contacting for process intensification. *Industrial & Engineering Chemistry Research* 44(25):9646-9652.
- Kreutzer MT, Kapteijn F, Moulijn JA. 2006. Shouldn't catalysts shape up? Structured reactors in general and gas-liquid monolith reactors in particular. *Catalysis Today* 111(1-2):111-118.
- Laane C, Boeren S, Vos K, Veeger C. 1987. Rules for Optimization of Biocatalysis in Organic-Solvents. *Biotechnology and Bioengineering* 30(1):81-87.
- Labarbera M. 1990. Principles of Design of Fluid Transport-Systems in Zoology. *Science* 249(4972):992-1000.
- Lawrence JR, Caldwell DE. 1987. Behavior of Bacterial Stream Populations within the Hydrodynamic Boundary-Layers of Surface Microenvironments. *Microbial Ecology* 14(1):15-27.
- Lee MY, Srinivasan A, Ku B, Dordick JS. 2003. Multienzyme catalysis in microfluidic biochips. *Biotechnology and bioengineering* 83(1):20-28.
- Levenspiel O. 1999. *Chemical reaction engineering*. New York: John Wiley & Sons. 665 p.
- Li T, Liu J, Bai R. 2008. Membrane aerated biofilm reactors: a brief current review. *Recent patents on biotechnology* 2(2):88-93.
- Liese A, Seelbach K, Wandrey C. 2006. *Industrial Biotransformations*. Weinheim: Wiley-VCH. 556 p.
- Machsun AL, Gozan M, Nasikin M, Setyahadi S, Yoo YJ. 2010. Membrane Microreactor in Biocatalytic Transesterification of Triolein for Biodiesel Production. *Biotechnology and Bioprocess Engineering* 15(6):911-916.
- Marques MPC, Fernandes P. 2011. Microfluidic Devices: Useful Tools for Bioprocess Intensification. *Molecules* 16(10):8368-8401.
- Marques MPC, Fernandes P, Cabral JMS, Znidarsic-Plazl P, Plazl I. 2010. On the feasibility of in situ steroid biotransformation and product recovery in microchannels. *Chemical Engineering Journal* 160(2):708-714.



- Martin K, Henkel T, Baier V, Grodrian A, Schon T, Roth M, Michael Kohler J, Metze J. 2003. Generation of larger numbers of separated microbial populations by cultivation in segmented-flow microdevices. *Lab on a chip* 3(3):202-7.
- Maruyama T, Uchida J, Ohkawa T, Futami T, Katayama K, Nishizawa K, Sotowa K, Kubota F, Kamiyaa N, Goto M. 2003. Enzymatic degradation of p-chlorophenol in a two-phase flow microchannel system. *Lab on a Chip* 3(4):308-312.
- Mateo C, Abian O, Fernandez-Lorente G, Pedroche J, Fernandez-Lafuente R, Guisan JM. 2002. Epoxy sepabeads: A novel epoxy support for stabilization of industrial enzymes via very intense multipoint covalent attachment. *Biotechnology Progress* 18(3):629-634.
- Mathys RG, Schmid A, Withold B. 1999. Integrated Two-Liquid Phase Bioconversion and Product-Recovery Processes for the Oxidation of Alkanes: Process Design and Economic Evaluation. *Biotechnol. Bioeng.* 64(4):459- 477.
- Mazutis L, Baret JC, Griffiths AD. 2009. A fast and efficient microfluidic system for highly selective one-to-one droplet fusion. *Lab on a chip* 9(18):2665-2672.
- Mazutis L, Griffiths AD. 2012. Selective droplet coalescence using microfluidic systems. *Lab on a chip* 12(10):1800-1806.
- Mendorf M, Agar DW. 2011. Scale-up of Capillary Extraction Equipment. *Chemie Ingenieur Technik* 83(7):1120-1124.
- Miller R, Fainerman VB, Makievski AV, Kragel J, Grigoriev DO, Kazakov VN, Sinyachenko OV. 2000. Dynamics of protein and mixed protein/surfactant adsorption layers at the water/fluid interface. *Advances in Colloid and Interface Science* 86(1-2):39-82.
- Mohr S, Fisher K, Scrutton NS, Goddard NJ, Fielden PR. 2010. Continuous two-phase flow miniaturised bioreactor for monitoring anaerobic biocatalysis by pentaerythritol tetranitrate reductase. *Lab on a chip* 10(15):1929-1936.
- Murray CD. 1926. The Physiological Principle of Minimum Work Applied to the Angle of Branching of Arteries. *The Journal of general physiology* 9(6):835-41.
- Nandakumar K, Obika H, Shinozaki T, Ooie T, Utsumi A, Yano T. 2003. Laser impact assessment in a biofilm-forming bacterium *Pseudoalteromonas carrageenovora* using a flow cytometric system. *Biotechnology and Bioengineering* 82(4):399-402.
- Neuhauser W, Steininger M, Haltrich D, Kulbe KD, Nidetzky B. 1998. A pH-controlled fed-batch process can overcome inhibition by formate in NADH-dependent enzymatic reductions using formate dehydrogenase-catalyzed coenzyme regeneration. *Biotechnol Bioeng* 60(3):277-82.
- Nicolella C, van Loosdrecht MCM, Heijnen SJ. 2000. Particle-based biofilm reactor technology. *Trends in Biotechnology* 18(7):312-320.
- Nord L, Backstrom K, Danielsson LG, Ingman F, Karlberg B. 1987. Extraction Rate in Liquid-Liquid Segmented Flow-Injection Analysis. *Analytica Chimica Acta* 194:221-233.
- Nord L, Karlberg B. 1984. Extraction Based on the Flow-Injection Principle .6. Film Formation and Dispersion in Liquid Liquid Segmented Flow Extraction Systems. *Analytica Chimica Acta* 164(Oct):233-249.
- Panke S, Held M, Wubbolts MG, Witholt B, Schmid A. 2002. Pilot-scale production of (S)-styrene oxide from styrene by recombinant *Escherichia coli* synthesizing styrene monooxygenase. *Biotechnol Bioeng* 80(1):33-41.
- Panke S, Witholt B, Schmid A, Wubbolts MG. 1998. Towards a biocatalyst for (S)-Styrene oxide production: Characterization of the styrene degradation pathway of *Pseudomonas* sp. strain VLB120 (vol 64, pg 2032, 1998). *Applied and Environmental Microbiology* 64(9):3546-3546.
- Park JB, Buhler B, Panke S, Witholt B, Schmid A. 2007. Carbon metabolism and product inhibition determine the epoxidation efficiency of solvent-tolerant *Pseudomonas* sp strain VLB120 Delta C. *Biotechnology and Bioengineering* 98(6):1219-1229.

- Piciooreanu C, van Loosdrecht MCM, Heijnen JJ. 2000. Effect of diffusive and convective substrate transport on biofilm structure formation: A two-dimensional modeling study. *Biotechnology and bioengineering* 69(5):504-515.
- Pompano RR, Li HW, Ismagilov RF. 2008. Rate of mixing controls rate and outcome of autocatalytic processes: Theory and microfluidic experiments with chemical reactions and blood coagulation. *Biophysical Journal* 95(3):1531-1543.
- Qureshi N, Maddox IS. 1988. Reactor Design for the Abe Fermentation Using Cells of *Clostridium Acetobutylicum* Immobilized by Adsorption onto Bonechar. *Bioprocess Engineering* 3(2):69-72.
- Ramelmeier RA, Blanch HW. 1989. Peroxidase-Catalyzed Oxidation of P-Anisidine with H<sub>2</sub>O<sub>2</sub> in Toluene. *Biotechnology and Bioengineering* 33(4):512-517.
- Rao AG, Ravichandra P, Joseph J, Jetty A, Sarma PN. 2007. Microbial conversion of sulfur dioxide in flue gas to sulfide using bulk drug industry wastewater as an organic source by mixed cultures of sulfate reducing bacteria. *Journal of Hazardous Materials* 147(3):718-725.
- Ratulowski J, Chang HC. 1990. Marangoni Effects of Trace Impurities on the Motion of Long Gas-Bubbles in Capillaries. *Journal of Fluid Mechanics* 210:303-328.
- Renken A, Kiwi-Minsker L. 2010. Microstructured catalytic reactors. In: Gates BC, Knözinger H, editors. *Advances in catalysis*: Elsevier. p 47-107.
- Rittmann BE. 1982. The Effect of Shear-Stress on Biofilm Loss Rate. *Biotechnology and Bioengineering* 24(2):501-506.
- Roach LS, Song H, Ismagilov RF. 2005. Controlling nonspecific protein adsorption in a plug-based microfluidic system by controlling interfacial chemistry using fluorosurfactants. *Analytical Chemistry* 77(3):785-796.
- Roberge DM, Zimmermann B, Rainone F, Gottsponer M, Eyholzer M, Kockmann N. 2008. Microreactor technology and continuous processes in the fine chemical and pharmaceutical industry: Is the revolution underway? *Organic Process Research & Development* 12(5):905-910.
- Rosche B, Li XZ, Hauer B, Schmid A, Buehler K. 2009. Microbial biofilms: a concept for industrial catalysis? *Trends in Biotechnology* 27(11):636-643.
- Ross AC, Bell G, Halling PJ. 2000. Organic solvent functional group effect on enzyme inactivation by the interfacial mechanism. *Journal of Molecular Catalysis B-Enzymatic* 8(4-6):183-192.
- Ruinatscha R. 2009. Asymmetric biocatalytic epoxidation in a scalable electrochemical reactor using FAD-dependent styrene monooxygenase. Dortmund: Technische Universität Dortmund. 173 p.
- Samant KD, Ng KM. 1998. Effect of kinetics and mass transfer on design of extractive reaction processes. *Aiche Journal* 44(10):2212-2228.
- Sambrook J, Russell WD. 2001. *Molecular Cloning: A Laboratory Manual*. New York: Cold Spring Harbor Laboratory Press.
- Sand W, Gerke T, Hallmann R, Schippers A. 1995. Sulfur Chemistry, Biofilm, and the (in)Direct Attack Mechanism - a Critical-Evaluation of Bacterial Leaching. *Applied Microbiology and Biotechnology* 43(6):961-966.
- Sayar NA, Chen BH, Lye GJ, Woodley JM. 2009a. Modelling and simulation of a transketolase mediated reaction: Sensitivity analysis of kinetic parameters. *Biochemical Engineering Journal* 47(1-3):1-9.
- Sayar NA, Chen BH, Lye GJ, Woodley JM. 2009b. Process modelling and simulation of a transketolase mediated reaction: Analysis of alternative modes of operation. *Biochemical Engineering Journal* 47(1-3):10-18.

- Schilke KF, Wilson KL, Cantrell T, Corti G, McIlroy DN, Kelly C. 2010. A novel enzymatic microreactor with *Aspergillus oryzae* beta-galactosidase immobilized on silicon dioxide nanosprings. *Biotechnology progress* 26(6):1597-605.
- Schmid A, Dordick JS, Hauer B, Kiener A, Wubbolts M, Witholt B. 2001. Industrial biocatalysis today and tomorrow. *Nature* 409(6817):258-68.
- Schrewe M, Magnusson AO, Willrodt C, Buhler B, Schmid A. 2011. Kinetic Analysis of Terminal and Unactivated C-H Bond Oxyfunctionalization in Fatty Acid Methyl Esters by Monooxygenase-Based Whole-Cell Biocatalysis. *Advanced Synthesis & Catalysis* 353(18):3485-3495.
- Sharma PK, Gibcus MJ, van der Mei HC, Busscher HJ. 2005a. Influence of fluid shear and microbubbles on bacterial detachment from a surface. *Applied and Environmental Microbiology* 71(7):3668-3673.
- Sharma PK, Gibcus MJ, van der Mei HC, Busscher HJ. 2005b. Microbubble-induced detachment of coadhering oral bacteria from salivary pellicles. *European Journal of Oral Sciences* 113(4):326-332.
- Sheldon RA. 2007. Enzyme immobilization: The quest for optimum performance. *Advanced Synthesis & Catalysis* 349(8-9):1289-1307.
- Siegel RR, Harder P, Dahint R, Grunze M, Josse F, Mrksich M, Whitesides GM. 1997. On-line detection of nonspecific protein adsorption at artificial surfaces. *Anal Chem* 69(16):3321-8.
- Slusarczyk H, Felber S, Kula M-R, Pohl M. 2000. Stabilization of NAD-dependent formate dehydrogenase from *Candida boidinii* by site-directed mutagenesis of cysteine residues. *European Journal of Biochemistry* 267(5):1280-1289.
- Sotowa KI, Miyoshi R, Lee CG, Kang Y, Kusakabe K. 2005. Mixing and enzyme reactions in a microchannel packed with glass beads. *Korean Journal of Chemical Engineering* 22(4):552-555.
- Srinivasulu S, Rao AGA. 1993. Kinetic and Structural Studies on the Interaction of Surfactants with Lipoxygenase L1 from Soybeans (*Glycine-Max*). *Journal of Agricultural and Food Chemistry* 41(3):366-371.
- Swarts JW, Kolfschoten RC, Jansen MCAA, Janssen AEM, Boom RM. 2010. Effect of diffusion on enzyme activity in a microreactor. *Chemical Engineering Journal* 162(1):301-306.
- Swarts JW, Vossenbergh P, Meerman MH, Janssen AE, Boom RM. 2008. Comparison of two-phase lipase-catalyzed esterification on micro and bench scale. *Biotechnology and bioengineering* 99(4):855-61.
- Syron E, Casey E. 2008. Membrane-aerated biofilms for high rate biotreatment: Performance appraisal, engineering principles, scale-up, and development requirements. *Environmental Science & Technology* 42(6):1833-1844.
- Tanaka Y, Slyadnev MN, Sato K, Tokeshi M, Kim HB, Kitamori T. 2001. Acceleration of an enzymatic reaction in a microchip. *Analytical Sciences* 17(7):809-810.
- Tice JD, Song H, Lyon AD, Ismagilov RF. 2003. Formation of Droplets and Mixing in Multiphase Microfluidics at Low Values of the Reynolds and the Capillary Numbers. *Langmuir* 19(22):9127-9133.
- Tyree MT, Ewers FW. 1991. The Hydraulic Architecture of Trees and Other Woody-Plants. *New Phytologist* 119(3):345-360.
- van Beilen JB, Duetz WA, Schmid A, Witholt B. 2003. Practical issues in the application of oxygenases. *Trends in Biotechnology* 21(4):170-177.
- van Beilen JB, Smits THM, Roos FF, Brunner T, Balada SB, Rothlisberger M, Witholt B. 2005. Identification of an amino acid position that determines the substrate range of integral membrane alkane hydroxylases. *Journal of bacteriology* 187(1):85-91.

- van der Vegt W, Norde W, van der Mei HC, Busscher HJ. 1996. Kinetics of Interfacial Tension Changes during Protein Adsorption from Sessile Droplets on FEP-Teflon. *Journal of Colloid and Interface Science*. p 57-65.
- Vankayala BK, Loeb P, Hessel V, Menges G, Hofmann C, Metzke D, Krtischil U, Kost HJ. 2007. Scale-up of process intensifying falling film microreactors to pilot production scale. *International Journal of Chemical Reactor Engineering* 5.
- Voloshin Y, Lawal A, Panikov NS. 2005. Continuous plug-flow bioreactor: experimental testing with *Pseudomonas putida* culture grown on benzoate. *Biotechnology and bioengineering* 91(2):254-9.
- Watts P, Haswell SJ. 2005. The application of micro reactors for organic synthesis. *Chemical Society Reviews* 34(3):235-246.
- Wirth T. 2008. *Microreactors in organic synthesis and catalysis*. Weinheim: Wiley-VCH.
- Woodley JM, Lilly MD. 1990. Extractive Biocatalysis - the Use of 2-Liquid Phase Biocatalytic Reactors to Assist Product Recovery. *Chemical Engineering Science* 45(8):2391-2396.
- Woodley JM, TitchenerHooker NJ. 1996. The use of windows of operation as a bioprocess design tool. *Bioprocess Engineering* 14(5):263-268.
- Young ME, Carroad PA, Bell RL. 1980. Estimation of Diffusion-Coefficients of Proteins. *Biotechnology and Bioengineering* 22(5):947-955.
- Yue J, Chen GW, Yuan Q, Luo LG, Gonthier Y. 2007. Hydrodynamics and mass transfer characteristics in gas-liquid flow through a rectangular microchannel. *Chemical Engineering Science* 62(7):2096-2108.

# Curriculum Vitae

## Personal data

Name	Rohan Rajaram Karande
Born	20 <sup>th</sup> February, 1982
Nationality	Indian
Family status	Married (1 child)

## Education

Since 2012	Post-doctoral researcher at the Laboratory of Chemical Biotechnology, TU Dortmund, under the supervision of Prof. Dr. Andreas Schmid and Dr. Katja Buehler. Dortmund, Germany
2007-2012	Doctoral thesis at the Laboratory of Chemical Biotechnology, TU Dortmund, under the supervision of Prof. Dr. Andreas Schmid and Dr. Katja Buehler. Dortmund, Germany
2004-2007	Master in Chemical Engineering (M. Sc.) Technische Universität Dortmund, Dortmund, Germany
1999-2003	Bachelor in Chemical Engineering (B.E) Shivaji University (P.V.P Institute of Technology) Kolhapur, India

## Peer-Reviewed Publications

Karande R., Schmid A. and Buehler K. (2010)

Enzyme catalysis in an aqueous/organic segment flow microreactor: ways to stabilize enzyme activity. *Langmuir*, 26(11):9152-9159

Karande R., Schmid A. and Buehler K. (2011)

Miniaturizing Biocatalysis: Enzyme catalyzed reactions in an aqueous/organic segmented flow capillary microreactor. *Advanced Synthesis and Catalysis*, 353(13):2511-2521

Ruinatscha R., Karande R., Buehler K. and Schmid A. (2011)

Integrated one-pot enrichment and immobilization of styrene monooxygenase (StyA) using Sepabead EC-EA and EC-Q1A anion-exchange carriers. *Molecules*, 16(7):5975-5988

## Patent

Karande R., Schmid A. and Buehler K. (2010)

Segmented flow biofilm reactor

WO/2012/152337

PCT/EP2011/057724

## Oral Presentations

Karande R., Buehler K. and Schmid A. (2009)

Application of segment flow microsystems to enzymatic catalysis.

Kolloquium der Fakultät BCI. 11. Nov. 2009, Dortmund, Germany

Karande R., Buehler K. and Schmid A. (2010)

Segment flow capillary microreactors as alternatives to two phase enzymatic batch reactors.

ESBES, 08. - 10. September 2010, Bologna, Italy

Karande R., Buehler K. and Schmid A. (2011)

Segmented flow capillary microreactors: a tool for bio-process intensification.

Bioverfahrenstechnik an Grenzflächen, 30. May - 01. June 2011, Potsdam, Germany

## Posters

Karande R., Buehler K. and Schmid A. (2008)

Asymmetric Enzymatic Hydrogenation in Capillary Microreactors.

MSB, 9. - 13. March 2008, Berlin, Germany

Karande R., Buehler K. and Schmid A. (2009)

Multiphase slug flow microreactor for enzyme based redox biocatalysis.

Dechema, Jahrestagung der Biotechnologen, 8. - 10. September 2009, Mannheim, Germany

Karande R., Buehler K. and Schmid A. (2010)

Asymmetric enzymatic hydrogenation in an aqueous/organic flow capillary microreactor.

Bioprozessorientiertes Anlagendesign, 10. - 12. May 2010, Nürnberg, Germany

Karande R., Buehler K. and Schmid A. (2011)

Applications of segmented flow microreactor for biocatalysis.

Biotrends, 8. - 9. December 2011, Dortmund, Germany